

NASA/TM-2003-21621/Rev-Vol II

*James L. Mueller, Giuletta S. Fargion and Charles R. McClain, Editors
J. L. Mueller, C. Pietras, S. B. Hooker, R.W. Austin, M. Miller, K.D. Knobelspiess, R. Frouin,
B. Holben and K. Voss, Authors.*

**Ocean Optics Protocols For Satellite Ocean Color Sensor
Validation, Revision 4, Volume II:
Instrument Specifications, Characterization and Calibration**

National Aeronautical and
Space administration

Goddard Space Flight Space Center
Greenbelt, Maryland 20771

January 2003

NASA/TM-2003-

**Ocean Optics Protocols For Satellite Ocean Color Sensor
Validation, Revision 4, Volume II:**

Instrument Specifications, Characterization and Calibration

*James L. Mueller, CHORS, San Diego State University, San Diego, California
Giulietta S. Fargion, Science Applications International Corporation, Beltsville, Maryland
Charles R. McClain, Goddard Space Flight Center, Greenbelt, Maryland*

*J. L. Mueller, and R.W. Austin
CHORS, San Diego State University, San Diego, California
Christophe Pietras
Science Applications International Corporation, Beltsville, Maryland
Stanford B. Hooker and Brent Holben
NASA Goddard Space Flight Center, Greenbelt, Maryland
Mark Miller
Department of Applied Science, Brookhaven National Laboratory, Upton, New York
Kirk D. Knobelspiesse
Science Systems and Applications, Inc., Greenbelt, Maryland
Robert Frouin
Scripps Institution of Oceanography, University of California, San Diego, California
Ken Voss
Physics Department, University of Miami, Florida*

National Aeronautical and
Space administration

Goddard Space Flight Space Center
Greenbelt, Maryland 20771

January 2003

Preface

This document stipulates protocols for measuring bio-optical and radiometric data for the Sensor Intercomparison and Merger for Biological and Interdisciplinary Oceanic Studies (SIMBIOS) Project activities and algorithm development. The document is organized into 7 separate volumes as:

Ocean Optics Protocols for Satellite Ocean Color Sensor Validation, Revision 4

Volume I: Introduction, Background and Conventions

Volume II: Instrument Specifications, Characterization and Calibration

Volume III: Radiometric Measurements and Data Analysis Methods

Volume IV: Inherent Optical Properties: Instruments, Characterization, Field Measurements and Data Analysis Protocols

Volume V: Biogeochemical and Bio-Optical Measurements and Data Analysis Methods

Volume VI: Special Topics in Ocean Optics Protocols

Volume VII: Appendices

The earlier version of *Ocean Optics Protocols for Satellite Ocean Color Sensor Validation, Revision 3* (Mueller and Fargion 2002, Volumes 1 and 2) is entirely superseded by the seven Volumes of Revision 4 listed above.

The new multi-volume format for publishing the ocean optics protocols is intended to allow timely future revisions to be made reflecting important evolution of instruments and methods in some areas, without reissuing the entire document. Over the years, as existing protocols were revised, or expanded for clarification, and new protocol topics were added, the ocean optics protocol document has grown from 45pp (Mueller and Austin 1992) to 308pp in Revision 3 (Mueller and Fargion 2002). This rate of growth continues in Revision 4. The writing and editorial tasks needed to publish each revised version of the protocol manual as a single document has become progressively more difficult as its size increases. Chapters that change but little, must nevertheless be rewritten for each revision to reflect relatively minor changes in, *e.g.*, cross-referencing and to maintain self-contained consistency in the protocol manual. More critically, as it grows bigger, the book becomes more difficult to use by its intended audience. A massive new protocol manual is difficult for a reader to peruse thoroughly enough to stay current with and apply important new material and revisions it may contain. Many people simply find it too time consuming to keep up with changing protocols presented in this format - which may explain why some relatively recent technical reports and journal articles cite Mueller and Austin (1995), rather than the then current, more correct protocol document. It is hoped that the new format will improve community access to current protocols by stabilizing those volumes and chapters that do not change significantly over periods of several years, and introducing most new major revisions as new chapters to be added to an existing volume without revision of its previous contents.

The relationships between the Revision 4 chapters of each protocol volume and those of Revision 3 (Mueller and Fargion 2002), and the topics new chapters, are briefly summarized below:

Volume I: This volume covers perspectives on ocean color research and validation (Chapter 1), fundamental definitions, terminology, relationships and conventions used throughout the protocol document (Chapter 2), requirements for specific *in situ* observations (Chapter 3), and general protocols for field measurements, metadata, logbooks, sampling strategies, and data archival (Chapter 4). Chapters 1, 2 and 3 of Volume I correspond directly to Chapters 1, 2 and 3 of Revision 3 with no substantive changes. Two new variables, Particulate Organic Carbon (POC) and Particle Size Distribution (PSD) have been added to Tables 3.1 and 3.2 and the related discussion in Section 3.4; protocols covering these measurements will be added in a subsequent revision to Volume V (see below). Chapter 4 of Volume I combines material from Chapter 9 of Revision 3 with a brief summary of SeaBASS policy and archival requirements (detailed SeaBASS information in Chapter 18 and Appendix B of Revision 3 has been separated from the optics protocols).

Volume II: The chapters of this volume review instrument performance characteristics required for *in situ* observations to support validation (Chapter 1), detailed instrument specifications and underlying rationale (Chapter 2) and protocols for instrument calibration and characterization standards and methods (Chapters 3 through 5). Chapters 1 through 5 of Volume II correspond directly to Revision 3 chapters 4 through 8, respectively, with only minor modifications.

Volume III: The chapters of this volume briefly review methods used in the field to make the *in situ* radiometric measurements for ocean color validation, together with methods of analyzing the data (Chapter 1), detailed measurement and data analysis protocols for in-water radiometric profiles (Chapter 2), above water measurements of remote sensing reflectance (Chapter III-3), determinations of exact normalized water-leaving radiance (Chapter 4), and atmospheric radiometric measurements to determine aerosol optical thickness and sky radiance distributions (Chapter 5). Chapter 1 is adapted from relevant portions of Chapter 9 in Revision 3. Chapter 2 of Volume III corresponds to Chapter 10 of Revision 3, and Chapters 3 through 5 to Revision 3 Chapters 12 through 14, respectively. Aside from reorganization, there are no changes in the protocols presented in this volume.

Volume IV: This volume includes a chapter reviewing the scope of inherent optical properties (IOP) measurements (Chapter 1), followed by 4 chapters giving detailed calibration, measurement and analysis protocols for the beam attenuation coefficient (Chapter 2), the volume absorption coefficient measured *in situ* (Chapter 3), laboratory measurements of the volume absorption coefficients from discrete filtered seawater samples (Chapter 4), and *in situ* measurements of the volume scattering function, including determinations of the backscattering coefficient (Chapter 5). Chapter 4 of Volume IV is a slightly revised version of Chapter 15 in Revision 3, while the remaining chapters of this volume are entirely new contributions to the ocean optics protocols. These new chapters may be significantly revised in the future, given the rapidly developing state-of-the-art in IOP measurement instruments and methods.

Volume V: The overview chapter (Chapter 1) briefly reviews biogeochemical and bio-optical measurements, and points to literature covering methods for measuring these variables; some of the material in this overview is drawn from Chapter 9 of Revision 3. Detailed protocols for HPLC measurement of phytoplankton pigment concentrations are given in Chapter 2, which differs from Chapter 16 of Revision 3 only by its specification of a new solvent program. Chapter 3 gives protocols for Fluorometric measurement of chlorophyll *a* concentration, and is not significantly changed from Chapter 17 of Revision 3. New chapters covering protocols for measuring, Phycoerythrin concentrations, Particle Size Distribution (PSD) and Particulate Organic Carbon (POC) concentrations are likely future additions to this volume.

Volume VI: This volume gathers chapters covering more specialized topics in the ocean optics protocols. Chapter 1 introduces these special topics in the context of the overall protocols. Chapter 2 is a reformatted, but otherwise unchanged, version of Chapter 11 in Revision 3 describing specialized protocols used for radiometric measurements associated with the Marine Optical Buoy (MOBY) ocean color vicarious calibration observatory. The remaining chapters are new in Revision 4 and cover protocols for radiometric and bio-optical measurements from moored and drifting buoys (Chapter 3), ocean color measurements from aircraft (Chapter 4), and methods and results using LASER sources for stray-light characterization and correction of the MOBY spectrographs (Chapter 5). In the next few years, it is likely that most new additions to the protocols will appear as chapters added to this volume.

Volume VII: This volume collects appendices of useful information. Appendix A is an updated version of Appendix A in Revision 3 summarizing characteristics of past, present and future satellite ocean color missions. Appendix B is the List of Acronyms used in the report and is an updated version of Appendix C in Revision 3. Similarly, Appendix C, the list of Frequently Used Symbols, is an updated version of Appendix D from Rev. 3. The SeaBASS file format information given in Appendix B of Revision 3 has been removed from the protocols and is promulgated separately by the SIMBIOS Project.

In the Revision 4 multi-volume format of the ocean optics protocols, Volumes I, II and III are unlikely to require significant changes for several years. The chapters of Volume IV may require near term revisions to reflect the rapidly evolving state-of-the-art in measurements of inherent optical properties, particularly concerning instruments and methods for measuring the Volume Scattering Function of seawater. It is anticipated that new chapters will be also be added to Volumes V and VI in Revision 5 (2003).

This technical report is not meant as a substitute for scientific literature. Instead, it will provide a ready and responsive vehicle for the multitude of technical reports issued by an operational Project. The contributions are published as submitted, after only minor editing to correct obvious grammatical or clerical errors.

Table of Contents and Author List

CHAPTER 1.....	1
<i>INSTRUMENT SPECIFICATIONS, CHARACTERIZATION AND CALIBRATION OVERVIEW</i>	
1.1 INTRODUCTION.....	1
1.2 INSTRUMENT PERFORMANCE SPECIFICATIONS.....	1
1.3 CHARACTERIZATION OF OCEANOGRAPHIC AND ATMOSPHERIC RADIOMETERS.....	1
1.4 CALIBRATION OF SUN PHOTOMETERS AND SKY RADIANCE SENSORS.....	2
1.5 STABILITY MONITORING OF FIELD RADIOMETERS USING PORTABLE SOURCES.....	2
1.6 CALIBRATION OF INHERENT OPTICAL PROPERTY SENSORS.....	3
1.7 CALIBRATION OF METEOROLOGICAL SENSORS.....	3
1.8 CTD CALIBRATION.....	3
1.9 PRESSURE TRANSDUCER CALIBRATIONS.....	3
REFERENCES.....	4
CHAPTER 2.....	5
<i>INSTRUMENT PERFORMANCE SPECIFICATIONS</i>	
2.1 INTRODUCTION.....	5
2.2 IN-WATER RADIOMETERS.....	5
<i>Spectral Characteristics</i>	5
<i>Responsivity, SNR, and Resolution</i>	7
<i>Linearity and Stability</i>	10
<i>Sampling Resolution</i>	10
<i>Angular Response Characteristics</i>	10
<i>Operating Depth</i>	10
<i>Instrument Attitude</i>	10
<i>Red and Near-Infrared Wavelengths</i>	11
2.3 SURFACE IRRADIANCE.....	11
<i>Surface Radiometer Characteristics</i>	11
2.4 ABOVE-WATER RADIOMETRY.....	12
2.5 INHERENT OPTICAL PROPERTY INSTRUMENTS.....	13
2.6 ATMOSPHERIC AEROSOLS.....	14
2.7 SPECTRAL SKY RADIANCE.....	15
2.8 PHYTOPLANKTON PIGMENTS.....	15
2.9 CTD PROFILES.....	15
REFERENCES.....	15
CHAPTER 3.....	17
<i>CHARACTERIZATION OF OCEANOGRAPHIC AND ATMOSPHERIC RADIOMETERS</i>	
3.1 INTRODUCTION.....	17
3.2 RADIOMETRIC RESPONSIVITY CALIBRATION.....	17
<i>Spectral Irradiance Calibrations</i>	19
<i>Spectral Radiance Calibrations</i>	22
3.3 PORTABLE STANDARDS.....	24
3.4 SPECTRAL BANDPASS CHARACTERIZATION.....	24
<i>Spectral Stray Light Characterization Using LASER-Illuminated Integrating Sphere Sources</i>	25
3.5 IMMERSION FACTORS.....	26
<i>Irradiance Sensor Immersion Factors</i>	26
<i>Radiance Immersion Factors</i>	28
3.6 RADIANCE FIELD-OF-VIEW.....	28
3.7 COLLECTOR COSINE RESPONSE.....	29
3.8 LINEARITY AND ELECTRONIC UNCERTAINTY.....	31
3.9 TEMPORAL RESPONSE.....	31
3.10 TEMPERATURE CHARACTERIZATION.....	31

3.11 PRESSURE EFFECTS	32
3.12 PRESSURE TRANSDUCER CALIBRATION	32
3.13 POLARIZATION SENSITIVITY	32
REFERENCES	32
CHAPTER 4.....	34
<i>CALIBRATION OF SUN PHOTOMETERS AND SKY RADIANCE SENSORS</i>	
4.1 INTRODUCTION	34
4.2 CALIBRATION TECHNIQUES FOR SUN PHOTOMETERS	35
<i>Langley – Bouguer Technique.....</i>	35
<i>Uncertainty of the Langley – Bouguer Technique.....</i>	36
<i>Cross-Calibration Technique.....</i>	37
<i>Accuracy and Limitations of the Cross Calibration Technique</i>	38
4.3 CALIBRATION TECHNIQUES FOR SKY RADIOMETERS	40
<i>Calibration of Unpolarized Sky Radiometers.....</i>	40
<i>Uncertainty of the Calibration of Unpolarized Sky Radiometers.....</i>	40
<i>Calibration of Polarized Sky Radiometers.....</i>	40
<i>Calibration and Characterization of Sky Radiance Distribution Cameras.....</i>	43
4.4 CALIBRATION OF SHADOW-BAND IRRADIANCE RADIOMETER.....	44
<i>Calibration of Instrument Circuitry and Temperature Stabilization of the Detector.....</i>	44
<i>Determination of the Extra-terrestrial Constants</i>	44
<i>Uncertainty of the Calibration of Shadow-Band Irradiance Radiometers</i>	45
REFERENCES	45
CHAPTER 5.....	49
<i>STABILITY MONITORING OF FIELD RADIOMETERS USING PORTABLE SOURCES</i>	
5.1 INTRODUCTION	49
5.2 THE SQM.....	49
5.3 OCS-5002	51
5.4 SQM-II	51
5.5 METHODOLOGY	52
5.6 DATA ANALYSIS	53
5.7 FUTURE APPLICATIONS	55
REFERENCES	56

Chapter 1

Instrument Specifications, Characterization and Calibration Overview

James L. Mueller

Center for Hydro-Optics and Remote Sensing, San Diego State University, California

1.1 INTRODUCTION

A central focus of the SIMBIOS program, and of independent validation activities in the SeaWiFS and other ocean color sensor projects, is the estimation of uncertainties in satellite determinations of normalized water-leaving radiance (or equivalently, normalized remote-sensing reflectance), atmospheric correction and bio-optical algorithms, and derived products. In most cases, statistical comparisons with *in situ* measurements – or quantities derived from *in situ* measurements – play a central role in estimating the uncertainties in the satellite ocean color measurements, algorithms and derived products. The uncertainty budgets of *in situ* measurements used for comparisons are obvious critical factors in such validation analyses, as also are details and uncertainties of critical design and performance characteristics of the instruments with which they are measured.

The chapters of this volume specify appropriate instrument characteristics and describe accepted laboratory procedures for characterizing instruments to determine and verify their compliance with those specifications. Chapter 2 provides a comprehensive specification of instrument performance characteristics required to meet the measurement uncertainties specified in Volume I. Detailed characterization and calibration protocols for radiometers and sun photometers are provided in Chapters 3 through 5. The status of each of these chapters, and topic areas in each where future advances and/or changes may be appropriate, are discussed briefly in sections 1.2 through 1.5. As is explained in Section 1.6, the calibration of IOP sensors is covered in Volume IV, rather than in the present volume. The protocol document does not provide detailed methods for calibrating meteorological sensors, CTD instruments, pressure transducers, and other ancillary sensors. Sections 1.7 through 1.9 emphasize the importance of using properly calibrated sensors to make these important supporting measurements, but a well-established infrastructure for these calibration services exists within the general oceanographic and atmospheric communities.

1.2 INSTRUMENT PERFORMANCE SPECIFICATIONS

Chapter 2 provides detailed specifications for performance-related characteristics of radiometers, and other types of instruments, that measure *in situ* variables used to validate satellite ocean color sensors, algorithms and derived products. The specifications in this revision (4.0) to the protocols are unchanged from those in Revision 3 (Mueller and Fargion 2002). Discussions with interested members of the community have not led to suggestions for any significant changes or additions.

1.3 CHARACTERIZATION OF OCEANOGRAPHIC AND ATMOSPHERIC RADIOMETERS

The procedures given here in Chapter 3 are essentially those from Mueller and Austin (1995). Changes and additions primarily reflect results and lessons learned from the SeaWiFS Intercomparison Round-Robin Experiment (SIRREX) series (e.g. Mueller *et al.* 1996; Johnson *et al.* 1996) and deal primarily with methods for transferring the NIST scale of spectral irradiance from an FEL lamp source to the responsivity scales of oceanographic and atmospheric radiometers. The SIMBIOS and SeaWiFS Project Offices are continuing the SIRREX, now SIMBIOS Radiometric Intercalibration (SIMRIC), series to assure maintenance of consistent radiometric calibration uncertainties throughout the community (Riley and Bailey 1998; Meister *et al.* 2002) and for better determination of, e.g., quantitative uncertainties associated with radiance calibrations using Spectralon plaques Hooker *et al.* 2002).

The Chapter 3 protocols recommend experimental determination of immersion factors for every individual underwater irradiance collector. In Mueller and Austin (1995), it was suggested that immersion factors determined for a prototype irradiance collector could be used for other radiance collectors of the same size, design and material specifications. The results of Mueller (1995) demonstrated that individual deviations between collectors of the same design, size and materials may be as large as 8 %, with a 3 % Root-Mean-Square (RMS) uncertainty for the group of such instruments tested. Using replicated tests and variations in setup configuration for each instrument tested, the experimental uncertainty associated with the immersion factor characterization procedure was shown to be less than 1 % (Mueller 1995). Recent experiments using an independent sample of radiometers, and including immersion tests replicated both within and between three laboratories (Zibordi *et al.* 2002), further confirmed the need to experimentally determine the spectral irradiance immersion factors for each instrument individually. The radiometers tested by Zibordi *et al.* (2002) are of a different design configuration and from a different manufacturer than those tested by Mueller (1995).

Topic areas in Chapter 3 that should be reviewed and considered for possible inclusion in future revisions:

1. Methods for applying to ocean radiometers (K. Carder and R. Steward, pers. comm.) the sun-based methods used in the atmospheric radiation community for calibrating sun photometers (Volume II, Chapter 4; Schmid *et al.* 1998) and other radiometers (Biggar 1998). In this regard, the question of continuing to use the Neckel and Labs (1984) $\bar{F}_o(\lambda)$ spectrum, or an alternative such as that of Thuillier *et al.* (1998), will become critically important (see the discussion in Volume I, Chapter 2).
2. Uncertainty budgets associated with the use of Spectralon reflectance plaques for calibrating radiance sensors continue to be inadequately understood, a difficulty noted during the last SIMRIC exercise (Meister *et al.* 2002). Recent experimental comparisons of several plaques (Hooker *et al.* 2002) provide anecdotal estimates of such uncertainty budgets, and have demonstrated the important effects of nonuniform illumination across a plaque by an FEL lamp. At this stage, however, a comprehensive treatment has yet to be completed.
3. A general protocol is needed giving improved methods for characterizing stray-light, spectral calibration, and slit responses in monochromator based hyperspectral spectrometers, which are increasingly being adopted and used within the ocean color research community. The innovative recent application, by NIST, of integrating-sphere sources illuminated by tunable LASERs to characterize stray light responses of the MOBY spectrographs represents a major advance (Volume VI, Chapters 2 and 5). It should be possible to develop a generalized stray-light characterization protocol within the next few years.

1.4 CALIBRATION OF SUN PHOTOMETERS AND SKY RADIANCE SENSORS

Chapter 4 is a reformatted version of Chapter 7 in Revision 3 (Mueller and Fargion 2002). The Chapter 4 protocols are based on the methods developed within the atmospheric radiation community, and by the AERONET Project at GSFC and its collaborating institutions around the world. Protocols for calibrating Shadowband Radiometers are presented here also. There is some overlap between Chapters 3 and 4, but the redundancies are not a serious drawback.

1.5 STABILITY MONITORING OF FIELD RADIOMETERS USING PORTABLE SOURCES

Mueller and Austin (1995) recommended the development and use of portable standards to verify the stability of radiometers during deployment on research cruises, or other field deployments, of several weeks duration. These general recommendations were based on limited experience with prototype analog sources developed by Austin and his colleagues in the 1980's at the Scripps Visibility Laboratory. Since 1995, joint research by investigators at NIST and GSFC developed a much-improved prototype of a portable source, the SeaWiFS Quality Monitor (SQM), suitable for shipboard use (Johnson *et al.* 1998) and demonstrated its ability to verify stability of radiometers with an uncertainty < 1 % (Hooker and Aiken 1998). Subsequently, less expensive versions of the SQM have been developed and become commercially available. Chapter 5 [formerly Chapter 8 in Revision 3 (Mueller and Fargion

2002)] provides a review of this development, detailed protocols for using SQM devices in the field, and uncertainty budgets.

1.6 CALIBRATION OF INHERENT OPTICAL PROPERTY SENSORS

Calibration of instruments used to measure Inherent Optical Properties (IOP) is covered in Volume IV, rather than here in Volume II. To obtain reliable IOP measurements, several currently used instruments require frequent, typically daily, recalibration during use at sea. In these circumstances, the calibration of the instrument becomes an intrinsic part of the field measurement methods and the protocols for calibration and measurement are best presented together.

1.7 CALIBRATION OF METEOROLOGICAL SENSORS

The uncertainties of several meteorological variables are significant components of uncertainty budgets associated with using *in situ* measurements to validate satellite ocean color measurements and algorithms. Uncertainty in barometric pressure can affect that of absorption terms in atmospheric correction algorithms. Uncertainty in surface wind velocity directly affects sun and sky glint reflection estimates used to correct water-leaving radiance determinations from satellites and *in situ* above-water radiometers. Anemometers, barometers, thermometers (air temperature), and hygrometers should be calibrated using methods and at intervals recommended by the World Meteorological Organization (WMO). Calibration services and certification are available through the vendors who supply meteorological instruments, and in the laboratories of some academic oceanographic and/or atmospheric institutions.

1.8 CTD CALIBRATION

The conductivity probe, temperature probe, and pressure transducer of the CTD should be recalibrated before and after each major cruise by a properly equipped physical oceanographic laboratory, including those maintained by many university oceanography departments and CTD manufacturers. In addition, the conductivity probe should be independently calibrated during the course of each cruise by obtaining salinity water samples simultaneous with CTD readings. These salinity samples are to be analyzed, either at sea or ashore, with a laboratory salinometer calibrated with International Association for the Physical Sciences of the Ocean (IAPSO) Standard Seawater.

1.9 PRESSURE TRANSDUCER CALIBRATIONS

It is important to frequently calibrate pressure transducers on oceanographic profiling instruments. For purposes of these protocols, the pressure in decibars is equivalent to depth in meters. Adjustments for the density of seawater are negligible in the present context. On the other hand, inaccurate calibration of the pressure sensor will lead to artifacts and increased uncertainty in, *e.g.*, the computation of the diffuse attenuation coefficients $K(z, \lambda)$. If an instrument's pressure transducer port is equipped with a threaded fitting, a hose filled with distilled water may be used to connect it to a hand-pump and NIST traceable dead weight tester (several models are commercially available). Another common arrangement is to immerse the instrument in a pressure chamber, which is connected in turn to the pump and pressure calibration device. In either case, water pressure is increased in steps to produce several readings spanning the operating range of the instrument under test, and a polynomial equation is fit to the data to relate transducer output to the pressures measured with the dead-weight tester. Detailed methods and a certificate of NIST traceable calibration should be obtained from the manufacturer of the pressure calibration device. Calibration services of this type are readily available, on a fee-for-service basis, at laboratories maintained by many oceanography departments and commercial vendors of oceanographic equipment.

If simultaneous deployment of the CTD with optical instruments having independent pressure transducers is practical, the two depths measured by the different instruments should be compared over the range of the cast. If depth measurements disagree significantly, these comparisons may be used to correct whichever transducer is found to be in error through analysis of pre- and post-cruise pressure transducer calibrations.

REFERENCES

- Biggar, S.F. 1998: Calibration of a visible and near-infrared portable transfer radiometer. *Metrologia*, **35**: 701-706.
- Hooker, S.B. and J. Aiken, 1998: Calibration evaluation and radiometric testing of field radiometers with the SQM. *J. Atmos. Oceanic Tech.*, **15**: 995-1007.
- Hooker, S.B., S. McLean, J. Sherman, M. Small, G. Lazin, G. Zibordi and J.W. Brown, 2002. The Seventh SeaWiFS Intercalibration Round-Robin Experiment (SIRREX-7), March 1999. *NASA Tech. Memo. 2002-206892, Vol. 17*. S.B. Hooker and E.R. Firestone [Eds.], NASA Goddard Space Flight Center, Greenbelt, MD. 69pp.
- Johnson, B.C., S.S. Bruce, E.A. Early, J.M. Houston, T.R. O'Brian, A. Thompson, S.B. Hooker and J.L. Mueller, 1996: The Forth SeaWiFS Intercalibration Round-Robin Experiment (SIRREX-4), May 1995. *NASA Tech. Memo. 104566, Vol. 37*, S.B. Hooker, E.R. Firestone and J.G. Acker, Eds., NASA GSFC, Greenbelt, Maryland, 65pp.
- Johnson, B.C., P-S. Shaw, S.B. Hooker and D. Lynch, 1998: Radiometric and engineering performance of the SeaWiFS Quality Monitor (SQM): a portable light source for field radiometers. *J. Atmos. Oceanic Tech.*, **15**: 1008-1022.
- Meister, G., P. Abel, R. Barnes, J. Cooper, C. Davis, M. Godin, D. Goebel, G. Fargion, R. Frouin, D. Korwan, R. Maffione, C. McClain, S. McLean, D. Menzies, A. Poteau, J. Robertson, and J. Sherman, 2002. The First SIMBIOS Radiometric Intercomparison (SIMRIC-1), April-September 2001. *NASA Tech. Memo. 2002-206892*, NASA Goddard Space Flight Center, Greenbelt, MD. 60pp.
- Mueller, J.L., 1995: Comparison of irradiance immersion coefficients for several marine environmental radiometers (MERs), In: Mueller, J.L. and others, Case Studies for SeaWiFS Calibration and Validation, Part 3. *NASA TM 104566, Vol. 27*: 3-15, Hooker, S.B., E.R. Firestone and J.G. Acker, Eds.
- Mueller, J.L., and R.W. Austin, 1995: Ocean Optics Protocols for SeaWiFS Validation, Revision 1. *NASA Tech. Memo. 104566, Vol. 25*, S.B. Hooker, E.R. Firestone and J.G. Acker, Eds., NASA GSFC, Greenbelt, Maryland, 67 pp.
- Mueller, J.L. and G.S. Fargion, 2002: Ocean Optics Protocols for Satellite Ocean Color Sensor Validation, Revision 3, *NASA TM 2002-210004*, NASA Goddard Space Flight Center, Greenbelt, Maryland, 308pp.
- Mueller, J.L., B.C. Johnson, C.L. Cromer, S.B. Hooker, J.T. McLean and S.F. Biggar, 1996: The Third SeaWiFS Intercalibration Round-Robin Experiment (SIRREX-3), 19-30 September 1994. *NASA Tech. Memo. 104566, Vol. 34*, S.B. Hooker, E.R. Firestone and J.G. Acker, Eds., 78 pp.
- Neckel, H., and D. Labs, 1984: The solar radiation between 3,300 and 12,500 AA. *Solar Phys.*, **90**: 205--258.
- Riley, T. and S. Bailey, 1998: The Sixth SeaWiFS Intercalibration Round-Robin Experiment (SIRREX-6) August—December 1997. *NASA/TM-1998-206878*. NASA, Goddard Space Flight Center, Greenbelt, MD. 26pp.
- Schmid, B., P.R. Spyak, S.F. Biggar, C. Wehrli, J. Seider, T. Ingold, C. Matzler and N. Kampfer. 1998: Evaluation of the applicability of solar and lamp radiometric calibrations of a precision Sun photometer operating between 300 and 1025 nm. *Appl. Opt.* **37**: 3923-3941.
- Thuillier, G., M. Herse, P.S. Simon, D. Labs, H. Mandel, D. Gillotay and T. Foujols. 1998: The visible solar spectral irradiance from 350 to 850 nm as measured by the SOLSPEC spectrometer during the Atlas I mission. *Solar Phys.* **177**: 41-61.
- Zibordi, G., D. D'Alimonte, D. van der Linde, J.F. Berton, S.B. Hooker, J.L. Mueller, G. Lazin and S. MacLean, 2002: The Eighth SeaWiFS Intercalibration Round-Robin Experiment (SIRREX-8), September – December 2001. *NASA Tech. Memo. 2002-206892, Vol. 21*, Hooker, S.B. and E.R. Firestone [Eds.], NASA Goddard Space Flight Center, Greenbelt, Maryland, 43pp.

Chapter 2

Instrument Performance Specifications

James L. Mueller and Roswell Austin

Center for Hydro-Optics and Remote Sensing, San Diego State University, California

2.1 INTRODUCTION

This report describes measurements of optical properties, and other variables, necessary for validating data obtained with satellite ocean color instruments, and for the development of in-water and atmospheric algorithms. The specifications herein are those required of instruments used on ships, or other platforms, to acquire that *in situ* data. In some cases, the specifications have been selected to allow use of instruments that are affordable and that either currently exist, or that can be developed without major improvements in today's state-of-the-art technology. In a few cases, new or improved instruments must be developed to realize the specified performance characteristics. The data uncertainty requirements for this program are more severe than those for a general ocean survey. Here, various investigators use a variety of instruments that are calibrated independently at a number of facilities, and contribute data to a common database used to validate SeaWiFS, and other satellite, ocean color measurements. The resulting radiometric and bio-optical database provides an essential means of detecting and quantifying on-orbit changes in the satellite instruments relative to their prelaunch calibrations and characterizations. This chapter specifies instrument characteristics and data uncertainties thought to be necessary, as well as sufficient, for this task. The validation analysis would be significantly degraded should calibration errors or differences of even a few percent, or wavelength errors or differences of a few nanometers, occur in (between) the instruments used to acquire the validation *in situ* bio-optical database.

2.2 IN-WATER RADIOMETERS

This section specifies radiometric characteristics for instruments that are used to measure $E_d(z,\lambda)$, $E_u(z,\lambda)$ and $L_u(z,\lambda)$. The specifications are applicable to filter radiometers and to spectroradiometers based on monochromators. Minimum performance characteristics are specified for spectral resolution, radiometric responsivity and resolution, signal-to-noise ratios (SNRs), radiometric saturation and minimum detectable values, angular response, temporal sampling resolution, linearity, and stability.

Spectral Characteristics

In-water radiometers shall be capable, as a minimum, of making measurements at the wavelengths shown in Table 2.1, which refers specifically to the SeaWiFS channels. The SeaWiFS channel wavelength combination is consistent with the recommended preferred ocean radiance channel combination (C3) recommended by the International Ocean Color Coordinating Group (IOCCG 1998), albeit with wider spectral bandwidths. For the SIMBIOS *in situ* validation database, the wavelength combinations in Table 2.1 must be expanded to provide radiance and irradiance measurements at the greater number of wavelengths represented by the full ensemble of ocean color sensors (Volume VII, Appendix A). For example, OCTS and POLDER each had a channel at 565 nm, rather than that at 555 nm on SeaWiFS. For purposes of these protocols, in-water radiometer channels at these additional wavelengths must match the satellite channel wavelengths and have full-width at half-maximum (FWHM) bandwidths within the same tolerances described below with reference to Table 2.1.

Table 2.1 presumes the use of properly blocked interference filters to provide the required spectral bandpass and out-of-band rejection (10^{-6} or better). Care must also be taken to avoid possible out-of-band leakage due to fluorescence by filter, or other optical component, materials. Filter radiometers should have channels with center wavelengths, as measured in the assembled instrument, matching those given in Table 2.1 to within 1 nm for 410 nm and 443 nm, and within 2 nm for all other spectral bands. Shifts of these magnitudes in center wavelengths will result in changes in measured radiometric values of approximately 1 % or less (R. Booth pers. comm.) and this specification should be met if possible. It is recognized, however, that enforcing a 1 nm hard-and-fast specification could be prohibitively expensive, and this tolerance should be regarded as a goal. With knowledge, to less than

0.2 nm, of the actual center wavelengths and complete spectral response functions, corrections probably can be made to infer effective radiometric quantities for the satellite instrument channels. Bandwidths must be 10 ± 2 nm FWHM. They are made narrower than, for example, the SeaWiFS channels to reduce the skewing of the parameters derived from underwater irradiance, or radiance, profiles in spectral regions where absorption by natural seawater exhibits rapid variation with wavelength.

Table 2.1: Recommended spectral bands for discrete-wavelength filter radiometers using 10nm FWHM bandwidths. In addition, out-of-band blocking in the tails of the instrument response functions should be 10^{-6} or better.

SeaWiFS Band	Wavelengths [nm]	E_d, E_u, L_u [nm]	E_s [nm]
1	402-422	412 ¹	412
2	433-453	443,435 ²	443
3	480-500	490	490
4	500-520	510	510
5	545-565	555	555
6	660-680	665,683	665 ³
7	745-785	⁴	780
8	845-885	⁴	875

1. A preferred option is to replace two separate 10nm FWHM bands centered at 406 and 416 nm with a single 412 nm channel. The two channels would allow more accurate modeling of L_{WN} (412), matching SeaWiFS characteristics.
2. An optional extra band is used to improve modeling of $L_{WN}(\lambda)$ radiances to match the SeaWiFS 443 nm channel.
3. E_s deck, only one channel in this band is necessary.
4. Due to the specialized nature of infrared in-water measurements, specialized sensors will be needed.

To maintain the above tolerances, it is anticipated that filters will be ordered to a center wavelength λ_0 with a tolerance of ± 1 nm and a FWHM bandwidth of 8.5 ± 1 nm. When the filter is installed in a radiometer with a 10° (half-angle) FOV, however, the spectral bandpass will broaden by 2 nm to 3 nm, and the center wavelength will shift. Furthermore, as a filter ages in use, its transmission curve may undergo changes to further broaden the FWHM bandpass and shift the peak. The tolerances specified above include an allowance for some degradation before expensive filter and detector changes must be done. In a single instrument, all channels at a given nominal wavelength should match within 1 nm, if possible. It is desirable, therefore, to obtain all of the filters used by an investigator for measurements at any nominal wavelength (λ_n) from a single manufacturing lot when possible. If this is done, $E_s(\lambda_n)$, $E_d(\lambda_n)$, $E_u(\lambda_n)$, and $L_u(\lambda_n)$, and any atmospheric radiometric quantities measured with that investigator's systems, would all have a greater likelihood of being measured over the same range of wavelengths, for each nominal wavelength (λ_n). In any event, the actual spectral response function of each instrument channel must be measured and known with an uncertainty less than 0.2 nm.

High-resolution monochromator-based spectroradiometers, with adequate sensitivity and stray light rejection characteristics, are also suitable instruments and are recommended for many algorithm development studies. Suitable specifications for such instruments are given in Table 2.2. (These instruments must also meet the specifications summarized in Tables 2.1 and 2.3.)

It is extremely difficult, if not impossible, to optically reject stray light within a single-grating spectrometer at the level specified in Table 2.1. On the other hand, recent capabilities developed at the National Institute of Standards and Technology (NIST) may be used to characterize the spectral stray-light response distribution function of a spectrometer using a set of tunable lasers (Brown *et al.* 2000). Stray light correction algorithms based on NIST characterizations are being developed for application to the Marine Optical Buoy (MOBY) spectrographs (Volume VI, Chapters 2 and 5). This correction is expected to reduce stray light uncertainties well below the level specified in Table 2.2. The tunable laser based stray light characterization procedure is too expensive to apply to every

radiometer used in this program, but its application is essential for key transfer radiometers. The radiometers in the MOBY facility, for example, are used to provide a common vicarious calibration reference for all satellite ocean color sensors embraced within the SIMBIOS program (Volume VI, Chapter 2), and the expense is well justified in this instance.

Table 2.2: Minimum specifications for the characteristics of high-resolution spectroradiometers.

<i>Optical Sensors</i>	
Spectral Range:	380 to 750 / 900 nm
Spectral Resolution:	5 nm (or less FWHM)
Wavelength Accuracy:	10 % FWHM of resolution (0.5 nm)
Wavelength Stability:	5 % FWHM of resolution (0.25 nm)
Signal-to-Noise Ratio:	1,000:1 (at minimum)
Stray Light Rejection:	10^{-6}
Radiometric Accuracy:	3 %
Radiometric Stability:	1 %
FOV Maximum:	10° (for radiance)
Temperature Stability:	Specified for 0–35°C
Linearity:	Correctable to 0.1 %
<i>Ancillary Sensors</i>	
Temperature:	0.2°C
Pressure:	0.1 % (full scale)
Horizontal Inclination:	1° over 40° range

Responsivity, SNR, and Resolution

The expected operating limits for radiometric responsivities, SNR, and digital resolution are specified in Table 2.3, the limits for which were derived as follows:

1. An E_d saturation value of $300 \mu\text{W cm}^{-2} \text{nm}^{-1}$ is assumed at all wavelengths.
2. Implicit, but not stated, in Table 2.3 is that the minimum required $E_d(0)$ is $20 \mu\text{W cm}^{-2} \text{nm}^{-1}$; it will not be appropriate to occupy validation stations when illumination is less than this minimum.
3. The minimum $E_d(0)$ implies a minimum detectable $E_d(z)$ value of $1 \mu\text{W cm}^{-2} \text{nm}^{-1}$ at 3 optical depths (3/K).
4. Digital resolution must be less than or equal to 0.5 % of the reading to maintain a 100:1 SNR. To permit a 1 % uncertainty in absolute calibration, if that goal can be met in the calibration laboratory, the instrument must digitally resolve 0.1 % of the irradiance (radiance) produced by the laboratory standards used; typical irradiance (radiance) values for calibration using 1,000 W FEL standard lamps traceable to the National Institute of Standards and Technology (NIST), and required digital resolutions at these signal levels, are given in Table 2.3 as “Calibration Irradiance” and “Digital Resolution (cal.)”, respectively. A SNR of 100:1 requires a resolution in $E_d(z)$ at three optical depths to $0.005 \mu\text{W cm}^{-2} \text{nm}^{-1}$ per count, i.e., 2.5 digit resolution. At the surface, $E_d(0)$ should be resolved to $0.05 \mu\text{W cm}^{-2} \text{nm}^{-1}$ per count.
5. The Case-1 saturation values of $E_d(0)$ represent the *Instrument Specification Subgroup's* (Mueller and Austin 1992) estimate of maximum reflectances to be expected in ordinary Case-1 waters: 12.5 % at 410 nm, 7.5 % at 488 nm and 0.5 % at 670 nm. These saturation values will be too low for measurements in Case-2 waters, or coccolithophorid blooms. In these situations, a maximum expected reflectance of 40 % for $\lambda < 660 \text{ nm}$ and 20 % for $\lambda \geq 660 \text{ nm}$ is assumed. This implies that the expected maximum irradiance in $E_d(0)$ should be $80 \mu\text{W cm}^{-2} \text{nm}^{-1}$ for $\lambda < 660 \text{ nm}$ and $40 \mu\text{W cm}^{-2} \text{nm}^{-1}$ for $\lambda \geq 660 \text{ nm}$.

6. The minimum required irradiances at three optical depths (as given in Table 2.3) assumes minimum reflectances of 1 % at 410 nm, 2 % at 488 nm, and 0.15 % at 670 nm.
7. The saturation and minimum radiances, and radiance responsivity resolutions, for $L_u(0)$ and $L_u(3/K_d)$ are calculated as $L_u/E_u = Q^{-1}$ times the corresponding specification for $E_u(0)$ or $E_u(z)$. In Mueller and Austin (1995) it was assumed that $Q = 5$, a constant at all wavelengths and depths. Morel and Gentili (1996) showed that Q actually varies between approximately 3.14 and 5 at 410 nm and 488 nm, and between approximately 3.14 and 5.7 at 670 nm (see Volume III, Chapter 4). Saturation radiances, for the extreme minimum case of $Q = 3.14$ (very clear waters with the sun nearly overhead), are increased by a factor of 1.6 at all three wavelengths relative to Mueller and Austin (1995). Minimum radiances at 670 nm, for the extreme maximum case of $Q = 5.7$ (turbid waters and solar zenith angle $> 60^\circ$), are decreased by a factor of 0.75, and the implied digital resolution at 670 nm was changed accordingly. Minimum expected radiances and required digital resolution at 410 nm and 488 nm are unchanged.

The specifications in Table 2.3 are meant as guidance to interpret the following required performance requirements:

1. The instrument must maintain a 100:1 SNR at every operating range encountered, during field measurements.
2. The data for measurements obtained in the field must be recorded with a digital resolution less than or equal to 0.5 % of reading.
3. The dynamic range of the instrument's linear sensitivity must extend to include the signal levels encountered during laboratory calibrations, and the calibration signals must be recorded with a digital resolution of 0.1 % of reading to permit 1 % uncertainty in calibration.

In general, the above performance specifications do not pose exceptionally difficult engineering challenges, with the possible exception of the full dynamic range implied by Case-2 or coccolith saturation radiance $L_u(665)$ to minimum expected $L_u(665)$. In any event, this situation will require specially designed radiometers (see also “*Red and Near-Infrared Wavelengths*” below). It is not necessary that every radiometer used for satellite ocean color sensor validation operate over the full dynamic ranges given in Table 2.3. A radiometer is merely required to maintain the above performance specifications over the dynamic ranges of irradiance and radiance existing at locations and associated illumination conditions where it is used for validation or algorithm development.

Table 2.3: Required instrument and sensitivities for SeaWiFS validation and algorithm development as a function of radiometric measured variable and wavelength.

<i>Property</i>	<i>Variable</i>	410 nm	488 nm	665 nm	<i>Comment</i>
$E_d(z, \lambda)$,	$E_d(0)_{\max}$	300	300	300	Saturation Irradiance
Downwelled	$E_d\left(\frac{3}{K_d}\right)$	1	1	1	Minimum Expected Irradiance
Irradiance	$\frac{dE}{dN}$	5×10^{-3}	5×10^{-3}	5×10^{-3}	Digital Resolution (profiles)
	$\frac{dE}{dN}$	5×10^{-2}	5×10^{-2}	5×10^{-2}	Digital Resolution (surface unit)
$E_u(z, \lambda)$,	$E_u(0)_{\max}$	120	120	60	Saturation Irradiance (Case-2/coccoliths)
Upwelled		37	22	1.5	Saturation Irradiance (Case-1)
Irradiance	$E_u\left(\frac{3}{K_d}\right)$	1×10^{-2}	2×10^{-2}	1.5×10^{-3}	Minimum Expected Irradiance
	$\frac{dE}{dN}$	5×10^{-4}	5×10^{-4}	5×10^{-5}	Digital Resolution (surface unit)
	$\frac{dE}{dN}$	5×10^{-5}	5×10^{-5}	5×10^{-6}	Digital Resolution (profiles)
$L_u(z, \lambda)$,	$L_u(0)_{\max}$	38	38	13	Saturation Radiance (Case-2/coccoliths)
Upwelled		12.0	7.2	0.5	Saturation Radiance (Case-1)
Radiance	$L_u\left(\frac{3}{K_d}\right)$	2×10^{-3}	4×10^{-3}	2.25×10^{-4}	Minimum Expected Radiance
	$\frac{dL}{dN}$	5×10^{-4}	5×10^{-4}	5×10^{-5}	Digital Resolution (surface unit)
	$\frac{dL}{dN}$	5×10^{-5}	5×10^{-5}	1×10^{-6}	Digital Resolution (profiles)
E_{cal} , Source	E_{cal}	2	5	15	Calibration Irradiance
Irradiance	$\frac{dE}{dN}$	2×10^{-3}	5×10^{-3}	1×10^{-2}	Digital Resolution (E_d , E_s , E_u cal.)
L_{cal} , Source	L_{cal}	0.6	1.5	4.5	Calibration Radiance
Radiance	$\frac{dL}{dN}$	6×10^{-4}	1×10^{-3}	4×10^{-3}	Digital Resolution (L_u cal.)

- Notes: 1. E_u and E_d are in units of $\mu\text{W cm}^{-2} \text{nm}^{-1}$ and L_u is in units of $\mu\text{W cm}^{-2} \text{nm}^{-1} \text{sr}^{-1}$.
 2. Responsivity resolution in radiometric units per digital count at the minimum required signal level.
 3. Specified ranges should maintain a 100:1 SNR.

Linearity and Stability

Errors attributable to linearity or stability should be less than 0.5 % of the instrumental readings over the dynamic ranges specified in Table 2.3. This is a challenging goal, but one which must be met if the equally challenging goal of achieving 1 % uncertainty in absolute calibration is to be meaningful.

Sampling Resolution

Sampling frequency should be compatible with the profiling technique being used. For the preferred multispectral filter radiometers and spectroradiometric (dispersion) instruments using array sensors, the minimum sampling frequencies are determined by the profiling rate and the depth resolution required. In general, five or more samples per meter should be obtained at all wavelengths. All channels of $E_d(z,\lambda)$, $E_u(z,\lambda)$ and $L_u(z,\lambda)$ at all wavelengths should be sampled within 10^{-2} s at each given depth. Alternatively, grating spectrometers using detector arrays to sample all channels simultaneously may be integrated for longer periods to achieve necessary signal-to-noise ratios.

The time response of the instrument to a full-scale (saturation to dark) step change in irradiance should be less than one second to arrive at a value within 0.1 %, or one digitizing step, whichever is greater, of steady state. In addition, the electronic e -folding time constant of the instrument must be consistent with the rate at which the channels are sampled, *i.e.*, if data are to be acquired at 10 Hz, the e -folding time constant should be 0.2 s to avoid aliasing. Individual data scans may be averaged to improve signal-to-noise performance, provided adequate depth resolution is maintained.

Angular Response Characteristics

Irradiance: The response of a *cosine collector* to a collimated light source incident at an angle (θ) from the normal must be such that:

1. for $E_u(\lambda)$ measurements, the integrated response to a radiance distribution of the form $L(\lambda, \theta) \propto 1 + 4 \sin \theta$ should vary as $\cos \theta$, within 2 %; and
2. for E_d measurement, the response to a collimated source should vary as $\cos \theta$ within less than 2 % for angles $0 \leq \theta \leq 65^\circ$ and 10 % for angles $65^\circ \leq \theta < 90^\circ$.

Departures from $\cos \theta$ will translate directly to approximately equal errors in E_d in the case of direct sunlight.

Radiance: The in-water FOV for upwelled radiance bands should be approximately 10° (half-angle). The resulting solid angle FOV (approximately 0.1 sr) is large enough to provide reasonable levels of flux, using silicon detectors, yet small enough to resolve the slowly varying (with θ for $\theta < 30^\circ$) field of upwelled radiance. Smaller FOV sensors are appropriate, of course, if all of the other performance specifications are satisfied.

Operating Depth

Instruments used for profiling in clear to moderately turbid Case-1 waters shall be capable of operating to depths of 200m. Depths should be measured with an uncertainty of 0.5 m and a repeatability of 0.2 m for radiometric profiles at visible wavelengths.

Instruments used for profiling in very turbid Case 1 and Case 2 waters require a much lower maximum pressure rating. On the other hand, in these waters it is necessary to resolve depth with an uncertainty < 5 cm, and with a differential uncertainty of approximately 2 cm.

Instrument Attitude

The orientations of the instrument with respect to the vertical shall be within $\pm 10^\circ$, and the attitude shall be measured with orthogonally oriented sensors from 0 - 30° with an uncertainty of $\pm 1^\circ$ in a static mode; it is not intended that this uncertainty be maintained while an instrument is subject to large accelerations induced by surface waves. These data shall be recorded with the radiometric data stream for use as a data quality flag.

Red and Near-Infrared Wavelengths

The fact that red and near-IR channels - *e.g.* SeaWiFS bands 6, 7, and 8 at wavelengths of 665 nm, 780 nm, and 865 nm, respectively - have such short attenuation lengths in water requires that special attention must be paid to these measurements. Problems due to instrument self-shading (Gordon and Ding 1992) and very rapid attenuation of $L_u(z,\lambda)$ must be considered at these wavelengths. Large diameter instruments, and radiometers mounted on large instrument packages, are not adaptable to these measurements.

Suggested procedures for making the measurements are to use either fiber optic probes carrying light back to a remote instrument, or very small single-wavelength discrete instruments. Each of these concepts is adaptable to deployment from a small floating platform. Care must be taken to avoid direct shading by the supporting platform, but at these wavelengths, the large attenuation coefficients of water makes shadowing by objects more than a few meters away irrelevant.

The minimum measurement scheme would be two discrete (10 nm FWHM) channels at 780 nm and 875 nm. Additional channels at 750 nm and 850 nm, or more elaborately, high-resolution spectroradiometry, would be useful in determining the spectral distribution of the upwelling light field in these bands.

These measurements should be performed as part of the standard validation data acquisition, because of their importance in the atmospheric correction algorithms. It is anticipated that in the majority of cases, and particularly in most Case-1 waters, these measurements will show negligible upwelling light. In Case-2 waters, cases of extremely high productivity, or in coccolithophorid blooms, reflectance at these wavelengths may be significant, and these measurements will become very important. When in-water measurements are performed at these wavelengths, the deck cell channels should be expanded to include bands at 750 and 875 nm (Table 2.1).

2.3 SURFACE IRRADIANCE

The spectral irradiance incident at the ocean surface shall be measured at wavelengths that correspond to the SeaWiFS spectral bands (Table 2.1), but with 10 nm FWHM bandwidth. A total radiation pyrometer may provide helpful ancillary information, but this is not a required instrument. Instruments mounted aboard ships must be positioned to view the sky with minimum obstruction or reflections from the ship's superstructure, antennas, etc. Particular care must be taken to prevent sun shadows from antennas falling on the irradiance-collecting surface. Gimbal mounting of the deck sensor may be helpful to keep the surface of the sensor horizontal. Improperly designed gimbal systems, however, can accentuate fluctuations caused by ship motion, and if there is obvious oscillation in the measured irradiance, the gimbal mechanism should be improved to eliminate the problem.

An intuitively attractive technique, which was suggested in previous versions of the optics protocols (Mueller and Austin 1992, 1995), would be to measure irradiance with a sensor floated a fraction of a meter below the sea surface, far enough away from the ship to avoid ship shadows. The flotation assembly would be designed to avoid shadowing the radiometric FOV and to damp wave-induced motions. This type of arrangement has an additional potential for supporting a small sensor to also measure upwelling radiance, $L_u(z,\lambda)$, just below the surface. Over the past several years, however, the ocean color community has gained experience with this approach, and has encountered consistent and significant difficulties due to wave-induced fluctuations in near-surface E_d . Zaneveld *et al.* (2001) compare theoretical characteristics of the effects of surface waves on near surface irradiance with examples of such measurements under low wind speed conditions. In the case of coherent surface waves, these effects become more pronounced and do not average linearly over time (Zaneveld, personal communication). The in-water reference radiometer method is no longer recommended for determining either $E_d(0^-, \lambda)$ or $E_s(\lambda)$. An acceptable variant of the approach is to use a similar flotation assembly, tethered to allow the instrument to drift away from the ship, but with the irradiance collector raised 50 to 100 cm above the sea surface to measure $E_s(\lambda)$ in air.

Surface Radiometer Characteristics

The specified number of channels and spectral characteristics of deck cells are the same as those for subsurface irradiance measurements as shown in Table 2.1, augmented as necessary for validation of satellite sensors other than SeaWiFS (Volume VII, Appendix A). Saturation irradiances are the same as for $E_d(\lambda)$ (Table 2.3). The dynamic operating range for these sensors needs to only be 25 db, with a SNR of 100:1, but it must include the nominal

calibration irradiance (Table 2.3). Linearity must be within $\pm 5\%$. Sampling frequency should match the frequency of the underwater radiometer, which should be 1 Hz or faster, and all wavelengths should be sampled within an interval less than or equal to 10^{-2} s. Cosine response characteristics should give relative responsivity to a collimated source (in air) which matches $\cos\theta$ within 2 % for $0 \leq \theta \leq 65^\circ$, and within 10 % for $65^\circ \leq \theta < 90^\circ$.

For some oceanographic process studies, it may be acceptable to use a radiometer measuring $E_s(\lambda)$ at only a single wavelength. If only a single channel deck radiometer is available, its spectral characteristic should closely match one of channels 2 through 5 (Table 2.1) with a 10 nm FWHM bandwidth. A broadband, or photosynthetically available radiation (PAR), radiometer should never be used for this purpose.

2.4 ABOVE-WATER RADIOMETRY

The performance characteristics to be specified for an above-water ocean color radiometer will vary, depending on how a particular instrument is to be employed in satellite ocean color sensor validation experiments. For radiometric comparisons with, *e.g.*, SeaWiFS and in-water measurements, the fundamental criterion to be met is that estimates of normalized spectral water-leaving radiance derived from shipboard or airborne measurements must have the same uncertainty specified for those derived from in-water measurements of $L_u(z, \lambda)$ (Table 2.3). A less accurate radiometer may be used to semi-quantitatively characterize spatial variability near ship stations.

In general, the spectral characteristics of above-water radiometers should match those specified for $L_u(\lambda)$ in Table 2.1. In some cases, however, it may be acceptable for a radiometer to match the SeaWiFS – or other sensor - specifications, which specify center wavelength within 2 nm and 20 nm FWHM bandwidth. Recalling the sensitivity of solar radiometry to the exact center wavelength and detailed spectral response function (Section 2.1), any use of airborne radiometers must quantitatively account for the different spectral responsivity functions between measurements of radiance by, *e.g.*, SeaWiFS, in-water radiometers, and above-water radiometers at each channel's nominal center wavelength.

A high-altitude imaging radiometer must have a radiometric uncertainty and SNR in all channels equal to those of the satellite ocean color instrument if its imagery is to be used for direct radiometric verification of the satellite sensor's radiometric performance. In some cases, the requisite SNR may be realized through pixel averaging to a 1 km spatial resolution commensurate with that of, *e.g.*, SeaWiFS. Direct radiometric comparisons between aircraft and SeaWiFS radiances, however, also require that the different atmospheric path effects be carefully modeled, and that the uncertainty in those modeled adjustments be independently estimated. This can be done most effectively when the aircraft measurements are combined with the full suite of shipboard in-water, atmospheric, and ancillary measurements (Volume I, Chapter 3, Table 3.1). In this case, direct comparisons between aircraft and ship radiometry may require that both the SNR and the uncertainties realized in combined analyses of the two data sets will represent a smaller spatial resolution than the nominal 1 km instantaneous field-of-view (IFOV) for SeaWiFS and other satellite sensors. Finally, the viewing zenith and azimuth angles at the matched pixel must also be nearly the same for both sensors, if uncertainties associated with modeled corrections for the ocean's surface and internal bidirectional reflectance distribution function (BRDF) are to be minimized (Volume III, Chapters 3 and 4).

Performance characteristic specifications are similar for ocean color radiometers used to measure water-leaving radiance from either the deck of a ship or an aircraft flown at low altitude, *i.e.*, 200m altitude or lower. Radiometric characteristics should match the criterion set forth for in-water $L_u(\lambda)$ radiometers in Section 2.1 and Tables 2-1 through 2-3. The instrument FOV should be between 5° and 10° (full angle), and all wavelengths must be coregistered within 10 % of the IFOV. All channels must be scanned simultaneously, or within less than 10^{-2} s (depending on the digitizing design), to avoid aliasing due to varying wave reflectance in shipboard measurements, and to avoid time-space aliasing in airborne measurements. This constraint precludes use of filter wheel radiometers and others which scan channels sequentially over a time interval greater than 10^{-2} s. Sampling over longer periods of time may be done by either electronic integration of all channels simultaneously, or by averaging multiple scans.

A radiometer's sensitivity to the polarization of aperture radiance is critical for ocean color remote sensing applications. Polarization sensitivity is likely to be present in any radiometer having mirrors, prisms or gratings in its optical path. To measure accurate water-leaving radiances using instruments of these types, it is necessary to depolarize aperture radiance using either fiber optics or a *pseudo-depolarizer*. Shipboard and airborne ocean color radiometers must have a polarization sensitivity of less than 2 % in all channels. The sole exception to this rule will occur in the case of instruments designed to actually measure the polarization components of aperture radiance, *e.g.*

the polarization channels of the French Polarization and Directionality of the Earth's Reflectances (POLDER) instrument and of the hand-held SIMBAD radiometers.

Each application of a particular above-water radiometer system, if it is proposed for satellite ocean color sensor validation, must be evaluated on its own merits. The instrument's responsivity, uncertainty, stability, FOV, and spectral characteristics must be evaluated in the context of the models to be used to compare its radiance measurements to in-water, or *e.g.* SeaWiFS, radiance measurements. The suitability of spatial averaging to improve SNRs must be evaluated in terms of the spatial variability prevailing in the experiment site, particularly when in-water and aircraft radiances are to be directly compared. Finer resolution aircraft imagery, or low-altitude trackline data, will often be essential for determining the validity of attempts to directly compare in-water and, *e.g.*, SeaWiFS radiances measured at a particular site.

In summary, airborne and shipboard above-water radiometry can obviously contribute valuable data for validating the radiometric performance of satellite ocean color instruments and the algorithms employed with their data. There is, however, a wide possible range of radiometer characteristics that can be applied to this program, and detailed specification of required characteristics can only be done in the context of each particular experiment's design. Only the guiding principals and desired end-to-end performance are specified here.

2.5 INHERENT OPTICAL PROPERTY INSTRUMENTS

The primary Inherent Optical Properties (IOP) are:

1. the beam attenuation coefficient, $c(z, \lambda)$, in units of m^{-1} ;
2. the absorption coefficient, $a(z, \lambda)$, in units of m^{-1} ; and
3. the volume scattering function, $\beta(z, \lambda, \Psi)$, in units of $\text{m}^{-1} \text{sr}^{-1}$, describing the distribution of photons scattered from an incident (path) direction (θ_o, ϕ_o) through an angle Ψ .

These quantities are defined in greater detail in Volume I, Chapter 2 and in Volume IV.

The integral of the volume scattering function over 4π sr is the total scattering coefficient, $b(z, \lambda)$, with units of m^{-1} . The integral of the volume scattering function over the back hemisphere is the backscattering coefficient, $b_b(z, \lambda)$, with units of m^{-1} .

It is possible to measure vertical profiles of $a(z, \lambda)$ and $c(z, \lambda)$ *in situ*. Instruments for making these measurements should, at a minimum, have the characteristics given in Table 2.4. In the case of beam attenuation coefficients, the requirements for uncertainty and precision correspond to changes in $c(\lambda)$ resulting from changes in concentration of approximately 5 and 2 $\mu\text{g L}^{-1}$ of suspended mass, respectively. Stability should be tested with instruments connected to the data acquisition system. Stability between successive calibrations should be better than 0.005 m^{-1} .

Dual path (reflective tube and open path) instruments for measuring $a(z, \lambda)$ and $c(z, \lambda)$ *in situ* are commercially available, meet the specifications of Table 2.4 for SeaWiFS wavelengths, and have found widespread use in the ocean optics and color communities. In some cases, two such instruments are mounted together, one having a 0.2 μm filter attached to the water inlet port. The filtered input instrument measures absorption and beam attenuation by dissolved substances, which allows the total absorption and attenuation measured by the unfiltered instrument to be partitioned into dissolved and particulate components. Hyperspectral resolution (<10 nm) instruments of this type are also commercially available, but the community has not yet established that the performance characteristics of these more sophisticated underwater spectrophotometers reliably meet the specifications of Table 2.4.

Table 2.4: Minimum instrument characteristics for measuring spectral absorption & attenuation coefficients.

Instrument Characteristics	
Spectral Resolution:	410, 443, 490, 510, 555 & 670 nm
Bandwidth:	10 nm
Uncertainty:	0.005 m ⁻¹
Precision for $\lambda < 650$ nm:	0.002 m ⁻¹
Precision for $\lambda \geq 650$ nm:	0.005 m ⁻¹
Stability with Temperature:	0.005 m ⁻¹ over 0–25° C
Sampling Interval:	≥ 4 samples m ⁻¹
Source Collimation Angle:	≤ 5 mrad
Detector Acceptance Angle:	≤ 20 mrad
Depth Capability:	200 m

The spectral total scattering coefficient cannot be measured directly. It can be obtained from $b(\lambda) = c(\lambda) - a(\lambda)$, with an uncertainty equal to the quadrature sum of the uncertainties in those measurements.

Using commercially available instruments, it is also possible to measure photons scattered at one or more fixed angles in the backward direction, and to estimate from this measurement $b_b(\lambda)$ *in situ*. The spectral backscattering coefficient, $b_b(\lambda)$ has the same requirements for spectral resolution, bandwidth, and linearity as $a(\lambda)$ and $c(\lambda)$ (Table 2.4). Since $b_b(\lambda)$ is not a transmission-like measurement, however, the uncertainty of its determination will be approximately 10 %.

The shape of the volume scattering function (VSF), $\beta(z, \lambda, \Psi)$, has until recently been determined *in situ* only crudely with devices like the ALPHA and Scattering Meter (ALSCAT) and the General Angle Scattering Meter (GASM), which were built more than two decades ago at the Visibility Laboratory of the Scripps Institution of Oceanography. These are single angle measurement devices, which must be scanned as a function of angle and wavelength. Because measuring scattering with these old instruments is a slow process, they do not lend themselves readily to incorporation into other instrument platforms. Recently developed new instruments, designed to measure the full VSF with modernized optical and electronic components, show considerable promise (*e.g.* Mobley *et al.* 2001). Protocols defining more detailed VSF measurement and analysis procedures are presented in Volume IV, Chapter 5.

2.6 ATMOSPHERIC AEROSOLS

Sun photometers should be used to measure atmospheric aerosol optical thickness. These sun photometers should have specifications in agreement with (or exceeding) the World Meteorological Organization (WMO) sun photometer specifications (Frohlich 1979). Specifically, the instruments should have a 2° FOV, temperature stabilization, and a precision of ± 0.01 %. The specific wavelengths of channels should correspond to the recommended WMO wavelengths of 380 nm, 500 nm, 675 nm, 778 nm, and 862 nm. Additional wavelengths corresponding to the SeaWiFS (Table 2.1), or other satellite ocean color sensors (Appendix A), channel combinations may be desirable in some applications, but they are not required for the SIMBIOS validation database. More detailed specifications associated with specific photometers are given in Volume II Chapter 4 and Volume III Chapter 5.

2.7 SPECTRAL SKY RADIANCE

Measurements of spectral sky radiance distribution should be made using a photoelectric all-sky camera. Spectral characteristics of the sky radiance camera channels are those specified for $E_s(\lambda)$ (Table 2.1). Data should be in a format such that absolute radiance values can be obtained with an uncertainty of 5 % and sky irradiance can be determined from integrals of the data to within 10 %. If the dynamic range of the camera is insufficient to capture both the sun and sky distribution, neutral density filters (or some other method) should be used so that radiance from both the sun and sky can be measured.

Alternatively, sky radiance distributions are determined using radiometers that are mechanically scanned through the solar principal plane. More detailed specifications for these instruments are described in Volume II Chapter 4 and Volume III Chapter 5.

2.8 PHYTOPLANKTON PIGMENTS

HPLC equipment and associated standards must conform to protocols specified in Volume V, Chapter 2. Bench fluorometers used to measure chlorophyll *a* concentration must conform to protocols specified in Volume V, Chapter 3. *In situ* fluorometers should resolve chlorophyll *a* concentration to 0.001 mg m^{-3} , or better.

2.9 CTD PROFILES

A calibrated CTD system should be used to make profiles of Conductivity, Temperature and Depth to maximum depths between 200 m and 500 m. The instrument should meet the minimum specifications given in Table 2.5.

Table 2.5: The minimum instrument characteristics for the measurement of hydrographic profiles.

<i>Parameter</i>	<i>Range</i>	<i>Uncertainty</i>	<i>Resolution</i>
Pressure [dbars]	0–500	0.3 %	0.005 %
Temperature [°C]	–2– 35	0.015° C	0.001° C
Salinity [PSU]	1– 45	0.03 PSU	0.001 PSU

REFERENCES

- Brown, S.W., G.P. Eppeldauer and K.R. Lykke, 2000: NIST facility for spectral irradiance and radiance response calibrations with a uniform source. *Metrologia*, **37**: 579-589.
- Frohlich, C., 1979: WMO/PMOD Sun photometer: instructions for manufacture. *World Meteor. Org.*, Geneva, Switzerland, 3 pp., (plus tables and drawings).
- Gordon, H.R., and K. Ding, 1992: Self shading of in-water optical instruments. *Limnol. Oceanogr.*, **37**, 491--500.
- IOCCG 1998. Minimum Requirements for an Operational Ocean-Colour Sensor for the Open Ocean. *Reports of the International Ocean-Colour Coordinating Group, No. 1*, IOCCG, Dartmouth Canada, 46pp.
- Mobley, C.D., L.K. Sundman and E. Boss, 2001: Phase function effects on oceanic light fields. *Appl Opt.*, (In press).
- Morel, A. and B. Gentili, 1996. Diffuse reflectance of oceanic waters. III. Implication of bidirectionality for the remote-sensing problem.

- Mueller, J.L., and R.W. Austin, 1992: Ocean Optics Protocols for SeaWiFS Validation. *NASA Tech. Memo. 104566, Vol. 5*, S.B. Hooker and E.R. Firestone, Eds., NASA Goddard Space Flight Center, Greenbelt, Maryland, 43 pp.
- Mueller, J.L., and R.W. Austin, 1995: Ocean Optics Protocols for SeaWiFS Validation, Revision 1. *NASA Tech. Memo. 104566, Vol. 25*, S.B. Hooker and E.R. Firestone, Eds., NASA Goddard Space Flight Center, Greenbelt, Maryland, 66 pp.
- Zaneveld, J.R.V., E. Boss and A. Barnard, 2001. Influence of surface waves on measured and modeled irradiance profiles. *Appl. Opt.*, **40**(9): 1442-1449.

Chapter 3

Characterization of Oceanographic and Atmospheric Radiometers

James L. Mueller and Roswell Austin

Center for Hydro-Optics and Remote Sensing, San Diego State University, California

3.1 INTRODUCTION

Presented in this chapter are procedures for characterizing environmental radiometers, including special characteristics of underwater radiometers, to verify compliance with the specifications of Volume II, Chapter 2. The characterization of any radiometer used to acquire field data for Sensor Intercomparison for Marine Biology and Interdisciplinary Oceanic Studies (SIMBIOS) validation and algorithm development purposes shall include the determination of those instrument characteristics that affect its calibration as used in the field environment. These characteristics include a sensor's:

1. spectral irradiance, or radiance, responsivity calibration, traceable to National Institute of Standards and Technology (NIST) standards;
2. spectral response functions (bandpass) of the various measurement channels;
3. spectral, out-of-band stray light sensitivity;
4. effects on responsivity caused by water immersion;
5. angular response sensitivities in the medium, i.e., air or water, in which it is to be used;
6. the temporal response of the system; and
7. the effects of temperature and pressure on the above characteristics.

The elements of radiometer characterization and calibration are outlined schematically in Figure 3.1. For any instrument to provide suitable data for SIMBIOS and Sea-viewing Wide Field-of-view Sensor (SeaWiFS) applications, the investigator must be certain that the instrument characterization has not changed beyond accepted limits and that the time history of the calibration is traceable. Certain attributes, such as a sensor's angular response characteristics, are sufficiently constant that they only need to be determined once, unless the instrument is modified. The exact nature of instrument modifications during maintenance will determine which characterization procedures must be repeated. When practical, on the other hand, radiometric calibrations and the assessment of system spectral characteristics of filter radiometers should be repeated before and after each major field deployment.

3.2 RADIOMETRIC RESPONSIVITY CALIBRATION

Determination of the absolute radiometric responses of the irradiance and radiance sensors requires the availability of a properly manned and equipped radiometric calibration facility. Such a facility must be equipped with suitable stable sources and radiometric scale transfer sensors, e.g., lamp standards of spectral irradiance and NIST calibrated transfer radiometers, respectively. The sources and transfer sensors must have defined spectral radiometric characteristics that are traceable to NIST. The calibration facility must also have a variety of specialized radiometric and electronic equipment, including: reflectance plaques, spectral filters, integrating spheres, and highly regulated power supplies for the operation of the lamps. Precision electronic measurement capabilities are also required, both for setting and monitoring lamp current and voltage and for measuring the output of the radiometer.

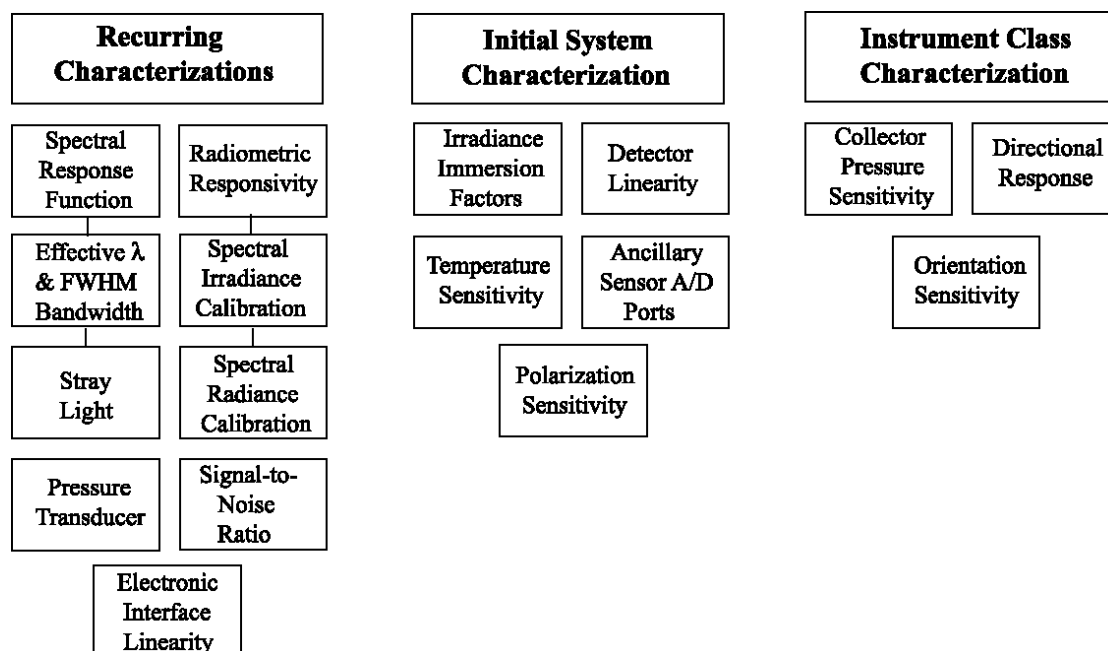


Figure 3.1: Elements of radiometer characterization and calibration.

It is not expected that every investigator will be able to independently perform radiometric calibrations. Instrument manufacturers and a few university laboratories are equipped and staffed to perform these calibrations for the ocean color research community. These facilities will perform frequent intercomparisons to assure the maintenance of the radiometric traceability to the NIST standard of spectral irradiance. The goal shall be to provide reproducible calibrations from 400 nm to 850 nm with 1 % uncertainty; the minimum requirement for radiometric data to be used in satellite ocean color sensor validation is for repeatable calibrations within less than 5 % (Volume I, Chapter 1).

This section describes sources and methods by which the NIST scale of spectral irradiance is transferred to calibrate irradiance and radiance sensors. The principal working standards used for spectral irradiance responsivity calibrations are FEL-type lamps¹ having assigned scales of spectral irradiance that have been transferred directly, or indirectly via secondary standards, from the scales of radiometric standards maintained by NIST. The spectral irradiance scales of the FEL lamps are in turn transferred to spectral radiance scales using plaques of known bidirectional reflectance, or integrating spheres, or both. The SeaWiFS Project Office initiated a series of SeaWiFS Intercalibration Round-Robin Experiments (SIRREXs) to assure internal consistency between the laboratories that calibrate radiometers for SeaWiFS validation (Mueller 1993 and Mueller *et al.* 1994). In SIRREX-3 (Mueller *et al.* 1996) and -4 (Johnson *et al.* 1996), it was demonstrated that with properly maintained FEL lamp secondary and working standards, thorough training of laboratory personnel in calibration procedures, and careful attention to

¹ “FEL” is a commercial lamp-type designator. The 1000 W FEL-type lamps used for spectral irradiance calibration are modified by welding on a special base, which has much larger terminals than are provided with the stock commercial bulbs (Walker *et al.* 1987). Following this modification, the spectral irradiance output of each lamp is scanned with a high-resolution monochromator, to assure that its spectrum is smooth and free from unwanted emission lines. Finally, the candidate calibration source lamp is “seasoned” by initially burning it for approximately 24-hours, using a highly regulated current source; its spectral irradiance output and lamp terminal voltage are carefully monitored. Lamps that do not achieve stable performance during the seasoning process are discarded. Several commercial vendors offer both seasoned FEL-type lamps, and seasoned lamps with a certified scale of spectral irradiance transferred from another FEL-type secondary standard lamp acquired directly from NIST.

measurement setups, it was possible to maintain an uncertainty level of $< 2\%$ for spectral irradiance and $< 3\%$ for spectral radiance calibrations.

The variety of instruments available for validation measurements makes it imperative that some common calibration traceability exists. Recognizing that it would be impractical to characterize and calibrate all oceanographic and airborne radiometers at GSFC, several remote calibration facilities were identified (instrument manufacturers and a few laboratories at academic and government institutions), and working standards and protocols used at these facilities may be traced directly to the NIST scale (Johnson *et al.* 1996). This organizational structure is shown schematically in Figure 3.2. Methods of standards intercomparison may include use of NIST calibrated filter radiometers to track and document the operation of each facility (radiometer wavelengths for this intercomparison will be determined). Round-robin calibration comparisons of a reference set of field instruments were implemented to benchmark the internal consistency of calibrations performed at the various facilities involved with calibrations throughout the ocean color community; the first of these (SIRREX-6) determined that the level of relative uncertainty between these laboratories is approximately 2% (Riley and Bailey, 1998).

In 2001, the SIMBIOS Project initiated a new series of SIMBIOS Radiometric Intercomparison (SIMRIC) round-robin comparisons of radiometric calibrations among the participating laboratories. Rather than comparing laboratory calibrations of radiance and irradiance sensors designed for field use, as in SIRREX-6, the SeaWiFS Transfer Radiometer SXR-II was used to compare the radiance scales of the calibration sources at the various laboratories (Meister *et al.* 2002). The SeaWiFS Transfer Radiometers, SXR and SXR-II, were built, and their calibrations are maintained directly, by NIST (Johnson *et al.* 1998). The SXR-II measures radiance in 6 wavelength-bands between 411 nm and 777 nm consistent with the SeaWiFS band (Table 5.1 of Chapter 5). Its angular Field of View (FOV) is approximately 2° Full-Width at Half-Maximum (FWHM) response. The SIMRIC-1 comparison procedure was to position the SXR-II to view the plaque, or sphere, radiance source(s) at each laboratory, and the instrument's calibrated response in each band was compared to the radiance scale at that wavelength interval as provided by the host laboratory; laboratory and SXR scales agreed within approximately 2% for most wavelength bands (Meister *et al.* 2002).

Spectral Irradiance Calibrations

Radiometric calibrations of irradiance sensors will be performed after it has been ascertained that: the conformity of the sensor angular response to the required cosine function is satisfactory, the sensor linearity is satisfactory, and the spectral sensitivity, including out-of-band stray-light blocking, is known and satisfactory.

The options available for radiometric calibration standards are limited to standard sources or standard detectors. The FEL-type lamp standard of spectral irradiance is traditionally used for radiometric calibration, mainly because of its ease of use, compared to the spectral radiance lamp. FEL-type lamp standards of spectral irradiance are provided by NIST, and FEL-type lamp secondary standards, with NIST-traceable spectral irradiance scales, are available from various commercial standardizing laboratories and manufacturers. The uncertainty cited by NIST for these standards is, at best, 1% in the visible and 2% is a more realistic estimate of absolute uncertainty attainable using lamp standards alone. In 2000, a detector-based realization was completed of the NIST scale of spectral irradiance, with a significantly improved uncertainty budget compared to that of the 1990 source-based scale of spectral irradiance (Yoon *et al.* 2002). The expanded combined uncertainty (2 standard uncertainties) of a NIST-issued secondary standard FEL based on the 2000 scale of spectral irradiance is approximately 1.1% to 1.6% in the ultraviolet and 0.5% to 0.6% in the visible and near-infrared (Yoon *et al.* 2002). In the wavelength region of principal interest for ocean color research, this represents an improvement of $\leq 0.2\%$ in the uncertainty (1 standard uncertainty) of the FEL working standards used to calibrate oceanographic radiometers. A NIST-issued FEL secondary standard of spectral irradiance is very expensive, and vendor-issued calibrated FEL working standards are only incrementally less expensive. Therefore, the recommended protocol is to continue using existing FEL lamps with scales based on the NIST 1990 scale of spectral irradiance, and to begin using FEL lamps with scales traced to the NIST 2000 scale when a laboratory's primary working standards are replaced, or recalibrated. NIST has published guidelines for the setup, alignment, and use of these standards (Walker *et al.* 1987). The vendors who manufacture and calibrate these lamps also issue guidelines for their use.

The irradiance calibration procedure (Walker *et al.*, 1987; Johnson, *et al.* 1996) may be summarized as follows:

- The irradiance sensor and a suitable lamp fixture for the FEL-type lamp standard are mounted on an optical bench. The lamp-sensor space shall be appropriately baffled and draped so that occulting the

direct path between lamp and sensor will result in a response of less than 0.1 % of the response to the lamp flux. Some laboratories place the lamp and sensor in different rooms, with a variable sized aperture so that illumination is confined near the edges of the irradiance collector (or plaque) – but the illumination beam should not be so tight that diffractive fringes fall on the irradiance collection area. Other laboratories use curtains and partitions to achieve the same result. However the baffling is accomplished, the most critical aspect is to eliminate on-axis reflections, e.g. as might result from a flat surface directly behind the lamp and perpendicular to the optical axis (Walker *et al.*, 1987)

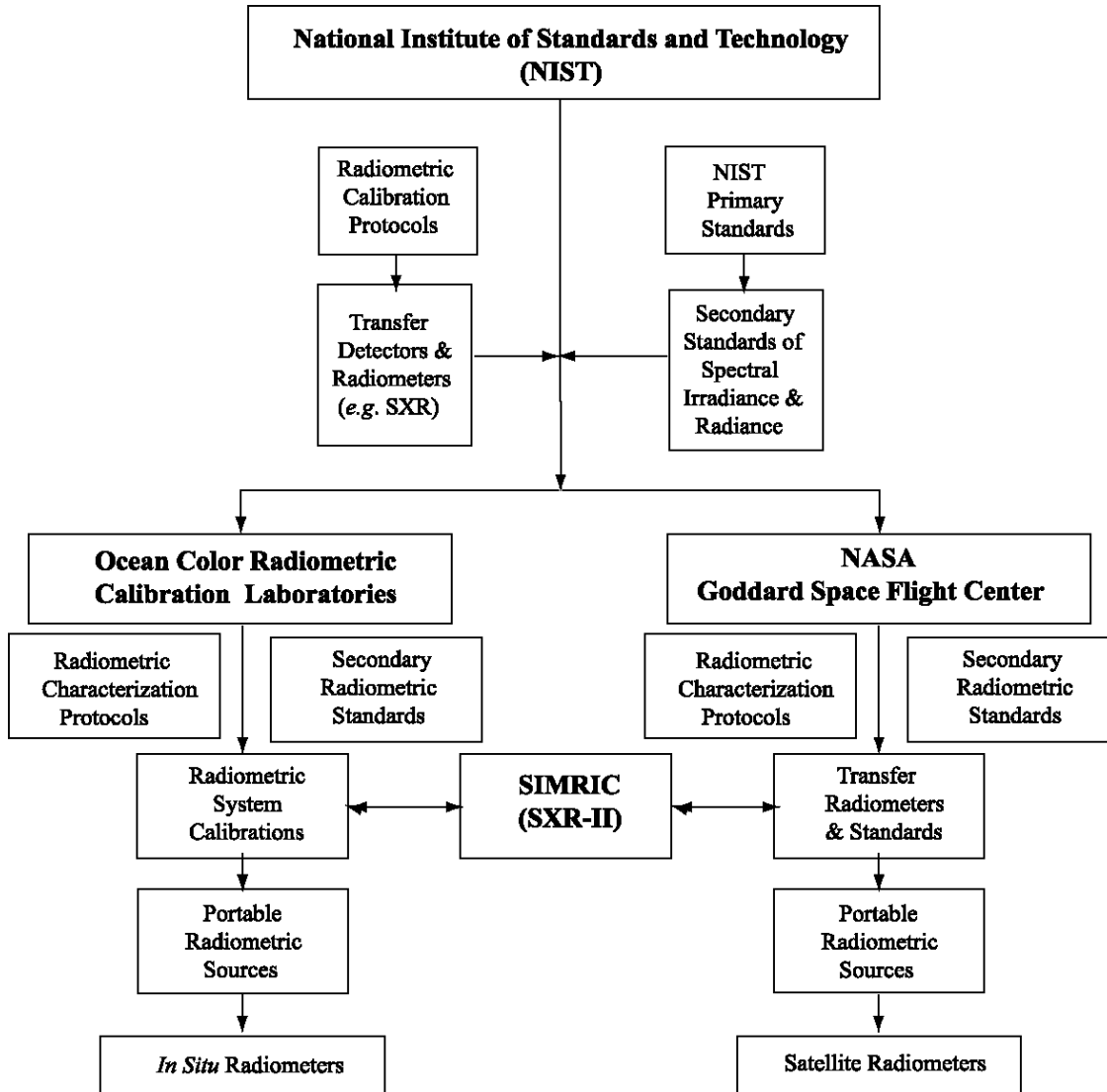


Figure 3.2: Organizational structure for radiometric instrument characterization and calibration within the SeaWiFS and SIMBIOS ocean color research community.

- An alignment reference target, having a window with cross hairs etched to mark the location of the lamp filament, is mounted in the lamp holder.
- An alignment LASER beam is directed normal to the target window; this alignment is achieved when the reflection from the window is directed back on the LASER aperture.

- The sensor is mounted on the optical bench with the irradiance collector centered on the alignment LASER beam, which marks the optical axis. The collector is aligned normal to the beam, using a mirror held flat against the collector to reflect the beam back through the lamp-target cross hairs to the LASER aperture.
- The FEL-type lamp spectral irradiance working standard is inserted into the lamp-holder, with its identification tag facing away from the sensor. The lamp terminals are connected to a current-regulated, direct current power supply, with careful attention to ensure proper polarity (as marked on the lamp). The power supply is turned on and ramped-up to the proper current for the particular lamp (given with the lamp calibration certificate). A shunt and 4.5 digit voltmeter should be used to monitor lamp current to the nearest 0.001 A. Following a 15 min warm-up, irradiance calibration measurements may be taken. The voltage present across the lamp terminals should be measured at frequent intervals during a calibration run, and compared to the voltage measured when the lamp was calibrated. A significant change in the lamp's operating voltage (at the specified current) indicates that the irradiance output of the lamp has probably changed also, and that the lamp is no longer usable as a working standard of spectral irradiance. On completion of the calibration session, it is good practice to also slowly ramp the lamp current down to avoid thermally shocking the filament.
- The distance r along the optical path between the collector surface and the lamp is measured to the front surface of the lamp's terminal posts. The standard reference distance for all NIST traceable FEL-type lamp scales of spectral irradiance is $r = 50.0$ cm .
- An occulting device is placed to occult the direct optical path between the lamp and collector, and the sensors responses $V_{\text{amb}}(\lambda)$ to ambient background light are recorded. If the ambient response is more than 0.1% of the instrument's dark response with the collector completely covered, then the baffling of the calibration setup is inadequate and should be improved.
- The occulting device is removed from the optical path and the irradiance sensor's responses $V_r(\lambda)$ are recorded, usually as digital counts in modern practice. The sensor's irradiance responsivity calibration factors (in air) are determined as

$$F_E(\lambda) = \frac{E_r(\lambda)}{V_r(\lambda) - V_{\text{amb}}(\lambda)}, \mu\text{W cm}^{-2}\text{nm}^{-1} [\text{digital count}]^{-1}. \quad (3.1)$$

If the lamp is at the standard distance $r = 50.0$ cm, $E_r(\lambda) = E_{50}(\lambda)$, where $E_{50}(\lambda)$ is the lamp's certified NIST-traceable scale of spectral irradiance at 50 cm. The spectral irradiance responsivity factors are applied to subsequent radiometric measurements as

$$E(\lambda) = F_E(\lambda) [V(\lambda) - V_{\text{dark}}(\lambda)], \mu\text{W cm}^{-2}\text{nm}^{-1}, \quad (3.2)$$

where $V_{\text{dark}}(\lambda)$ are the instruments dark responses as determined in the field (e.g. Volume III, Chapter 2).

- Should an irradiance sensor saturate when it is illuminated at a lamp distance of 50 cm, it will be necessary to reduce the irradiance level by increasing r , with the adjusted irradiance scale $E_r(\lambda)$ determined as

$$E_r(\lambda) = E_{50}(\lambda) \left[\frac{50 + \Delta f}{r + \Delta f} \right]^2, \mu\text{W cm}^{-2}\text{nm}^{-1}, \quad (3.3)$$

where Δf is the distance that the center of the lamp filament is offset behind the front plane of its terminal posts. The magnitude of this offset is typically $\Delta f \approx 3$ mm, but it may vary significantly between individual FEL lamps. One approach to determining Δf is to estimate the location of the center of the filament, and measure its distance behind the plane of the front surface of the terminal posts using a mechanical jig. Alternatively, the filament offset can be determined for a particular lamp by measuring an irradiance sensor's responses with the lamp positioned at 50 cm and a series of N

distances r_n between 50 cm and 300 cm. Assuming that the response of the sensor is linear, combining (3.2) and (3.3) leads to

$$\frac{V_n(\lambda) - V_{\text{amb}}(\lambda)}{V_{50}(\lambda) - V_{\text{amb}}(\lambda)} = \left[\frac{50 + \Delta f}{r_n + \Delta f} \right]^2 \quad (3.4)$$

The solution to (3.4) at each distance r_n and wavelength λ_m is

$$\Delta f_{nm} = \frac{X_{nm} r_n - 50}{1 - X_{nm}} \quad (3.5)$$

where $X_{nm} \equiv \left[\frac{V_n(\lambda_m) - V_{\text{amb}}(\lambda_m)}{V_{50}(\lambda_m) - V_{\text{amb}}(\lambda_m)} \right]^{\frac{1}{2}}$. The filament offset Δf may then be determined as the average

of the NxM estimates obtained using (3.5) at N distances r_n and M wavelengths λ_m . To determine the actual filament offset, this experiment is best done using an integrating sphere cosine collector. If a solid diffuser collector is used, the resulting offset will represent the sum of the lamp's filament offset from the terminal post front, plus the effective distance within the diffuser material representing the irradiance collector's effective entrance plane (which may vary somewhat with wavelength). On the other hand, the combined distance offset would be the appropriate one to use with that particular radiometer and FEL combination. The effective offset may also be determined using a reflectance plaque and a narrow field-of-view radiance sensor (see below under *Spectral Radiance Calibrations*).

Spectral Radiance Calibrations

Radiance responsivity calibrations require a uniform, *i.e.* a Lambertian, source of known radiance that will fill the angular field of view of the radiance sensor. The two procedures that are most frequently used to calibrate ocean color radiance sensors are given below.

1. *Reflectance Plaque Radiance Calibrations:* An FEL-type lamp working standard of spectral irradiance is used, at a known distance r , to illuminate a plaque of near-Lambertian reflectance, with a known bidirectional reflectance distribution function (BRDF) $\rho(\lambda, \theta_o, \theta)$; the BRDF for plaques used in this procedure are most frequently calibrated for normal illumination, *i.e.* $\theta_o = 0$, and a viewing angle $\theta = 45^\circ$. For this geometry, the setup is identical to that described above for *Spectral Irradiance Calibrations*, with the reflectance plaque substituted for the irradiance collector. All of the above comments pertaining to effective baffling, and determination of the lamp filament offset, apply to this radiance calibration procedure as well. The procedure (see also Johnson et al. 1996) may be summarized as follows:

- The alignment of the lamp optical axis normal to the center of the reflectance plaque is best done using an alignment LASER, FEL target and mirror placed against the plaque surface at its center, and adjusting the apparatus to achieve retroreflection of the LASER beam from both the FEL target and plaque alignment mirror. This initial alignment procedure is identical to that described above for *Spectral Irradiance Calibrations*.
- The standard lamp is positioned on an axis normal to the center of the plaque at distance r . To assure uniform illumination across the surface of the plaque, r must typically be greater than 1.5 m, and for wide FOV instruments as large as 3 m. Hooker *et al.* (2002) measured the spatial distributions of radiance reflected from the central 40 cm x 40 cm area 45 cm square plaque illuminated by 4 different FEL lamps at $r = 50$ cm, and by one of the FEL's at $r = 130$ cm and $r = 210$ cm. At $r = 50$ cm, all lamps produced variations in reflected radiance of up to 20% over the area of the surface viewed by the FWHM FOV's of a typical field radiometer. Spatial variations of reflected radiance within the FWHM FOV area decreased to 8% at $r = 130$ cm, and to 3% at $r = 210$ cm.
- The filament offset Δf may be determined by the methods described above under *Spectral Irradiance Calibrations*. If this is done using measurements at varying distances with equation

(3.5), the FWHM FOV of the radiance sensor must be small enough to subtend an area of diameter ≤ 3 cm located at the center of the plaque. If a larger area of the surface is viewed, changes in the spatial distribution of illumination by the FEL (Hooker *et al.* 2002) may be confounded with the systematic variation associated with the filament offset. Biggar (1998) found an FEL filament offset of $\Delta f = 3.2$ mm, a “typical” value adopted, on an *ad hoc* basis, by some of the laboratories participating in SIMRIC-1 (Meister *et al.* 2002). The effect of a 3 mm filament offset in equation (3.3) amounts to increases, relative to $\Delta f = 0$, of 0.6 % at $r = 100$ cm and of approximately 1 % in the range $200 \leq r < 300$ cm. Because FEL-specific variations with distance over the range $200 \leq r < 300$ cm are a greater source of uncertainty in this calibration procedure (for the wide FOV instruments typically used in ocean color research), a significant segment of the community feel that applying a non-zero filament offset is neither necessary, nor beneficial. Countering this argument, SIMRIC-1 intercomparison results consistently showed improvements, of order 1 %, in agreement between calculated plaque radiances and SXR-II NIST-calibrated radiances when the $\Delta f = 3.2$ mm (Biggar 1998) adjustment was applied (Meister *et al.* 2002). On this basis, the use of either a default $\Delta f = 3.2$ mm, or an improved, locally determined FEL and plaque specific filament offset, is recommended as a provisional protocol for this type of radiance calibration.

- The radiance sensor is positioned to view the plaque at an angle $\theta = 45^\circ$, measured from the plaque normal (any other angle at which the diffuse reflectance of the plaque is known is acceptable also). It must be established that the plaque fills the sensor's FOV and that the presence of the sensor case has not perturbed the irradiance on the plaque. The angular alignment of the instrument aperture can be done by rotating the plaque about its vertical axis to, e.g., 22.5° (measured with an indexing column) and adjusting the instrument to achieve retroreflection (see, for example, Hooker *et al.* 2002 and Meister *et al.* 2002).
- The lamp is occulted to record the sensor's ambient responses $V_{\text{amb}}(\lambda)$. The occulter is removed and the responses $V_r(\lambda)$ to radiance reflected from the plaque are recorded.
- The radiance reflected by the plaque and viewed by the sensor in this geometry is determined as

$$L(\lambda) = \frac{1}{\pi} \rho(\lambda, 0^\circ, 45^\circ) E_r(\lambda), \quad (3.6)$$

where the spectral irradiance $E_r(\lambda)$ is calculated using equation (3.3).

2. *Integrating Sphere Radiance Calibrations:* An alternative approach to calibrating multispectral radiance sensors is to view an integrating sphere that is uniformly illuminated by stable, appropriately baffled lamps, and that also has an exit port large enough to completely fill the sensor's FOV. The sphere and exit port must be large enough to place the radiance sensor far enough away to prevent significant secondary illumination of the sphere walls due to reflections off the sensor's entrance optics; if the sensor is too close, the reflected light will both increase and distort the uniformity of the radiance distribution within the sphere. The spectral radiance scale of an integrating sphere source may be transferred from the spectral irradiance scale of an FEL-type lamp standard², and then used to calibrate radiance sensors for field measurements, using the following procedure (Johnson *et al.* 1996):

- An irradiance scale transfer radiometer, configured with an integrating sphere having a circular entrance aperture of radius r_2 as its cosine collector, is calibrated using a FEL-type standard of spectral irradiance by the method outlined above under “*Spectral Irradiance Calibrations*”.

² In some laboratories, the radiance scale of a sphere is assumed constant for relatively lengthy periods of time between infrequent scale transfers from an FEL source. Often, these laboratories rely on monitoring the sphere output with detectors at one or more wavelengths. A single wavelength monitor can give a misleading impression of sphere stability, however, as patterns of degradation in sources and optical coatings are often highly wavelength dependent (J. Butler and G. Meister, Pers. Comm.).

- The irradiance scale transfer radiometer is positioned with the entrance aperture of its integrating sphere collector parallel to and centered coaxially at a distance d from the circular aperture, with radius r_1 , of the integrating sphere source.
- The spectral irradiance $E(\lambda, d, r_1, r_2)$ of the integrating sphere source's exit port is measured using the irradiance scale transfer radiometer. The ambient reference $V_{\text{amb}}(\lambda)$ is recorded with the source exit port covered, the cover is removed to record $V_d(\lambda)$, and source irradiance is calculated using (3.2).
- Assuming a uniform radiance distribution within the sphere's exit port, the spectral irradiance scale of the integrating sphere is calculated as (Johnson *et al.* 1995)

$$L(\lambda) = \frac{E(\lambda, d, r_1, r_2) [d^2 + r_1^2 + r_2^2]}{\pi r_1^2} [1 + \delta + \delta^2 + \dots], \quad (3.7)$$

where $\delta = r_1^2 r_2^2 (d^2 + r_1^2 + r_2^2)^{-2}$.

- The radiance sensor to be calibrated is substituted for the transfer radiometer, and views the center of the source aperture. Its responses $V_d(\lambda)$ and are recorded.

In either approach, the radiance responsivity calibration coefficients of the field radiometer are determined as

$$F_L(\lambda) = \frac{L(\lambda)}{V_r(\lambda)}, \mu\text{W cm}^{-2}\text{nm}^{-1}\text{sr}^{-1} [\text{digital count}]^{-1}, \quad (3.8)$$

substituting $V_d(\lambda)$ for $V_r(\lambda)$ in the integrating sphere case, and applied to derive radiance from field measurements $V(\lambda)$ as

$$L(\lambda) = F_L(\lambda) V(\lambda), \mu\text{W cm}^{-2}\text{nm}^{-1}\text{sr}^{-1}. \quad (3.9)$$

3.3 PORTABLE STANDARDS

The portable irradiance and radiance reference standard to be used to trace instrument stability during field deployments (Volume II, Chapter 5) should be placed in position on the sensor immediately following the calibration to establish the instrument response to this reference unit. In the field, an instrument should be connected to the portable standard and its response recorded daily, keeping a record of instrument responsivity throughout an experiment. These comparison records provide an essential warning of problems, if they appear.

3.4 SPECTRAL BANDPASS CHARACTERIZATION

Oceanographic radiometers should be characterized to define the nominal wavelengths and bandwidths, defined as the full width of the passband as measured to the FWHM intensity points. The nominal, or center wavelength, will usually be defined as the wavelength halfway between wavelengths at which the normalized response is 0.5, and the channel is characterized by this wavelength and the FWHM bandwidth. The determination of the spectral response function, *i.e.* the passband, will be made for each channel with a scanning monochromatic source, with a bandwidth less than 0.2 nm; the source output must be normalized to a detector of known spectral sensitivity. The response function thus measured is then normalized to the maximum (peak).

Although the results of this characterization are usually represented by only the nominal wavelength and FWHM bandpass, the complete normalized response function should be recorded for use in detailed wavelength adjustments and comparisons with the SeaWiFS and other sensor channel response functions, which must be characterized before launch. It is further recommended that the internal instrument temperature be monitored during these tests, and that the test be repeated at two temperatures at least 15° C apart, e.g., 10° and 25° C. If a significant shift, greater than 1.0 nm, with temperature of either the center wavelength or bandwidth is detected, then additional temperature calibration points are recommended. Dark offsets must be recorded during each test.

For spectral characterizations of irradiance diffusers, the entire surface of the diffuser should be illuminated by the monochromator's output. In the case of radiance detectors, a diffuser should be used to diffuse the monochromator slit image and uniformly fill the instrument's FOV.

The wavelength response of a monochromator-based radiometer is calibrated by scanning over line sources, with sharp peaks at well-known wavelengths. Suitable spectral calibration sources, such as, mercury, cadmium, and neon lamps, are provided by several vendors, together with tabulations of the wavelengths of the emission lines generated by each source.

The width of the slit function of a monochromator may be estimated by scanning over a laser line, *e.g.* helium-neon, at a very small wavelength interval. The instrument FOV must be filled during the test.

It is anticipated that the monochromator-based spectral characterization will not be able to adequately measure leakage of broadly distributed out-of-band radiation; therefore, blocking of blue light in channels longer than 540 nm must be routinely tested. Where continuous wave (CW) argon lasers are available, out-of-band response should be measured at 488 nm. One recommended test that can be performed during the absolute calibrations at $\lambda \leq 640$ nm is the sequenced measurement of three Schott BG-18 filters, each 1 mm thick, using a FEL-type light source. The procedure is to measure the channel signal using each filter separately, then in combination, and comparing the computed and measured transmissions. If a significantly higher combined transmission of the three filters, when they are used in combination, is measured relative to the calculated transmittance, then spectral leakage is present. At wavelengths greater than 640 nm, other filters that attenuate the wavelength of interest, with a transmission value of less than or equal to 0.1 and which pass shorter wavelength light with significantly greater transmission, should be substituted for the BG-18.

Consideration must also be given to unblocked fluorescence by the filters, or other optical elements, as a possible source of light leaks. Methods to test for fluorescence contamination specifically are not well established at this time.

While leakage of blue light into red channels is the most significant oceanographic optical problem, the leakage of red and IR light into blue channels can cause significant errors when the instrument is calibrated using a red-rich source. A convenient way to measure this leakage is to place a long wavelength-pass, sharp-cut, absorbing glass filter that does not exhibit fluorescence between a broadband (*e.g.*, incandescent) source and the sensor. A non-zero response indicates unwanted out-of-band red response and the need for improved red blocking.

Spectral Stray Light Characterization Using LASER-Illuminated Integrating Sphere Sources

Scientists at NIST have recently developed tunable, monochromatic sources that enable the characterization of a sensor's spectral responsivity, at the $<10^{-6}$ level, to illumination at wavelengths far outside its primary bandpass. This new NIST facility, named Spectral Irradiance and Radiance responsivity Calibrations with Uniform Sources (SIRCUS), is based on integrating sphere sources illuminated by LASERS; an ensemble of tunable and fixed frequency LASERS are utilized to cover the full spectral ranged of interest (Brown, Eppeldauer, and Lykke 2000). Very small exit apertures are used to provide sources of monochromatic irradiance, and large exit apertures are used as sources of monochromatic radiance, as appropriate to uniformly fill a particular sensor's entrance pupil. The source's absolute scale of spectral irradiance (radiance) at each monochromatic wavelength setting is transferred from the scale of a transfer radiometer calibrated, in turn, with a NIST primary standard. Thus, when the sensor under test views the source, its response is used to determine its absolute spectral irradiance (radiance) responsivity to the source wavelength at the sensor's nominal wavelength of interest. The absolute response function determination, using SIRCUS to provide monochromatic illumination scanned over the full spectral range of interest (*e.g.* 350 nm to 1000 nm) while the sensor's responses are recorded at all of its resolved wavelengths of interest, provides the information necessary for spectral stray light corrections with very low (albeit yet to be determined) uncertainty levels. Initial work to characterize the stray light responsivity functions of the spectrographs used to measure downwelled spectral irradiance and upwelled spectral radiance on the Marine Optical Buoy (MOBY), and more details about SIRCUS and its applications, are described in Volume VI, Chapters 2 and 5, and references cited therein.

3.5 IMMERSION FACTORS

Irradiance Sensor Immersion Factors

When a plastic, opal-glass, or Teflon diffuser is immersed in water, its light transmissivity is less than it was in air. Since an instrument's irradiance responsivity is calibrated in air, a correction for this change in collector transmissivity must be applied to obtain irradiance responsivity coefficients for underwater measurements.

The change in a collector's immersed transmissivity is the net effect of two separate processes: a change in the reflection of light at the upper surface of the collector, and internal scattering and reflections from the collector's lower surface. A small part of the light flux falling on the collector is reflected at the air-plastic, or water-plastic, interface, and the majority of the flux passes into the collector body. The relative size of this reflectance, called *Fresnel reflectance*, depends on the relative difference in refractive indices between the diffuser material and the surrounding medium.

The refractive index of the collector material is always larger than that of either water or air, and because the refractive index of water is larger than that of air, Fresnel reflectance is smaller at a diffuser-water interface than at a diffuser-air interface. Therefore, the initial transmission of light through the upper surface of an irradiance collector is larger in water than in air. The immersed upper surface is, on the other hand, also less effective at reflecting the upward flux of light backscattered within the diffuser body and light reflected at the lower diffuser-air interface in the instrument's interior, processes that are not affected by immersion. Therefore, a larger fraction of the internally scattered and upwardly reflected light passes back into the water column than would be lost into air. Because the increased upward loss of internally reflected flux exceeds the gain in downward flux through the diffuser-water interface, the net effect of these competing processes is a decrease in the collector's immersed transmissivity.

Experience has shown that the immersion factors for an irradiance collector must be experimentally characterized in the laboratory. Some manufacturers perform this characterization procedure only for a prototype of a particular collector design and material specification. They sometimes then provide only these nominal immersion factors for all production radiometers using that collector design. Mueller (1995) applied the characterization procedure described below to determine irradiance immersion factors for 11 radiometers having cosine collectors of the same design and material. The measurements were replicated 2 to 4 times for each radiometer, using independent setups on different days and varying the lamp-to-collector distance between replications, to determine that Type A uncertainty associated with the experimental procedure is less than 1 %. On the other hand, root-mean-square differences between immersion factors in this group of irradiance sensors ranged from 3 % to 5 %, at different wavelengths, and differences between individual collectors were as large as 10 % at some wavelengths. Zibordi et al. (2002) recently measured discrepancies of this magnitude between collectors for radiometers of a design and manufacturer different from those studied by Mueller (1995).

To measure this effect, a suggested and acceptable procedure (Petzold and Austin 1988) is as follows:

1. The instrument is placed in a tank of water with the irradiance collector level and facing upward.
2. A tungsten-halogen lamp with a small filament, powered by a stable power supply, is placed at a carefully measured distance above the surface of the irradiance collector. An initial reading is taken in air, before the water level in the tank is raised above the dry collector. Lamp voltage and shunt current should be monitored throughout the duration of the experimental procedure to assure stable output. As a further assurance of lamp output stability, some laboratories also monitor the lamp output continuously with a separate irradiance sensor (in air) (Zibordi *et al.* 2002).
3. The water is raised initially to a carefully measured depth z above the collector surface and readings are recorded for all wavelengths. Repeatable results at the $< 1\%$ level of uncertainty require careful attention to the cleanliness of the water (Zibordi *et al.* 2002). An affordable approach to achieve adequate water quality is to recycle the water through a diatomaceous earth swimming pool filter.
4. The water level is then increased stepwise in, *e.g.*, 5 cm increments, and the instrument responses are measured and recorded for each depth z . A maximum water depth of 40 cm to 50 cm is normally adequate to obtain data covering a sufficient range of responses.
5. The water level is then lowered, and data recorded, over a similar series of incremental depths.

6. A final reading is taken with the water level below the collector, after drying the collector. It is recommended to then change and remeasure the lamp-to-collector distance d , and repeat the entire procedure to verify that a Type A experimental uncertainty less than 1 % has been achieved.

A minimum water depth of 5 cm is recommended to avoid artifacts due to multiple reflections between the collector and water surfaces. These reflections would otherwise artificially increase the transmitted flux, and therefore, decrease the apparent immersion effect. The magnitude of this artifact will increase with decreased depth z below some critical limit, which is the order of the diameter of the collector. With very small diameter collectors, it may be possible to acquire good immersion effect data at values of $z < 5$ cm, but the absence of this artifact should be demonstrated experimentally if this is done.

The amount of energy arriving at the collector varies with the water depth and is a function of several factors:

1. the attenuation at the air-water interface, which varies with wavelength;
2. the attenuation over the water pathlength, which is a function of depth and wavelength; and
3. the change in solid angle of the light leaving the source and arriving at the collector, caused by the light rays changing direction at the air-water interface, which varies with wavelength and water depth.

Using Fresnel reflectance equations, the transmittance through the surface is

$$T_s(\lambda) = \frac{4n_w(\lambda)}{[1+n_w(\lambda)]^2}, \quad (3.10)$$

where $n_w(\lambda)$ is the index of refraction of the water at wavelength λ . The transmittance through the water path is given by

$$T_w(\lambda) = e^{-K(\lambda)z}, \quad (3.11)$$

where $K(\lambda)$ is the attenuation coefficient of the water and z is the path length in corresponding units.

The change with water depth z of the refracted solid angle subtended by the collector, as viewed from the lamp filament, is given by the factor

$$G(z, \lambda) = \left[1 - \frac{z}{d} \left(1 - \frac{1}{n_w(\lambda)} \right) \right]^{-2}, \quad (3.12)$$

where d is the distance of the lamp source from the collector surface.

The immersion correction factor $F_i(\lambda)$ for irradiance is then calculated for each depth z as

$$F_i(\lambda) = \frac{E_a(\lambda)}{E_w(z, \lambda)} T_s(\lambda) T_w(\lambda) G(z, \lambda), \quad (3.13)$$

where $E_a(\lambda)$ and $E_w(\lambda, z)$ are the irradiance in air and the irradiance underwater at depth z , respectively.

There are two unknowns in (3.10)-(3.13): the attenuation coefficient of the water $K(\lambda)$ and the immersion factor $F_i(\lambda)$. A minimum of three measurements must be made to solve for $F_i(\lambda)$ and $K(\lambda)$: one in air to get $E_a(\lambda)$, and two at different water depths for $E_w(\lambda, z)$. The recommended method is to take readings of $E_w(\lambda, z)$ at many water depths. If (3.11) is substituted into (3.13), and the result is log transformed and rearranged, each measurement $E_w(\lambda, z)$ and depth z may be expressed as

$$\ln \left[\frac{E_a(\lambda)}{E_w(z, \lambda)} T_s(\lambda) G(z, \lambda) \right] = \ln [F_i(\lambda)] + K(\lambda)z. \quad (3.14)$$

The unknown slope $K(\lambda)$, and intercept $\ln[F_i(\lambda)]$, are then determined by a linear least-squares regression analysis. The complete derivation of (3.10) – 3.14) is given in Petzold and Austin (1988).

Radiance Immersion Factors

The absolute calibration for the spectral radiance channels is found by viewing a surface of known radiance in air in the laboratory. When the instrument is submerged in water, a change in responsivity occurs and a correction must be applied. This change in responsivity is caused by the change in the indices of refraction of the different media in which the instrument is immersed--in this case air and water. Two optical changes occur, both of which are caused by the change in refractive index. The two effects to be corrected are:

1. the change in transmission through the interface between the air and the window during calibration, and the same effect through the water-window interface during data measurement, and
2. the change in the solid angle included in the underwater FOV relative to that in air.

Since $n_w(\lambda)$ is a function of wavelength, the correction factor $F_i(\lambda)$ is also a function of wavelength. If the refractive index of air is assumed to be 1.000 at all wavelengths, and if $n_g(\lambda)$ is the index of refraction for the (glass) window, the correction for the change in transmission through the window, $T_g(\lambda)$, is (Austin 1976)

$$T_g(\lambda) = \frac{[n_w(\lambda) + n_g(\lambda)]^2}{n_w(\lambda)[1 + n_g(\lambda)]^2}, \quad (3.15)$$

and the correction for the change in the FOV is

$$F_v(\lambda) = [n_w(\lambda)]^2. \quad (3.16)$$

The index of refraction of a PlexiglasTM window, $n_g(\lambda)$, may be computed, using an empirical fit to the Hartmann formula, as

$$n_g(\lambda) = 1.47384 + \frac{7.5}{\lambda - 174.71}, \quad (3.17)$$

where λ is the wavelength in nanometers (Austin 1976). The refractive indices of other window materials must be obtained from the manufacturer.

The index of refraction for seawater $n_w(\lambda)$ may be similarly computed, using an empirical fit of the data from Austin and Halikas (1976), as

$$n_w(\lambda) = 1.325147 + \frac{6.6096}{\lambda - 137.1924}. \quad (3.18)$$

Finally, the immersion factor $F_i(\lambda)$ for a radiance sensor is obtained as

$$F_i(\lambda) = T_g(\lambda)F_v(\lambda), \quad (3.19)$$

or by substitution from (3.15) and (3.16), in expanded form as

$$F_i(\lambda) = \frac{n_w(\lambda)[n_w(\lambda) + n_g(\lambda)]^2}{[1 + n_g(\lambda)]^2}. \quad (3.20)$$

3.6 RADIANCE FIELD-OF-VIEW

It is required that the radiance FOV of the instrument be known. The FOV should not normally enter into the absolute calibration, however, if the FOV is fully filled by a calibration source of uniform radiance.

In this test, the instrument is placed on a rotational stage with the entrance aperture of the radiometer over the rotation axis. A stable light source with a small filament is placed several meters in front of the instrument, which is then scanned from -30° to $+30^\circ$ in 2° increments. The uncertainty in angle positioning should be $\leq 0.1^\circ$. The on axis, *i.e.* 0° , mechanical alignment is made using the window surface as reference, by adjusting to get the reflection of the lamp filament to return on axis. The uncertainty in this alignment is approximately 0.1° . The in-air

measurement angles θ_a are converted to corresponding angles θ_w in seawater using the relation $\theta_w = \frac{\theta_a}{n_w(\lambda)}$, where $n_w(\lambda)$ is given by Equation (3.18).

3.7 COLLECTOR COSINE RESPONSE

The directional response of cosine collectors must be characterized. The directional response of the deck cell is determined in air, and those of the in-water instruments are measured immersed in water. Full spectral determinations are required. For instruments measuring upwelling irradiance $E_u(z, \lambda)$ it is recommended that the cosine response of each instrument be measured individually. For downwelling irradiance $E_d(z, \lambda)$ instruments, checking a production run may be satisfactory if the vendor's material and design are demonstrated to be uniform throughout the duration of the run. Given the variations observed in immersion factors of collectors of the same design and materials (Mueller 1995; Zibordi *et al.* 2002), however, this possibility should be accepted only with caution. Whenever possible, it is strongly recommended that the cosine response of irradiance collectors be characterized individually.

Absolute responsivity calibration of an irradiance meter is done in air, using light incident normal to the collector. To properly measure irradiance incident on the plane at all angles θ (relative to the normal), the instrument's response should follow a cosine function. In other words, for an instrument response $V(\lambda, 0)$ to a given collimated irradiance incident at $\theta = 0^\circ$, if the instrument is rotated to the angle θ away from the original normal axis, the response should be $V(\lambda, \theta) = V(\lambda, 0)\cos\theta$. If this criterion is met, then the on-axis calibration is sufficient and the device will correctly measure irradiance arriving at the plane of the collector, regardless of the directional distribution at which the light arrives.

The preferred in-water irradiance collector design has an improved cosine response over that of a simple flat plate diffuse collector (Boyd 1955 and Tyler and Smith 1979). This improvement is mostly for near-grazing angles (θ approaching 90° to the normal) and is particularly important when measurements of the upwelling underwater irradiance are made, *i.e.*, with the collector facing downward. In that case, most of the light is incident from the sides, *i.e.* in the region of these near-grazing angles.

Since $E_d(z, \lambda)$ and $E_u(z, \lambda)$ measurements are made underwater, the tests to determine the fidelity with which the instruments directional response follows the cosine function must be made with the instrument submerged. A description of the suitable experimental procedure follows (Petzold and Austin 1988).

The instrument is suspended in a tank of water while supported by a fixture designed to allow rotation about an axis through the surface and center of the collector. A tungsten-halogen lamp with a small filament is enclosed in a housing with a small exit aperture and placed approximately 1 m from a large window in the tank. The collector is placed approximately 25 cm behind this window. A circular baffle should be placed immediately in front of the window to reduce stray light. The water should be highly filtered to the extent that the effects of scattered light are indiscernible.

The equivalent air path lamp-to-collector distance should be approximately 1.25 m or greater. At this distance, the fall-off at the outer edge of a 6 cm diameter diffuse collector would be 0.9994, or -0.06 %, when the diffuser is at $\theta = 0^\circ$ with the normal. The net effect over the entire area of the diffuser would be 0.9997 or -0.03 %. When $\theta = 90^\circ$, with the diffuser edge-on to the lamp, the distance to the lamp varies for different points on the surface. The net error over the entire surface for this condition is 0.99997 or -0.003 %. All other angles fall between these limiting cases.

The $\theta = 0^\circ$ alignment should place the center of the collector on the axis of illumination, with the collector surface oriented normal to the axis. One method of effecting this alignment is to pass a laser (or autocollimator) beam through the location of the filament to the center of the collector. The collector is rotated until a mirror held flat against it reflects the laser (or autocollimator) beam back on itself. The rotational indexing scale should be zeroed in this position. With the alignment laser (or autocollimator) still in place, the collector should be slowly rotated to the $\theta = 90^\circ$; the beam should just graze the collector at $\theta = 90^\circ$ and remain in the center of the collector

at the intermediate angles. The alignment and rotational apparatus should be adjusted until these angular alignment criteria are satisfied. Note that success in this alignment procedure also depends on orienting the illumination axis normal to the tank's window.

The instrument responses $V(\lambda, 0)$ are initially recorded for $\theta = 0^\circ$. The instrument alignment is rotated at 5° intervals to $\theta = 90^\circ$, and the instrument responses $V(\lambda, \theta)$ measured for each alignment angle. The $V(\lambda, 0)$ responses are recorded at the beginning, the middle, and the end of each run and examined as a measure of lamp and instrument stability over the time involved. If the angular indexing mechanism allows rotation in either direction, the procedure should then be repeated in the $-\theta$ direction to complete the characterization of directional response in one plane perpendicular to the collector surface. If the apparatus allows rotation in only one direction, then the instrument should be rotated about the optical axis (normal to the collector), and the procedure repeated to complete the plane. At least two sets of such runs should be made about different axes through the surface of the diffuser.

The directional response of the instrument (for each azimuth scanned) is expressed as $\frac{V(\lambda, \theta)}{V(\lambda, 0)}$, which should ideally equal $\cos\theta$. The angular distribution of relative error in a radiometer's cosine-response is, therefore, $\frac{V(\lambda, \theta)}{V(\lambda, 0)\cos\theta} - 1$.

Assuming the average response to the four measurements made at each θ_i (four separate azimuth angles about the normal to the collector) adequately represent the overall mean cosine response of the collector, then the error, ε in measuring irradiance for a uniform radiance distribution is approximately

$$\varepsilon = \frac{\sum_{i=0}^N \bar{V}(\theta_i) \sin \theta_i \Delta\theta}{\sum_{i=0}^N \cos \theta_i \sin \theta_i \Delta\theta} - 1, \quad \theta_0 = 0, \quad \theta_N = \frac{\pi}{2} \quad \text{and} \quad \Delta\theta = \frac{\pi}{2N}, \quad (3.21)$$

using a simple trapezoidal quadrature. Similarly, for a radiance distribution of the form $1 + 4\sin\theta$, to simulate upwelled irradiance, the approximate error is

$$\varepsilon = \frac{\sum_{i=0}^N \bar{V}(\theta_i) (1 + 4\sin \theta_i) \sin \theta_i \Delta\theta}{\sum_{i=0}^N \cos \theta_i (1 + 4\sin \theta_i) \sin \theta_i \Delta\theta} - 1, \quad \theta_0 = 0, \quad \theta_N = \frac{\pi}{2} \quad \text{and} \quad \Delta\theta = \frac{\pi}{2N}. \quad (3.22)$$

The asymmetry of the cosine response, δ is equivalent to an effective tilt of an ideal cosine collector with respect to the instrument's mechanical axis, which can be quantified as

$$\delta = \frac{\int_{\theta_1}^{\theta_2} \cos(\theta + \theta_t) \sin \theta d\theta}{\int_{\theta_1}^{\theta_2} \cos(\theta - \theta_t) \sin \theta d\theta}, \quad (3.23)$$

where θ_t is the tilt angle.

The measured asymmetry is computed as the ratio of sums of measurements at opposite azimuth angles $\phi(\theta \geq 0)$ and $-\pi(\theta < 0)$ in the same plane, that is,

$$\delta = \frac{\sum_{i=0}^N \bar{V}(\theta_i, 0) \sin \theta_i \Delta\theta}{\sum_{i=0}^N \bar{V}(\theta_i) \sin \theta_i \Delta\theta} - 1, \quad \theta_0 = 0, \quad \theta_N = \frac{\pi}{2} \quad \text{and} \quad \Delta\theta = \frac{\pi}{2N}. \quad (3.24)$$

Variations in asymmetry from channel to channel may be due to the placement of the individual detectors behind the diffuser. Any offset of the average asymmetry with the mechanical axis could be due to any one of a variety of causes:

- the alignment on the rotating test fixture not being correct,
- tilt of the diffuser,
- the detector array not being centered,
- nonuniformity of the reflectance of the internal surfaces of the instrument between the diffuser and the sensor array, or
- nonuniformity of the diffuser.

3.8 LINEARITY AND ELECTRONIC UNCERTAINTY

The linearity of the radiometric channels must be determined over their expected range of use. The above-surface (deck cell) and underwater irradiance sensors intended for the measurement of downwelling irradiance have full-scale (saturation) values that are not readily obtained with the usual incandescent blackbody sources, such as 1000 W, 3200 K tungsten-halogen projection lamps. The linearity at the high end of the calibrated range may be determined by using 900 W to 2,000 W high pressure xenon arc lamps, which provide a small, stable source of high intensity (approximately 6000 K) radiation. With such lamps, irradiance levels approximating full sunlight can be attained. Using such sources for the high-end of the sensor's response range, and the more easily managed tungsten-halogen lamps over the range below 20 % to 30 % of full scale, the linearity of the response characteristic of the radiometric channels can be assessed. The flux should be changed in 5 db (0.5 log), or less, steps using a proven and accepted procedure for controlling irradiance such as inverse square law, or calibrated apertures. These suggested procedures for testing linearity at the higher levels are not well established in practice, and research is needed to determine the precision that can be attained.

If departures from linearity are found, they must be incorporated into the calibration function for the instrument and be properly applied to the raw data to obtain calibrated irradiance and radiance data.

It is recommended that all instruments utilizing inputs from ancillary sensors, e.g., transmissometers, be characterized for the linearity and uncertainty of the voltage measurement covering the full output range of the ancillary sensor. For instruments with range dependent gain changing, either manual or automatic, the scale offset and linearity for each range should, at a minimum, be tested annually. Uncertainties exceeding 0.1 % of any reading within the normal working range must be investigated and corrected.

Other characteristics of electronic sensor systems may adversely affect measurement uncertainty. During the design and engineering prototype development of a radiometer, the design and implementation must be analyzed to characterize, and correct as needed, possible effects of hysteresis, overload, recovery times, cross talk between either optical transducers or electronic channels, and sensitivity to orientation in the Earth's magnetic field, which is particularly likely with photomultiplier tubes.

3.9 TEMPORAL RESPONSE

The temporal response of a spectrometer may be examined by introducing a step function of near full-scale flux to the system using an electrically operated shutter and measuring the system's transient response at 0.1 s, or shorter, intervals. The response should be stable within one digitizing step, or 0.1 %, whichever is greater, of the steady state value in one second or less.

3.10 TEMPERATURE CHARACTERIZATION

Two major types of temperature-induced variation may be seen in an optical radiometric instrument: 1) offset or *dark* changes, and 2) scale *responsivity* changes. Each underwater instrument must be individually characterized over the range of $-2\text{ }^{\circ}\text{C}$ to $40\text{ }^{\circ}\text{C}$. In the case of deck cells, the temperature range for testing should be extended to $10\text{ }^{\circ}\text{C}$ to $45\text{ }^{\circ}\text{C}$. Sensors exhibiting temperature coefficients greater than 0.01 % per $^{\circ}\text{C}$ over this temperature range, should be fully characterized over their respective ranges to establish the means and precision with which

post-acquisition processing can be used to correct for temperature dependency. Although knowledge of the zero, or dark current, drift is essential for working at the lowest radiances or irradiances, it should be emphasized that more significant near-surface errors may be induced by temperature variations in responsivity.

These possible responsivity changes must be individually determined across the spectrum. In the above discussion, the temperatures cited are *environmental* temperatures, but it should be emphasized that any correction must use the temperature of the affected element, which is normally in the interior of the instrument. This is best accomplished by routinely using temperature sensors placed at critical locations within the instrument. For highest precision, dynamic temperature testing involving temporal transients, as well as possible temperature gradients within an instrument, may be appropriate.

3.11 PRESSURE EFFECTS

Pressure can cause radiometric measurement errors by deforming irradiance collectors. Pressure coefficients associated with polytetrafluoroethylene (PTFE) based irradiance diffusers are known to exist, but they are not uniform and there may be hysteresis effects. It is recommended that each type of irradiance detector be examined for variations in responsivity with pressure. If a significant effect is observed, then pressure-dependent responsivity coefficients should be determined separately for each instrument and collector. The pressure characterization should also test for, and quantify, hysteresis and temporal transients in responsivity under a time varying pressure load. The characterization of pressure effects has not previously been common practice, and the requisite procedures are therefore poorly defined; new protocols must be developed.

3.12 PRESSURE TRANSDUCER CALIBRATION

The radiometer's pressure transducer, which is used to measure instrument depth during profiles, should be tested and calibrated before and after each major cruise (Volume II, Chapter 1, Sect. 1.9).

3.13 POLARIZATION SENSITIVITY

Polarization sensitivity is more critical in above-water radiometry than underwater radiometry. If a radiometer measures polarization components of radiance, then its responsivity and rejection of cross-polarization radiance must be characterized for each component channel. For above-water scalar radiance instruments, as with the SeaWiFS and other ocean color radiometers, sensitivity to linear polarization must be less than 2 %, and the actual degree of polarization sensitivity must be characterized for each channel. A protocol for characterizing the polarization sensitivity of a radiometer is described in Volume II, Chapter 4 (Sect. 4.3). Other laboratory procedures for characterizing polarization sensitivity of a radiometer are described by Hooker *et al.* (2002).

REFERENCES

- Austin, R.W. and G. Halikas, 1976: The index of refraction of seawater. *SIO Ref. 76-1*, Vis. Lab., Scripps Inst. of Oceanography, La Jolla, California, 64pp.
- Biggar, S.F. 1998: Calibration of a visible and near-infrared portable transfer radiometer. *Metrologia*, **35**: 701-706.
- Brown, S.W., G.P. Eppeldauer and K.R. Lykke, 2000: NIST facility for spectral irradiance and radiance response calibrations with a uniform source. *Metrologia*, **37**: 579-589.
- Hooker, S.B., S. McLean, J. Sherman, M. Small, G. Lazin, G. Zibordi and J.W. Brown, 2002. The Seventh SeaWiFS Intercalibration Round-Robin Experiment (SIRREX-7), March 1999. *NASA Tech. Memo. 2002-206892, Vol. 17*. S.B. Hooker and E.R. Firestone [Eds.], NASA Goddard Space Flight Center, Greenbelt, MD. 69pp.
- Johnson, B.C., S.S. Bruce, E.A. Early, J.M. Houston, T.R. O'Brian, A. Thompson, S.B. Hooker and J.L. Mueller, 1996: The Fourth SeaWiFS Intercalibration Round-Robin Experiment (SIRREX-4), May 1995. *NASA Tech. Memo. 104566, Vol. 37*, S.B. Hooker, E.R. Firestone and J.G. Acker, Eds., NASA GSFC, Greenbelt, Maryland, 65 pp.

- Johnson, B. C., J.B. Fowler, and C.L. Cromer, 1998: The SeaWiFS Transfer Radiometer (SXR). *NASA Tech. Memo. 1998-206892, Vol. 1*, S.B. Hooker and E.R. Firestone, Eds., NASA Goddard Space Flight Center, Greenbelt, Maryland, 58 pp.
- McLean, J.T., and B.W. Guenther, 1989: Radiance calibration of spherical integrators. *Optical Radiation Measurements II, SPIE*, 1, **109**, 114--121.
- Meister, G., P. Abel, R. Barnes, J. Cooper, C. Davis, M. Godin, D. Goebel, G. Fargion, R. Frouin, D. Korwan, R. Maffione, C. McClain, S. McLean, D. Menzies, A. Poteau, J. Robertson, and J. Sherman, 2002. The First SIMBIOS Radiometric Intercomparison (SIMRIC-1), April-September 2001, *NASA Tech. Memo. 2002-206892*, NASA Goddard Space Flight Center, Greenbelt, MD. 60pp.
- Mueller, J.L., 1993: The First SeaWiFS Intercalibration Round-robin Experiment SIRREX-1, July 1992. *NASA Tech. Memo. 104566, Vol. 14*, S.B. Hooker and E.R. Firestone, Eds., NASA Goddard Space Flight Center, Greenbelt, Maryland, 60 pp.
- Mueller, J.L., 1995: Comparison of irradiance immersion coefficients for several marine environmental radiometers (MERs), In: Mueller, J.L. and others, Case Studies for SeaWiFS Calibration and Validation, Part 3. *NASA TM 104566, Vol. 27*: 3-15, Hooker, S.B., E.R. Firestone and J.G. Acker, Eds.
- Mueller, J.L., B.C. Johnson, C.L. Cromer, J.W. Cooper et al. 1994: The Second SeaWiFS Intercalibration Round-robin Experiment SIRREX-2, June 1993. *NASA Tech. Memo. 104566, Vol. 16*, S.B. Hooker and E.R. Firestone, Eds., NASA Goddard Space Flight Center, Greenbelt, Maryland, 121 pp.
- Mueller, J.L., and R.W. Austin, 1995: Ocean Optics Protocols for SeaWiFS Validation, Revision 1. *NASA Tech. Memo. 104566, Vol. 25*, S.B. Hooker and E.R. Firestone, Eds., NASA Goddard Space Flight Center, Greenbelt, Maryland, 66 pp.
- Mueller, J.L., B.C. Johnson, C.L. Cromer, S.B. Hooker, J.T. McLean and S.F. Biggar, 1996: The Third SeaWiFS Intercalibration Round-Robin Experiment (SIRREX-3), 19-30 September 1994. *NASA Tech. Memo. 104566, Vol. 34*, S.B. Hooker, E.R. Firestone and J.G. Acker, Eds., 78 pp.
- Petzold T.J. & R.W. Austin 1988: Characterization of MER-1032. *Tech.Memo.EV-001-88t*, Vis.Lab.,Scripps Institution of Oceanography, La Jolla, California, 56 pp.
- Riley, T. and S. Bailey, 1998: The Sixth SeaWiFS Intercalibration Round-Robin Experiment (SIRREX-6) August—December 1997. *NASA/TM-1998-206878*. NASA, Goddard Space Flight Center, Greenbelt, MD. 26pp.
- Walker, J.H., R.D. Saunders, J.K. Jackson, and D.A. McSparron, 1987: Spectral Irradiance Calibrations. NBS Special Publication 250--20, U.S. Dept. of Commerce, National Bureau of Standards, Washington, DC, 37 pp. plus appendices.
- Walker, J.H., C.L. Cromer, and J.T. McLean, 1991: Technique for improving the calibration of large-area sphere sources. *Ocean.Optics*, B.W. Guenther, Ed., SPIE, **1,493**, 224-230
- Yoon, H.W., C.E. Gibson and P.Y. Barnes, 2002: The realization of the NIST detector-based spectral irradiance scale. *Appl. Opt.* (submitted).
- Zibordi, G., D. D'Alimonte, D. van der Linde, J.F. Berton, S.B. Hooker, J.L. Mueller, G. Lazin and S. MacLean, 2002: The Eighth SeaWiFS Intercalibration Round-Robin Experiment (SIRREX-8), September – December 2001. *NASA Tech. Memo. 2002-206892, Vol. 21*, Hooker, S.B. and E.R. Firestone [Eds.], NASA Goddard Space Flight Center, Greenbelt, Maryland, 43pp.

Chapter 4

Calibration of Sun Photometers and Sky Radiance Sensors

Christophe Pietras¹, Mark Miller², Kirk D. Knobelspiesse³, Robert Frouin⁴, Brent Holben⁵ and Ken Voss⁶

¹*Science Applications International Corporation, Beltsville, Maryland*

²*Department of Applied Science, Brookhaven National Laboratory, Upton, New York*

³*Science Systems and Applications, Inc., Greenbelt, Maryland*

⁴*Scripps Institution of Oceanography, University of California, San Diego, California*

⁵*Biospheric Sciences Branch, NASA Goddard Space Flight Center, Greenbelt, Maryland*

⁶*Physics Department, University of Miami, Florida*

4.1 INTRODUCTION

Atmospheric sensors are designed to measure direct solar signals and sky radiances in order to retrieve the radiative properties of the atmosphere. There are two major types of instruments in use to perform these measurements: sun photometers and sky radiance scanning systems including fast rotating shadow-band radiometers.

Sun photometers capture photometric intensity of the direct solar beam. Their fields of view are small, typically between 1° and 3°, in order to minimize contamination of the transmitted solar signal by scattered skylight. Some photometers are manually aimed at the sun using sun-sighting optics, while other types of photometers are fixed in place and are equipped with automatic sun-tracking mechanisms.

MicroTops II (Morys *et al.* 1998; Porter *et al.* 1999) and SIMBAD (Deschamps *et al.* 2000; Fougnie *et al.* 1999a, 1999b) are two examples of hand-held sun photometers. The fields of view (FOV) of hand-held sun photometers are typically between 2° and 3°, which is generally larger than the FOVs of the automatic sun-tracking photometers (Table 4.1). The wider FOV allows the user to manually aim the instrument at the sun from the rolling deck of a ship. The even wider field of view of SIMBAD (Table 4.1) is intended to measure marine reflectance as well as the solar signal. An improved version, called SIMBADA, has been recently developed and is available since 2001. SIMBADA new features are an integrated GPS and 11 channels.

Examples of fixed, automated tracking sun photometers include the CIMEL (Holben *et al.*, 1998) and the PREDE (Nakajima *et al.*, 1996). The design of a particular sun tracking mechanism is dependent on whether it is to be used on a moving platform (e.g., PREDE POM-01 Mark II), or on a stable station (e.g., CIMEL, PREDE POM-01L). CIMEL and PREDE instruments perform both sun photometric and sky radiance measurements. In sky radiance mode, these instruments measure sky radiances within 3° of the sun in the aureole, and also scan the sky radiance distribution in the principal solar plane. The FOV of the CIMEL and PREDE instruments are less than 1.5° and the instruments are equipped with collimators for stray light rejection (O'Neill *et al.*, 1984; Holben *et al.* 1998; Nakajima *et al.* 1996).

Fast rotating shadow-band radiometers measure solar intensity values indirectly from diffuse and global upper hemispheric irradiance. They have a 2π FOV and are equipped with a solar occulting apparatus. Finally, electronic camera systems equipped with “fisheye” lenses may be used to measure the full sky radiance distribution (Voss *et al.* 1989).

Sun photometers and sky radiometers commonly have several channels from 300 nm to 1020 nm and narrow bandwidths (approximately 10 nm). Their characteristics are summarized in Table 4.1. This chapter will describe calibration techniques, and uncertainties of the sun photometers and sky radiometers. Measurement and data analysis protocols and procedures are discussed in Volume III, Chapter 5.

4.2 CALIBRATION TECHNIQUES FOR SUN PHOTOMETERS

To calibrate sun photometers, it is necessary to take into account degradation of detectors and interference filters. The absolute calibration using lamp standards is generally not recommended for the retrieval of aerosol optical thickness (AOT). However, in case of a strong loss of sensitivity over time, Schmid *et al.* (1998) advised combining lamp calibration with solar calibration and discussed the applicability and accuracy of the method. The following subsections will present techniques commonly used with sun photometers and their validities.

Langley – Bouguer Technique

The signal measured by a sun photometer, assuming that the instrument is aimed directly into the sun and its spectral channels are not affected by gaseous absorption, may be expressed as

$$V(\lambda) = V_o(\lambda) \left(\frac{d_o}{d} \right)^2 e^{-M(\theta_o)[\tau_R(\lambda) + \tau_{O_3}(\lambda) + \tau_a(\lambda)]}, \quad (4.1)$$

where $V_o(\lambda)$ is the signal representing the instrument response to solar flux at the top of the atmosphere (TOA) as derived from the Langley-Bouguer calibration procedure, $\left(\frac{d_o}{d} \right)^2$ is the earth-sun distance correction obtained according to Iqbal (1983), θ_o is the solar zenith angle, air mass $M(\theta_o)$ is a function of the solar zenith angle computed according to Kasten and Young (1989), $\tau_R(\lambda)$ is the Rayleigh optical thickness calculated according to Penndorf (1957), $\tau_{O_3}(\lambda)$ is the ozone optical thickness calculated from the ozone amount retrieved from a satellite ozone sensor, such as Total Ozone Mapping Spectrometer (TOMS), and $\tau_a(\lambda)$ is the aerosol optical thickness (AOT).

The purpose of the Langley-Bouguer technique is to obtain the unknown instrument response to the solar flux at the top of the atmosphere, $V_o(\lambda)$. This is achieved by plotting the logarithm of the signal $V(\lambda)$ against the air mass $M(\theta_o)$, and extrapolating the signal to $M = 0$. The slope of the logarithmic signal is the total optical depth (Rayleigh, ozone and aerosol). The protocol is detailed below:

1. As $M(\theta_o)$ varies from 1 to 6 over the course of the day, take five successive measurements each time the air mass changes by 0.25.
2. Measure the dark current frequently to avoid temperature effects.
3. Record the sky condition in case of clouds or thin cirrus occurrences (includes cloud coverage and cloud positions in the sky).
4. Stop when M reaches 7, or the sky condition changes.

The main constraint in the Langley-Bouguer technique is the stability of the atmospheric optical extinction. Hence, the uncertainty greatly depends on the geographical location of the calibration experiment. The calibration is generally performed in conditions where the stability of the atmosphere and a low aerosol contribution enable high accuracy of the method (Holben *et al.* 1998; Schmid *et al.* 1998). The site of Mauna Loa Observatory (MLO), Hawaii, is particularly well suited for calibrating optical instruments. The facilities and research activities at the observatory are reported on its web site <http://mloserv.mlo.hawaii.gov/>. The altitude of the Mauna Loa site (3397 m) reduces the uncertainties due to variability in aerosols and water vapor, both of which commonly affect measurements in the lower atmospheric layers.

Variations in the atmosphere dramatically affect $V_o(\lambda)$ retrievals. Several improvements to the Langley-Bouguer technique have been proposed, such as using a calibrated reference channel (Soufflet *et al.* 1992) and the circumsolar radiation (Tanaka *et al.* 1986). A review of different methods and their uncertainties are discussed in Forgan, 1994.

Uncertainty of the Langley – Bouguer Technique

The Langley-Bouguer technique has been commonly used, although it is not an absolute calibration method and has large uncertainties. Combining several Langley-Bouguer sessions in high altitude conditions minimizes of the uncertainties. AERONET reference instruments are typically recalibrated at MLO every 2-3 months using the Langley-Bouguer technique. According to Holben *et al.* (1998), the uncertainties in TOA voltages are estimated to be as low as 0.2 % to 0.5 % for the MLO calibrated instruments. Therefore, the uncertainty in AOT due to the ambiguities in TOA voltages for the reference instruments is better than 0.002 to 0.005 in absolute values.

Figure 4.1 presents typical Langley-Bouguer plot for CIMEL #101 at MLO (circles) and at GSFC (squares). The total optical thickness at MLO is nearly half that of GSFC. The maximum difference in AOTs derived from GSFC and MLO sites is 0.05 for the air mass of 1. Therefore, MLO is an attractive calibration site for this technique.

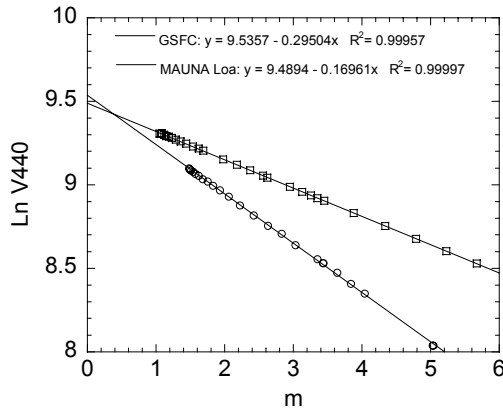


Figure 4.1: The Langley-Bouguer technique applied to CIMEL # 10 sun photometer measurements at 440nm. (o) - Mauna Loa Observatory, September 11, 1999, and (□) - GSFC, October 15, 1999.

In addition to the uncertainty in the retrieval of $V_o(\lambda)$, there are other sources of uncertainty in the Langley-Bouguer technique, including computations of the solar zenith angle, air mass, earth-sun distance and Rayleigh and ozone corrections:

1. **Solar zenith angle computation:** The solar position is retrieved using a simple algorithm based on codes from Michalsky (1988) and Spencer (1989), and *The Astronomical Almanac*. The uncertainty of the solar position calculated using this algorithm is 0.01^0 until the year 2050.
2. **Earth-sun distance correction:** The earth-sun distance correction $\left(\frac{d_o}{d}\right)^2$ is dependent on the ratio of the average to the actual earth-sun distance. It can be computed according to Iqbal (1983) as

$$\left(\frac{d_o}{d}\right)^2 = 1 + \left[0.034 \cos\left(\frac{2\pi J}{365}\right)\right], \quad (4.2)$$

where J is the sequential day of the year. This factor is sometimes computed using an alternative approximation due to Platridge (1977). Differences between the two algorithms vary between 0 and 3%.

3. **Air mass computation.** The precise Langley-Bouguer technique requires taking into account the structure of atmospheric constituents that attenuate sunlight (Schotland *et al.* 1986; Forgan 1988). $M(\theta_o)$ can be computed according to Kasten (1966), or Kasten and Young (1989) [used here as

Equation (5.3) in Volume III, Chapter 5]. For solar zenith angles $\theta_0 \leq 75^\circ$, the differences between these two formulations are lower than 0.1 %. For larger zenith angles, the air mass changes differently for different atmospheric attenuation components. This problem is avoided by limiting the range of θ_0 in the Langley-Bouguer technique. Various authors use different computations of the air mass for determining attenuation by ozone. Holben *et al.* (1988) used the ozone air mass calculation proposed by Komhyr *et al.* (1989), while Schmid *et al.* (1998) used the formulation introduced by Stählerin *et al.* (1995).

4. **Ozone and Rayleigh correction:** The ozone optical depth is determined from TOMS measurements of ozone amounts in Dobson units. Ozone absorption coefficients are derived from Nicolet *et al.* (1981). The Rayleigh optical depth is computed using values from Penndorf (1957), corrected for the site elevation, but Deschamps *et al.* (1983) use a different algorithm. Differences between the results are less than 2.5 % in the spectral range from 300 nm to 1020 nm. The principal uncertainty in the Rayleigh optical thickness is associated with variability in atmospheric pressure. Eck *et al.* (1989) computed the combined uncertainties associated with calibration, ozone optical thickness, and Rayleigh optical thickness. The total combined uncertainty in AOT was estimated to range between 0.010 to 0.021 for field instruments, and 0.002 to 0.009 for the reference instruments calibrated using the Langley-Bouguer technique.

Cross-Calibration Technique

The cross-calibration technique is a cost-effective and efficient method for calibrating sun photometers relative to instruments that have been calibrated using the demanding Langley-Bouguer method at ideal locations like MLO. The cross-calibration technique is based on simultaneous measurements taken from both calibrated and non-calibrated sun photometers. Observations with minimal time differences between measurements and an air mass less than 3 are required. TOA voltages are computed as

$$V_o(\lambda) = V_o^{\text{ref}}(\lambda) \frac{V(\lambda)}{V^{\text{ref}}(\lambda)}, \quad (4.3)$$

where $V_o^{\text{ref}}(\lambda)$ is the TOA signal of a reference CIMEL sun photometer calibrated at Mauna Loa by the Langley-Bouguer technique and $V(\lambda)$ and $V^{\text{ref}}(\lambda)$ are the signals measured by the non-calibrated and reference sun photometers, respectively, for channels at the same wavelength λ .

Some sun photometers have channels λ_i that are slightly different from the wavelengths of any of the channels of the reference sun photometer. In this situation, the channel of the reference sun photometer with the wavelength λ_j that is nearest to λ_i is used. To calculate TOA voltages as

$$V_o(\lambda_i) = V_o^{\text{ref}}(\lambda_j) \frac{V(\lambda_i)}{V^{\text{ref}}(\lambda_j)} e^{M(\theta_0) \{ [\tau_R(\lambda_i) - \tau_R(\lambda_j)] + [\tau_{O_3}(\lambda_i) - \tau_{O_3}(\lambda_j)] + \tau_a(1 \mu\text{m})(\lambda_i^\alpha - \lambda_j^\alpha) \}}, \quad (4.4)$$

where the exponential term is the ratio of transmittances expressed as differences in Rayleigh, ozone and aerosol optical depths for wavelengths λ_i and λ_j , which in this instance are expressed in μm . The variables α and $\tau_a(1 \mu\text{m})$ are, respectively, the Angström coefficient and the aerosol optical thickness at $\lambda = 1 \mu\text{m}$, determined from the reference CIMEL measurements. Using the Angström law, AOT at any other wavelength is conveniently determined as

$$\tau_a(\lambda) = \tau_a(1 \mu\text{m}) \lambda^{-\alpha}. \quad (4.5)$$

The reference sun photometer is one of a selected set of CIMEL sun photometers managed by the AERONET group and calibrated every three months, using the Langley-Bouguer technique at MLO. As shown in Table 4.2, most of the sun photometers have common channels with the CIMEL reference sun photometer, allowing for the application of the cross-calibration technique. The stability of the aerosol extinction is not very critical with this method. However, standard deviations of TOA voltages over time still need to be determined. The protocol is summarized below:

1. Set the GMT time on both calibrated and non-calibrated sun photometers.

2. Initiate measurements as soon as the calibrated sun photometer starts working.
3. Take measurements concurrently with the calibrated sun photometer.
4. Take all the measurements between 10 a.m. and 3 p.m. local time to have suitable air mass.
5. Measure the dark current in order to avoid temperature effects.
6. Record the sky condition in case of clouds or thin cirrus occurrences (cloud coverage and cloud positions in the sky).
7. Stop when M reaches 3 or the sky condition changes.

Accuracy and Limitations of the Cross Calibration Technique

SIMBIOS sun photometers are routinely cross-calibrated at least every three months, or before each campaign. Calibrations are performed during days with clear and stable atmospheric conditions (AOT at 440 nm typically lower than 0.15). The uncertainties of the cross-calibration are composed of uncertainties in the calibrated reference sun photometer and the non-calibrated sun photometer. The calibration of the reference sun photometers is performed by the AERONET group. The calibration transfer from the MLO reference sun photometers to non-calibrated instruments at least doubles the $V_o(\lambda)$ uncertainty for instruments of the same design. According to Holben *et al.* (1998), the uncertainty in AOTs obtained for cross-calibrated CIMEL instruments are estimated to be 0.01 to 0.02. The uncertainties are higher when the cross-calibrated sun photometer is not of the same design as the reference sun photometer.

For cross-calibrated MicroTops, SIMBAD and PREDE the TOA voltages are determined with uncertainties lower than 1 % (i.e. 0.02 in terms of AOT). Figure 4.2 shows the time series of TOA voltages obtained at GSFC since 1998 (in 2001 for the PREDE). Channels 440 nm and 870 nm are presented. Four reference CIMELs were (S/N 94, 37, 27 and 101) calibrated at MLO were used. TOA voltages retrieved in all bands are reported in Table 4.2. The decay of calibration over time is generally less than 5% per year for SIMBAD and MicroTops. A cross calibration every 3 months allows accounting for the decay over time. However, a larger decay (10%/yr) is observed in some of the channels of MicroTops. The decay is significant and requires a change of the corresponding filter and eventually the photodiode of the instrument. The main source of error in retrieving AOT using sun photometry is the TOA voltages. Since Voltz (1959), several papers have discussed different methods to improve the solar calibration. Schmid *et al.* (1998) used lamp and solar calibrations in conjunction with each other. O'Neill *et al.* (1984) combined solar aureole and solar beam extinction. Soufflet *et al.* (1992) and Holben *et al.* (1998) used a well-calibrated sun photometer as a reference.

The degradation of interference filters is the most important source of the long-term variability in the cross calibration. Although major improvements have been made on the filter design (e.g., ion-assisted deposition interference filters), degradation over time in filter spectral transmittances remains as the main factor limiting the performance of sun photometers. Degradation of filters necessitates frequent calibration of sun photometers, and measurements of the filter transmission or the relative system response (Schmid *et al.*, 1998). The degradation of the filters mounted on the CIMEL sun photometers has been monitored since 1993. Degradation reported by Holben *et al.* (1998) was between 1 and 5% during the first 2 years of CIMEL operation by the AERONET Project.

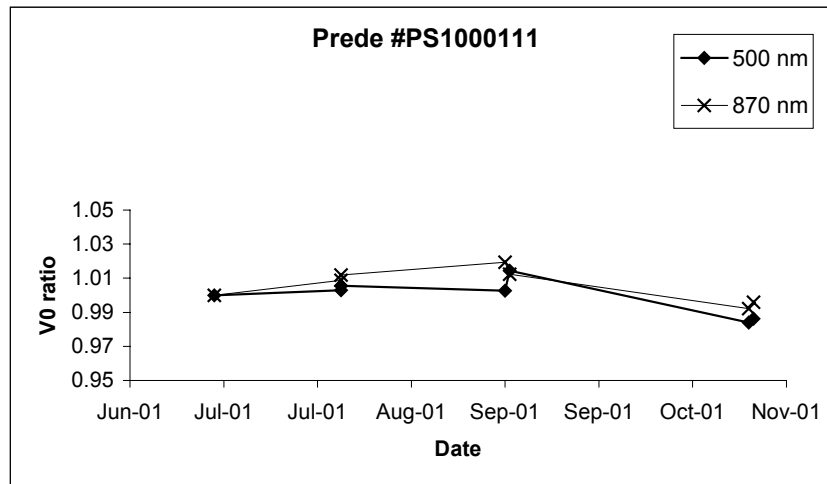
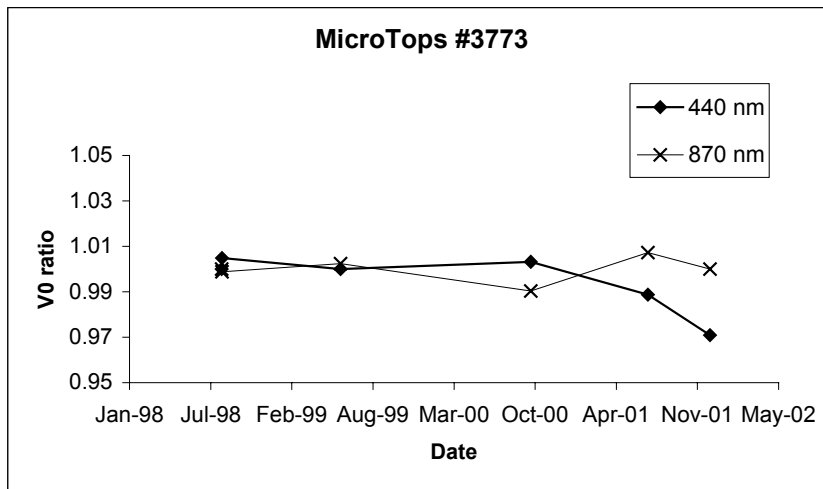
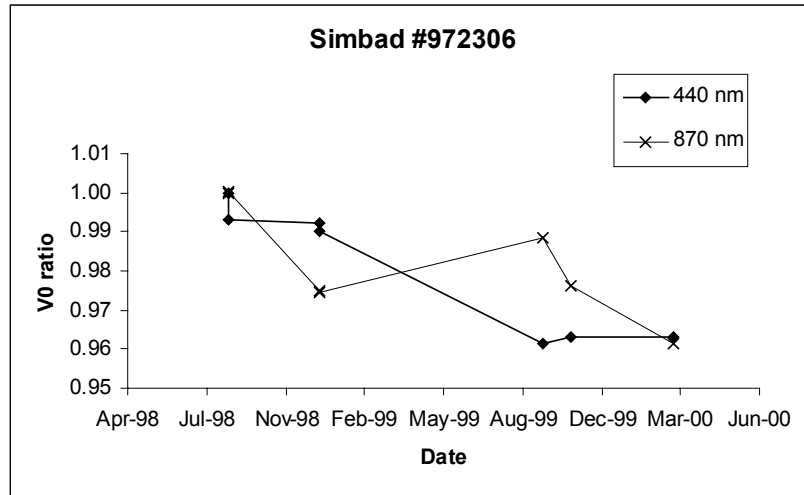


Figure 4.2: Time series of cross calibration since 1998 for SIMBAD and MicroTops, in 2001 for PREDE

4.3 CALIBRATION TECHNIQUES FOR SKY RADIOMETERS

Sky radiance scanning systems are automated instruments dedicated to measure sky radiances in the aureole and in the principle plane of the sun. Radiative properties of aerosols are retrieved using an inversion algorithm of the sky radiances (Dubovik *et al.* 2000; Nakajima *et al.* 1996) and of the polarized component of the sky radiances (Vermeulen *et al.* 2000). This section is dedicated to the description of calibration techniques for accurate retrievals of sky radiances.

Calibration of Unpolarized Sky Radiometers

Unpolarized radiometers, such as CIMEL and PREDE, are calibrated using an integrating sphere (Volume II, Chapter 3 Sect. 3.2). The radiometer is aligned in front of the sphere (Figure 4.3, top) and 10 measurements are taken for each channel. Radiances of the integrating sphere are then integrated through the domains of each channel of the radiometer. As a result, ratios of raw radiometer voltages to the integrated sphere radiances are obtained. These ratios constitute radiometer calibration parameters C_i :

$$C_i = \frac{V_i}{\int L(\lambda) R_n^i(\lambda) d\lambda}, \quad (4.6)$$

where V_i is the voltages measured in the considered channel i , $R_n^i(\lambda)$ is the normalized spectral response function of the radiometer channel, and $L(\lambda)$ is the spectral radiance scale of the integrating sphere.

Uncertainty of the Calibration of Unpolarized Sky Radiometers

The accuracy of the radiometer calibration is dependent on the calibration of the integrating sphere, sphere's size, clarity of the calibration protocols and precision of the calibration process. A two-meter integrating sphere is available and managed by NASA GSFC Calibration Facility (<http://spectral.gsfc.nasa.gov/>). The uncertainty of the radiances provided by this integrating sphere is estimated to be less than 5%.

Calibration of Polarized Sky Radiometers

The technology to calibrate polarized sun photometers is now available to the SIMBIOS Project. The method was initially designed by the Laboratoire d'Optique Atmosphérique (LOA), Lille, France, for the calibration of POLDER sensor (POLarization and Directionality of the Earth's Reflectances), its airborne (Deuze *et al.* 1992) and space version (Bret-Dibat T. *et al.* 1995; Hagolle *et al.*, 1999).

The polarization box named "POLBOX" is a passive system including neither optical source nor electrical power supply. POLBOX transforms natural light to polarized light. The user's guide for the device (Balois 1999) is available at LOA and GSFC. A Lambertian source is necessary to provide the input light to the box, therefore, an integrating sphere is usually used. POLBOX is composed of two adjustable glass blades that have a high refractive index. The blades are placed in a black anodized aluminum alloy box. The box can turn around the optical axis. The degree of polarization and the direction of the linear polarization plane are tunable by the user by adjusting the position of the box and the blades. The alignment of the blades, relative to the optical axis, is performed by auto-collimation using a basic laser and a mirror. Alignment is required each time the blades are cleaned and replaced in the POLBOX. The required equipment consists of:

1. Polarization device POLBOX.
2. Calibrated light source (integrating sphere).
3. Lambertian light source (integrating sphere or lamp with scattering opaline diffuser).
4. Sun photometer.

The calibration process for polarized radiometers is composed of the following steps:

1. Perform the absolute calibration using the calibrated sphere (Figure 4.3, top) for all radiometer channels, including the polarized ones.
2. Place POLBOX between an integrating sphere and the sun photometer (Figure 4.3, bottom). The integrating sphere is highly recommended for the stability, but its calibration is not essential for determining the relative polarized responses of the instrument.
3. Perform one measurement for each tilt of both blades in POLBOX. A combined tilt is defined and measured by the rotating unit. The tilt of each blade is identical in absolute degrees but shifted in opposite directions.
4. The degree polarization of the light transmitted through the POLBOX to the sensor is given by:

$$P_c(\theta_i) = \frac{A(n)\cos^2(2\theta_i) + B(n)\cos(\theta_i) + C(n)}{D(n)\cos^2(2\theta_i) + E(n)\cos(\theta_i) + F(n)}, \quad (4.7)$$

where A , B , C , D , E , and F are functions of the refractive index n of the blades, and θ_i is the tilt angle of the blades (the same but opposite).

5. Plot the computed degree of polarization against the measured polarization and obtain the intercept of 0° polarization and the slope.

Due to the mechanical limitations of the POLBOX system the maximum degree of polarization that can be reached is 60 %. A 100 % polarization can be obtained using an analyzing polarizing sheet. If needed, the orientation of the polarization can also be determined using POLBOX. Indeed, the orientation of the polarized light is marked on the POLBOX device and a rotating system allows turning POLBOX around the optical axis in order to change the orientation.

The polarized version of CIMEL sun photometers has three polarized channels, each with identical spectral characteristics centered at 870 nm. The polarization axes of the three channels are positioned at intervals exactly 120° apart. The rotating filter wheel of the CIMEL photometer has 9 filter positions, including one opaque filter to measure the dark current. Polarizing covers attached to the filter wheel allow measurement of the three components of the polarized light.

The CIMEL calibration process measures non-polarized signals from the calibrated integrating sphere. The signals are noted V_S^0 , $V_S^{-60^\circ}$, and $V_S^{+60^\circ}$. The use of an unpolarized source implies that each polarized channel measures the same signal. A normalization of the measured signals is then required in order to define the coefficients K_1 and K_2 as

$$K_1 = \frac{V_S^0}{V_S^{-60^\circ}}, \text{ and } K_2 = \frac{V_S^0}{V_S^{+60^\circ}}. \quad (4.8)$$

Next, the sun photometer is placed in front of the POLBOX device and an integrating sphere is used as a light source (Figure 4.3, bottom). Polarized signals are measured in the three polarized channels and noted V_0 , V_{-60} , V_{+60} . The degree of polarization of the light is consequently derived as

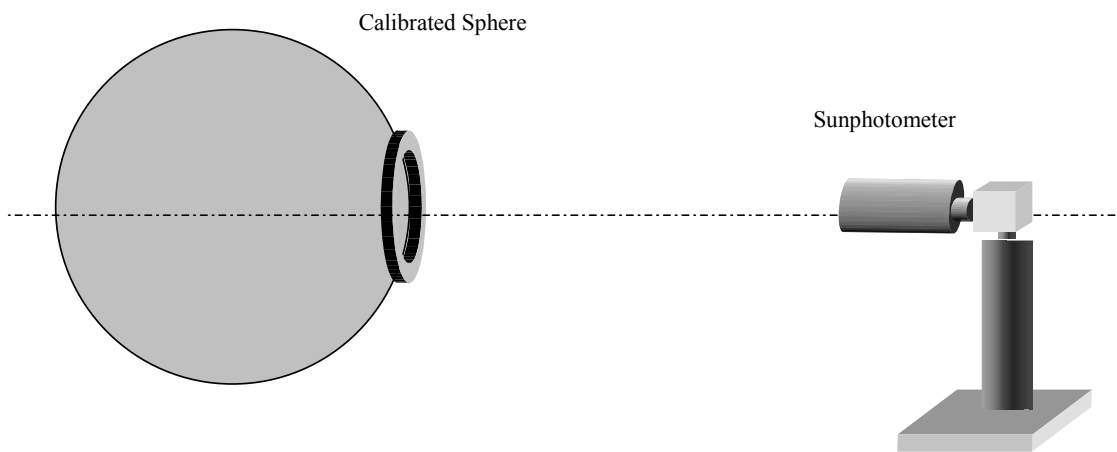
$$P_m = \frac{2\sqrt{K_1^2 V_{-60}^2 + V_0^2 + K_2^2 V_{+60}^2 - K_1 V_{-60} V_0 - K_2 V_{+60} V_0 - K_1 K_2 V_{-60} V_{+60}}}{K_1 V_{-60} + V_0 + K_2 V_{+60}}. \quad (4.9)$$

The calibration is accomplished by plotting the computed degree of polarization against the measured polarization to obtain the 0° of polarization, P_0 , and the slope b . Figure 4.4 presents the calibration of the CIMEL #191 performed at GSFC in May 1999. The angle of the polarized light (Ψ) may also be retrieved as

$$\tan(2\Psi) = \frac{\sqrt{3}(V_{+60} - V_{-60})}{2V_0 - V_{+60} - V_{-60}}. \quad (4.10)$$

Uncertainty of the Calibration of Polarized Sky Radiometers The uncertainty of the calibration of polarized radiometers depends on the uniformity of the ‘‘Lambertian’’ light source, and on the optical characteristics of the polarization device, which must be kept in good condition. Dirty glass blades may introduce a polarization by the device itself. Greasy prints on blade surfaces need to be avoided when manipulating the device during cleaning and maintenance.

The degree of polarization obtained at the output of the device is 60% at maximum due to the mechanical design of POLBOX. 100% of degree of polarization can be obtained using polarizing sheets placed in front of the radiometer. However, it is highly recommended to use the same polarizing sheets as those mounted on the radiometer. Then, adjustment of the polarizing sheets to obtain the extinction of the signal can be performed accurately.



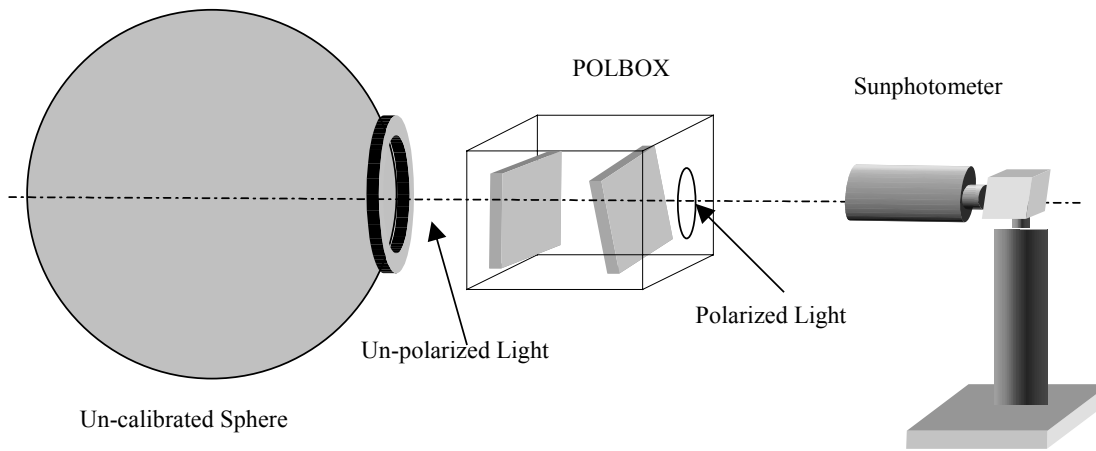


Figure 4.3: Absolute calibration of the CIMEL sun photometer (top); and calibration of the polarized channels of the CIMEL sun photometer (bottom).

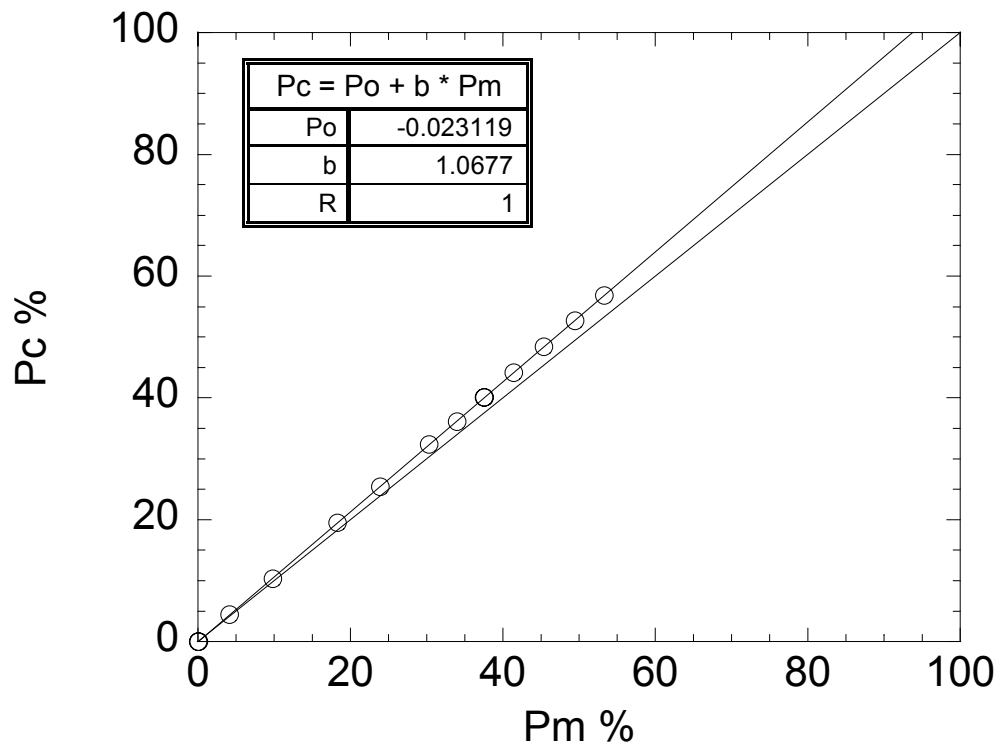


Figure 4.4: Degree of computed polarization versus measured polarization by the CIMEL #191 in May 1999 at GSFC Calibration Facilities.

Calibration and Characterization of Sky Radiance Distribution Cameras

Camera systems for sky radiance distribution measurements, and their uses, are described in Volume III, Chapter 5 of these protocols. Absolute and spectral response calibrations should be performed on the radiance distribution camera before and after each cruise. A full characterization of the instrument should be performed initially, including camera lens roll-off characteristics for each camera (Voss and Zibordi 1989), in addition to the characterization protocols specified in Volume II, Chapter 3. If attenuation devices are used to prevent solar saturation, these should be calibrated frequently to track drift. Linearity calibrations should also be performed with the same frequency as the absolute and spectral response calibrations. Procedures for characterizing this class of instruments are essentially the same as for other radiance detector systems (Volume II, Chapter 3). Each individual detector element in the detector array is essentially regarded as an independent radiometer.

4.4 CALIBRATION OF SHADOW-BAND IRRADIANCE RADIOMETER

Calibration is the most essential element of the shadow-band radiation measurement program. A thorough and on-going calibration process is required before the fast rotating shadow-band radiometer (FRSR) can make accurate radiometric measurements at sea. To insure accurate measurements, there are two important elements for FRSR measurement protocol: calibration of the instrument circuitry, which includes temperature stabilization of the detector during measurements, and determination of the extra-terrestrial constants. The following two subsections discuss these elements and establish protocols.

Calibration of Instrument Circuitry and Temperature Stabilization of the Detector

Laboratory calibration is done in two parts: the optical detector and the electronics attached to the detector. The electronic gains are combined with the direct-normal detector irradiance gains coefficients to make a single calibration equation relating direct-normal irradiance to the electronic measurement in mV.

Initial values for the detector calibration, band-pass response, and zenith angle correction are supplied by the vendor. In addition, the instrument should be periodically recalibrated using the protocols of Volume II, Chapter 3. Each of the narrow-band filters has a bandwidth of approximately 10 nm and the vendor calibration provides gains at 1 nm spacing. The zenith angle correction is measured on two planes, one on a south-to-north plane and one on a west-to-east plane. The zenith angle corrections are determined by holding the head in a tilting fixture under a collimated beam and tilting the head through 180° in one-degree steps from horizon to horizon in each plane (see also Volume II, Chapter 3, Section 3.7)

The end-to-end electronic gains are calibrated using the data collection software and a precision reference voltage source in place of each radiometer channel. One-minute averages and standard deviations of voltages for each channel are logged for a full range of input voltages. Electronic calibrations are repeated at regular intervals and for a variety of ambient temperatures. Calibration of the electronics is performed before and after each deployment.

A silicone cell photodiode has a small leakage current which is called a “dark current”. After amplification in the electronics a “dark voltage” results, and if the dark voltage is not negligible, it must be measured and removed. In some instruments, such as the MICROTUPS II hand-held sun photometer, the operator covers the detector before taking a solar measurement. For an autonomous instrument an electronic design eliminates the dark voltage. For the FRSR, the largest deviation from a straight-line fit is less than 0.1 % of full scale and no “dark voltage” adjustment is required.

Calibration drift in the multi-frequency head has caused a great deal of concern in the sun photometer community. Calibration shift is detectable as a permanent change in the apparent extraterrestrial irradiance E_o as computed by the Langley-Bouguer technique. Calibration shift is erratic and quite variable; it can occur suddenly, over a few weeks, or can degrade slowly over months. The 610 nm and 660 nm channels are most prone to drift, though all narrow-band channels are suspect due to gain drift and shifting bandpass response functions. In earlier heads, the filter material, a stack of laminated films, apparently became delaminated as a result of temperature cycling and humidity. A different filter material became available after approximately December 1998 and many researchers are in the process of retrofitting their heads with the new material.

Determination of the Extra-terrestrial Constants

The Langley-Bouguer technique works whenever the skies are perfectly clear, no cirrus or other layers are present, and if the atmospheric optical depth τ is constant over the time duration of the observations. In practice, a Langley-Bouguer calibration can be produced from about one hour of clear sky in the early morning just after sunrise, or late evening just before sunset when $2 < M(\theta_o) < 6$ (i.e. $60^\circ < \theta_o < 80^\circ$). All measurements of E_N , the normal-beam solar irradiance (see section 14.4), are plotted on a log-linear plot and a best estimate straight line is fitted to the data. For sites other than ideal calibration locations, such as the MLO described below, a median-fitting algorithm provides the best objective fit to the data. Over the ocean, there are almost always clouds on the horizon. In the tropics these are usually high cumulus clouds or cirrus. As a result, Langley-Bouguer measurements from ships are rare gems that must be collected whenever they occur.

As a protocol, E_o 's used in final data products should be computed using the Langley-Bouguer technique at Mauna Loa. The Langley-Bouguer technique should also be used at sea as often as possible as a quality assurance tool, because it provides an excellent means of detecting calibration changes. The top-of-the-atmosphere irradiance, $F_o(\lambda)$, depends on the sun-earth separation, but its mean value, should not change significantly over time. The absolute calibration of the instrument can be compared to the mean reference solar irradiance at the top of the atmosphere, $\bar{F}_o(\lambda)$ (Neckel and Labs, 1984) by integrating the reference solar spectrum over the bandpass of each channel to obtain

$$\bar{F}_o = \frac{\int_0^\infty R_n(\lambda) \bar{F}_o(\lambda) d\lambda}{\int_0^\infty R_n(\lambda) d\lambda}, \quad (4.11)$$

where R_n is the normalized spectral response function of the channel under consideration. For a well-calibrated absolute instrument, $E_o \cong \bar{F}_o$. However, as long as the calibration constant, E_o , is constant, as determined from multiple applications of the Langley-Bouguer technique, accurate AOT estimates are possible. While many investigators use raw voltages to calibrate their instruments, the extra step of computing E_o is important, since it defines the radiative impact of the aerosol at the surface.

Uncertainty of the Calibration of Shadow-Band Irradiance Radiometers

The filter material in shadow-band radiometers is sensitive to temperature. If the head temperature varies from 20 °C to 30 °C, the 500 nm filter will drift by less than 1 nm (Mark Beaubean, Yankee Environmental Systems, personal communication, 1999). Keeping the temperature of the optical detector relatively stable over the range of conditions encountered on a ship can be a challenge. The internal heater in the optical detector is occasionally insufficient for the observed conditions. Providing adequate insulation is the best deterrent, although this issue remains problematic in some conditions and is the subject of current engineering efforts.

The calibration of the shadow-band radiometer is realized using the Langley-Bouguer technique. The technique is subject to the same accuracy constraints and limitations as the Langley-Bouguer calibrated sun photometers described earlier in the chapter.

REFERENCES

- Balois J.Y., 1998: Polarizing box POLBOX User's Guide, *Tech. Report*, Laboratoire d'Optique Atmosphérique, Lille, France, 12pp.
- Bret-Dibat T., Y. Andre' and J.M. Laherrere, 1995: Pre-flight calibration of the POLDER instrument, in *SPIE Proc. Infrared spaceborne remote sensing III*, **2553**, 218-231.
- Deschamps P. Y., B. Fougnie, R. Frouin, P. Lecomte and C. Verwaerde, 2000: SIMBAD: an advanced field radiometer to measure aerosol optical thickness and marine reflectance, *Applied Optics* (submitted).
- Deschamps P. Y., M. Herman M. and D. Tanre, 1983: Model calculation of the reflected solar radiation by the atmosphere and the earth between 0.35 and 4 μm ., *ESA Report*, **4393/80/F/DD**, 156pp.
- Deuze J.L., F.M. Breon, P.Y. Deschamps, P. Goloub and M. Herman, 1992: Polarization measurements with the airborne version of the POLDER instrument, in *SPIE Proc. Polarization and Remote Sensing*, **1747**, 178-187.
- Dubovik O., and M.D. King, 2000: A flexible inversion algorithm for retrieval of aerosol optical properties from Sun and sky radiance measurements, *J. Geophys. Res.* (submitted).
- Eck, T.F, B.N. Holben, J.S. Reid, O. Dubovik, A. Smirnov, N.T. O'Neill, I. Slutsker and S. Kinne, 1999: The wavelength dependence of the optical depth of biomass burning urban and desert dust aerosols, *J. Geophys. Res.*, **104**, 31, 333-31,350.
- Forgan B. W., 1988: Bias in a solar constant determination by the Langley method due to Structured atmospheric aerosol: comment, *App. Opt.*, **27**, **12**, 2546-2548.

- Forgan B. W., 1994: General method for calibrating Sun photometers, *App. Opt.*, **33**, **21**, 4841-4850.
- Fougnie B., R. Frouin, P. Lecompte and P.Y. Deschamps, 1999a: Reduction of skylight reflection effects in the above-water measurements of diffuse marine reflectance, *Appl. Opt.*, **38**, **18**, 3,844-3,856.
- Fougnie B., P.Y. Deschamps, R. Frouin, 1999b: Vicarious Calibration of the POLDER ocean color spectral bands using in situ measurements, *IEEE Trans. Geosc. & Remote Sensing*, ADEOS special issue, **37**, **3**, 1,567-1,574.
- Goloub P., J.L. Deuze, M. Herman and Y. Fouquart, 1994: Analysis of the POLDER polarization measurements performed over cloud covers, *IEEE Trans Geosc. & Remote Sensing.*, **32**, **1**, 78-88.
- Hagolle O., P. Goloub, P.Y. Deschamps, H. Cosnefroy, X. Briottet, T. Bailleul, J.M. Nicolas, F. Parol, B. Lafrance and M. Herman, 1999: Results of POLDER in-flight calibration, *IEEE Trans. Geosc. & Remote Sensing*, **37**, **3**, 1550-1566.
- Holben B.N., T.F. Eck, I. Slutsker, D. Tanre, J.P. Buis, A. Setzer, E. Vermote, J.A. Reagan, Y.L. Kaufman, T. Nakajima, F. Lavenu, I. Jankowiak, A. Smirnov, 1998: A federated instrument network and data archive for aerosol characterization, *Remote Sens. Environ.*, **66**, 1-16.
- Iqbal M., 1983: An introduction to Solar Radiation, Academic, San Diego, CA, 390pp.
- Kasten F. and A.T. Young, 1989: Revised optical air mass tables and approximation formula, *Appl. Opt.*, **28**, **22**, 4735-4738.
- Kasten F., 1965: A new table and approximation formula for relative optical airmass, *Arch. Meteorol. Geophys. Bioklimatol. Ser.*, **B14**, 206-223.
- Komhyr W. D., R.D. Grass, and R.K. Leonard, 1989: Dobson Spectrophotometer 83: a standard for total ozone measurements, 1962-1987, *J. Geophys. Res.*, **94**, 9847-9861.
- Morys, M., F.M. Mims, S.E. Anderson, 1998: Design calibration and performance of MICROTOPS II hand-held ozonemeter, <http://www.solar.com/ftp/papers/mtops.pdf>, 12pp.
- Nakajima T., G. Tonna, R. Rao, P. Boi, Y.L. Kaufman, B. Holben, 1996: Use of Sky brightness measurements from ground for remote sensing of particulate polydispersions, *Appl. Opt.*, **35**, **15**, 2672-2686.
- Neckel, H. and D. Labs, 1984: The solar radiation between 3,300 and 12,500 AA. *Solar Phys.*, **90**, 205-258.
- Nicolet M., 1981: The solar spectral irradiance and its action in the atmospheric photodissociation processes, *Planet. Space Sci.*, **29**, 951-974.
- O'Neill N.T., and J.R. Miller, 1984: Combined solar aureole and solar beam extinction measurement, 1: Calibration considerations, *Appl. Opt.*, **23**, 3691-3696.
- Penndorf R., 1957: Tables of the refractive index for standard air and the Rayleigh scattering coefficient for the spectral region between 0.2 and 20.0 microns and their application to atmospheric optics, *J. Opt. Soc. Am.*, **47**, 176-182.
- Porter, J.N., M. Miller, C.Pietras, C. Motell, 1999: Ship Based Sun Photometer Measurements Using Microtops Sunphotometers, *J. Atmos. Ocean. Technol.* (submitted), 21pp.
- Schmid B. and C. Wehrly, 1995: Comparison of Sun photometer calibration by Langley technique and standard lamp, *Appl. Opt.*, **34**, 4500-4512.
- Schmid B., P.R. Spyak, S.F. Biggar, C. Wehrli, J. Sekler, T. Ingold, C. Mätzler, and N. Kämpf, 1998: Evaluation of the applicability of solar and lamp radiometric calibrations of a precision Sun photometer operating between 300 and 1025 nm, *Appl. Opt.*, **37**, **18**, 3923-3941.
- Schotland R. M. and T.K. Lea, 1986: Bias in a solar Constant Determination by the Langley Method due to Structured Atmospheric Aerosol, *App. Opt.*, **25**, 2486-2491.
- Soufflet V., C. Devaux, D. Tanre, 1992: A modified Langley Plot method for measuring the spectral aerosol optical thickness and its daily variations, *Appl. Opt.*, **31**, 2154-2162.
- Stahelin J., H. Schill, B. Högger, P. Viatte, G. Levrat, and A. Gamma, 1995: Total ozone observation by Sun photometry at Arosa, Switzerland, *Opt Eng.*, **34**, 1977-1986.

- Tanaka M., T. Nakajima, M. Shiobara, 1986: Calibration of a sunphotometer by simultaneous measurements of direct-solar and circumsolar radiations, *App.Opt.*, **25**, 7, 1170-1176.
- Vermeulen A., C. Devaux., and M. Herman, 2000: Retrieval of the scattering and microphysical properties of aerosols from ground-based optical measurements including polarization, *Appl.Opt.* (submitted).
- Volz F., 1959: Photometer mit selen-photoelement zur spectralen messung der sonnenstrahlung und zur bestimmung der wellenlangenabhangigkeit der dunstrubung, *Arch. Meteor. Geophys. Bioklimatol. Ser.*, **B10**, 100-131.
- Voss, K.J., and G. Zibordi, 1989: Radiometric and geometric calibration of a spectral electro-optic ``fisheye" camera radiance distribution system. *J. Atmos. Ocean. Technol.*, **6**, 652-662.

Table 7.1: Characteristics of sun photometers.

Channels (nm)	MicroTops	SIMBAD	SIMBADA	CIMEL	PREDE
315					✓
340				✓	
350			✓		
380			✓	✓	
400					✓
410			✓		
440	✓	✓	✓	✓	
490		✓	✓		
500	✓			✓	✓
510			✓		
560		✓	✓		
620			✓		
675	✓	✓	✓	✓	✓
750			✓		
870	✓	✓	✓	✓	✓
940	✓			✓	✓
1020				✓	✓
FOV	2.5°	3°	3°	1.2°	1.5°

Table 7.2: Top-of-atmosphere (TOA) voltages since 1998 for three sun photometers cross-calibrated with respect to reference CIMELs.

MicroTops 03773	Cimel#	440 nm	500 nm	675 nm	870 nm	
8/21/1998	37	1244	988	1218	824	
6/9/1999	101	1238	987	1198	827	
9/20/2000	37	1242	984	1194	817	
7/6/2001	101	1224	980	1202	831	
12/6/2001	101	1202	984	1208	825	
SIMBAD 932706		440 nm	490 nm	560 nm	675 nm	870nm
8/21/1998	37	388591	479121	406870	421086	304820
12/14/1998	94	388269	473101	394874	410455	311944
9/23/1999	94	376205	464224	391526	416182	300000
10/28/1999	101	376820	462637	387034	410887	302475
3/6/2000	37	382815	465574	382168	408538	301005
Land Prede PS1000111		440 nm	500 nm	675 nm	870 nm	1020 nm
7/6/2001	101	1.480E-04	2.866E-04	3.643E-04	2.743E-04	1.530E-04
8/2/2001	101	1.446E-04	2.874E-04	3.668E-04	2.767E-04	1.530E-04
9/6/2001	94	1.451E-04	2.873E-04	3.646E-04	2.796E-04	1.552E-04
9/7/2001	94	1.460E-04	2.907E-04	3.635E-04	2.777E-04	1.542E-04
10/28/2001	94	1.817E-04	2.820E-04	3.557E-04	2.721E-04	1.533E-04

Chapter 5

Stability Monitoring of Field Radiometers Using Portable Sources

Stanford B. Hooker

NASA Goddard Space Flight Center, Greenbelt, Maryland

5.1 INTRODUCTION

Mueller and Austin (1995) included a discussion on tracking instrument performance in between calibration activities with stable lamp sources in rugged, fixed geometric configurations. The recommended specifications of the device included the stability of the lamp output and the repeatability of measurement must be sufficient to detect 2 % variations in an instrument's performance. In terms of the protocols for using the source, it was recommended that an instrument should be connected to the portable standard and its response recorded daily, keeping a record of instrument responsiveness throughout an experiment. Furthermore, these sources would provide an essential warning of problems if they appear.

One of the more important requirements in the use of the portable source was it must be available when the complete radiometric calibrations are performed, so a baseline may be established and maintained for each sensor channel, but recognizing that the source cannot be a substitute for complete calibrations. The temporal record they provide will, however, be invaluable in cases where the pre-and post-cruise calibrations disagree or if the instrument is disturbed, e.g., opened between calibrations, subjected to harsh treatment during deployment or transport, or if the data quality are otherwise suspect. These portable standards are an important part of the recommended instrument package.

5.2 The SQM

Although Mueller and Austin (1995) specified the need for, and described some of the requirements of, a portable source, no such device was then commercially available. In response to the need for a portable source, NASA and NIST developed the SQM. The engineering design and characteristics of the SQM are described by Johnson et al. (1998), so only a brief description is given here. A separate rack of electronic equipment, composed principally of two computer controlled power supplies and a multiplexed, digital voltmeter (DVM), are an essential part of producing the stable light field. All of the external components are controlled by a computer program over a general purpose interface bus (GPIB).

The SQM has two sets of halogen lamps with eight lamps in each set; both lamp sets are arranged symmetrically on a ring and operate in series, so if one lamp fails, the entire set goes off. The lamps in one set are rated for 1.05 A (4.2 V) and are operated at 0.95 A, and the lamps in the other set are rated for 3.45 A (5.0 V) and are operated at 3.1 A; the lamp sets are hereafter referred to as the 1 A and 3 A lamps, respectively. The lamps are operated at approximately 95 % of their full amperage rating to maximize the lifetime of the lamps.

A low, medium, and high intensity flux level is provided when the 1 A, 3 A, and both lamp sets are used, respectively. Each lamp set was aged for approximately 50 hours before deploying the SQM to the field. The interior light chamber has bead-blasted aluminum walls, so the diffuse component of the reflectance is significant. The lamps illuminate a circular plastic diffuser protected by safety glass and sealed from the environment by o-rings. The diffuser is resilient to ultraviolet yellowing, but can age nonetheless. The exit aperture is 20 cm in diameter and has a spatial uniformity of 98 % or more over the interior 15 cm circle. The SQM does not have, nor does it require, an absolute calibration, but it has design objectives of better than 2 % stability during field deployments.

A faceplate or *shadow collar* provides a mounting assembly, so the device under test (DUT), usually a radiance or irradiance sensor, can be positioned in the shadow collar. The DUT has a D-shaped collar fitted to it at a set distance, 3.81 cm (1.5 inch), from the front of the DUT. This distance was chosen based on the most restrictive clearance requirement of the radiometers used in the different deployment rigs. The D-shaped collar ensures the DUT can be mounted to the SQM at a reproducible location and orientation with respect to the exit aperture each time the DUT is used. The former minimizes uncertainties (principally with irradiance sensors) due to distance

differences between measurement sessions, while the latter minimizes uncertainties (principally with radiance sensors) due to inhomogeneities in the exit aperture light field. In either case, the D-shaped collar keeps these sources of uncertainties below the 1 % level. A schematic of the original SQM is given in Fig.5.1. The SQM faceplate can be changed to accept a variety of instruments from different manufacturers. Radiometers above a certain size, approximately 15 cm, would be difficult to accommodate, but the entire mounting assembly can be changed to allow for reasonable viewing by seemingly difficult to handle radiometers. To date, three radiometer designs have been used with the SQM, and there were no problems in producing the needed faceplates, D-shaped collars, or support hardware to accommodate these units.

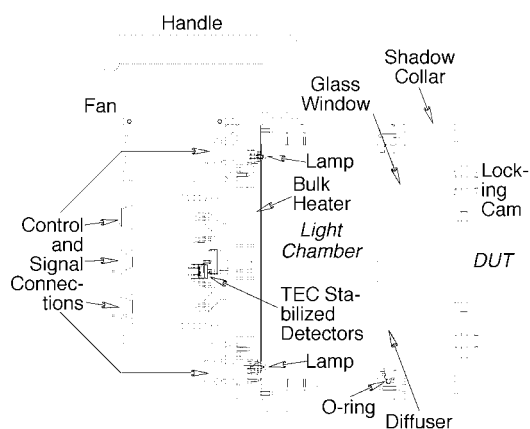


Figure 5.1: A schematic of the SQM showing a DUT kinematically mounted to the shadow collar.

The SQM light field can change because of a variety of effects; for example, the presence of the DUT, the aging of the lamps, a deterioration in the plastic diffuser, a change in the transmittance of the glass cover, a drift in the control electronics, a repositioning of a mechanical alignment, etc. To account for these changes, three photodiodes, whose temperatures are kept constant with a precision thermoelectric cooler (± 0.01 K), measure the exit aperture light level: the first has a responsivity in the blue part of the spectrum, the second in the red part of the spectrum, and the third has a broadband or *white* response. All three internal monitors view the center portion of the exit aperture. A fan cools the back of the SQM to prevent a build up in temperature beyond that which the thermoelectric cooler can accommodate. The SQM has an internal heater to help maintain temperature stability in colder climates and to shorten the time needed for warming up the SQM.

Another SQM quality control procedure is provided by three special DUTs called *fiducials*: a white one, a black one, and a black one with a glass face (the glass is the same as that used with the field radiometers). A fiducial has the same size and shape of a radiometer, but is non operational. The reflective surface of a fiducial is carefully maintained, both during its use and when it is not being used. Consequently, the reflective surface degrades very slowly, so over the time period of a field expedition, it remains basically constant. A field radiometer, by comparison, has a reflective surface that is changing episodically from the wear and tear of daily use. This change in reflectivity alters the loading of the radiometer on the SQM and is a source of variance for the monitors inside the SQM that are viewing the exit aperture, or the radiometer itself when it is viewing the exit aperture. The time series of a fiducial, as measured by the internal monitors, gives an independent measure of the temporal stability of the light field.

The SQM has been used to track changes in instruments between calibrations and on multiple cruises lasting approximately 5--6 weeks each (Hooker and Maritorena 2000). Although there was some controversy at the design stage about operating the lamps below their rated current (approximately 95 % of rating), there has been no observable degradation in the performance of the lamps as a result of this--indeed, they have survived long shipment routes (US to UK to Falkland Islands and back) on repeated occasions, as well as, the high vibration environment of a ship. The SQM is clearly a robust instrument well suited to the task of calibration monitoring in the field at the 1 % level (Hooker and Aiken 1998). There are two commercialized versions of the SQM: the OCS-5002 built by Yankee Environmental Systems (YES), Inc. (Turners Falls, Massachusetts), and the SQM-II built by Satlantic, Inc. (Halifax, Canada). Although both companies based their designs on the SQM, the OCS-5002 is most like the original.

5.3 OCS-5002

The OCS-5002 is composed of the lamp housing, with shadow collar and kinematic mounting system, plus a power supply, both of which are operated and monitored via a serial port interface to a computer. All system operations, including powering on and off the lamps, controlling the cooling fan and preheater, as well as monitoring system performance during warm up and operation are controlled by the external software. The power supply and control system were specially designed to enhance performance and are enclosed in a waterproof enclosure. A picture of the lamp housing with shadow collar attached is shown in Fig. 5.2.

An internal thermally stabilized current regulation circuit ensures precise current regulation to the two independent lamp sets (with low- and high-power lamps). The lamps in the original design were potted into aluminum mounts that held the bulbs in their correct orientations. The mounts were soldered to a circular circuit board and were difficult to replace. In the OCS-5002, porcelain sockets are used for each lamp, which are held in place with epoxy in aluminum mounting rings. This design allows for rapid individual bulb replacement.

Shunt temperatures as well as the lamp housing temperatures are monitored during operation. A two-channel filter-detector and a third unfiltered detector are positioned within the lamp housing to permit direct optical monitoring of the lamp rings and the integrating cavity itself. These three detectors are thermally stabilized via a thermoelectrically cooled housing to approximately 35°C, and their outputs are continuously monitored during system operation.



Figure 5.2: A picture of the OCS-5002 without a DUT mounted to the shadow collar

5.4 SQM-II

The main difference between the SQM-II (Fig. 5.3) and the original unit is the high degree of integration in the former. The entire system consists of two components, a deck box that provides DC power to the SQM-II, and the SQM-II itself (McLean et al. 1998). The latter contains the lamp rings (which use the same lamps as the original SQM), heating and cooling subsystems, control circuitry, the system computer, plus display and data storage. The SQM-II system is designed to be self contained and does not require a computer to operate. Only two cables are required to complete system assembly (an AC power cord for the deck box and a DC power cord to link the deck box to the SQM-II). Although this integration reduces system complexity, it comes with increased vulnerability: a failure in any one of the subsystems can render the entire system inoperable with no opportunity for simply swapping in a new (external) subassembly, like a power supply or DVM. As was done with the original SQM, Satlantic recommends running the SQM-II on an uninterruptible power supply (UPS).

User input to start and monitor the system is via a simple 4-button keypad and a 4 x 20 fluorescent display at the rear of the device. Commands can be entered using the menus on the display or remotely from a computer. A

computer can also be connected to the system to log data during a measurement session, or the data can be stored internally in a flash card and downloaded later.

The differences between the two SQM units are not restricted to their control architecture. The SQM-II has many improvements that use of the original unit has shown to be desirable under different circumstances:

1. The bulbs are mounted at the front, facing away from the exit aperture, which increases the average path length of the light emitted by each bulb, and it makes it easier to service the lamps (individually and as a subassembly);
2. The light chamber is lined with Spectralon, so the emitted flux is higher, and the aperture uniformity is greater; and
3. At 490 nm, the SQM-II is about seven times more intense than the SQM (the apparent blackbody temperature of the SQM-II is 3,100 K, whereas, the SQM is about 2,400 K).

Although the greater flux of the SQM-II is a desirable attribute for the blue part of the spectrum, the high output in the red saturates many in-water field radiometers. This was subsequently corrected by adding a blue filter to the exit aperture.

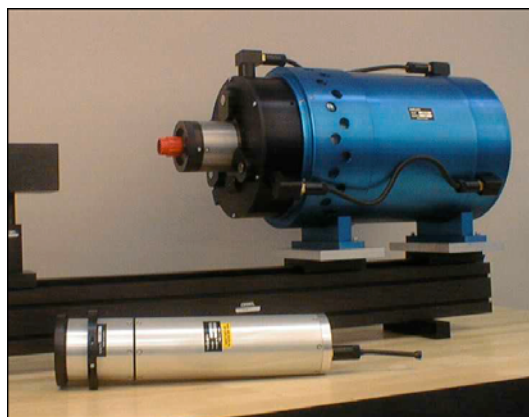


Figure 5.3: A picture of the SQM-II with a DUT mounted to the shadow collar.

5.5 METHODOLOGY

To check the stability of radiometers in the field, and to monitor the performance of the SQM, a calibration evaluation and radiometric testing (CERT) session and a data acquisition sequence (DAS) needs to be defined. In its simplest form, a CERT session is a sequence of DAS events, which are executed following a prescribed methodology. Each DAS represents enough data to statistically establish the characteristics of the instrument involved within a reasonable amount of time. In most cases, 3 minutes is sufficient. A typical sequence of procedures for each CERT session is as follows:

1. The electronics equipment (the lamp power supplies and the digital multimeter, the SQM fan and internal heater power supplies, the lamp timers, etc.) is turned on 1-2 hours before the CERT session begins. The total numbers of hours on each lamp set are tracked by recording the starting and ending number of hours on each lamp set.
2. The SQM is preheated using the internal electrical heater for 30--60 minutes, depending on the environmental conditions at the time. This is done to achieve a time efficient thermal equilibrium of the instrument from the power dissipation of the lamps.
3. If the mixture of radiometers used in the CERT sessions change over time, at least one radiometer (preferably two of different types, i.e., radiance and irradiance) should be recurrently used in all sessions. The first data collected during the CERT session should be the dark voltages for this radiometer (usually achieved by putting an opaque cap on the radiometer) and the SQM internal dark voltages (usually acquired by blocking the SQM exit aperture with a fiducial).
4. Once the SQM is powered up at the selected lamp level, it should be allowed to warm up for at least 1 hour (and frequently for as long as 2 hours in highly variable environments). The warm-up period can

be considered completed when the internal SQM monitor data are constant to within 0.1 %. The radiometric stability usually coincides with a thermal equilibrium as denoted by the internal thermistors.

5. Upon the completion of the warm-up period, the individual radiometers are tested sequentially. First, the previous DUT is removed and replaced with a fiducial. Second, dark voltages for the radiometer to be tested and SQM monitor data for glass fiducial are simultaneously collected. Third, the fiducial is removed from the SQM and replaced with the radiometer. Finally, data from the SQM and the radiometer are recorded. Each time a DUT is mounted to the SQM, the lamp voltages and internal temperatures of the SQM are recorded.
6. If multiple flux levels are to be measured, and the current lamp set is not to be used, it is powered down. The needed lamp set is powered on and allowed to warm up for 1-2 hours. The individual radiometers are tested sequentially with fiducial measurements taken during dark voltage measurements (step 5).
7. Before the SQM is finally shut down, any remaining fiducials are measured. These measurements, plus the fiducial data acquired in between the radiometer dark and light (SQM) measurements, are the primary sources for tracking the stability of the SQM flux. After the lamps are powered down, the ending number of hours on each lamp set is recorded.

It is important to note the warm-up process only involves the SQM and it is done only once before the individual DUTs are measured; the DUTs are not warmed up *per se*, although, they are usually kept in the same room as the SQM, so they are at room temperature.

The point for radiometric stability of the internal SQM monitors (0.1 %) is usually achieved within 30-90 minutes of powering up the lamps, depending on the amount of preheating. In general, the warm-up period is extended another 30 minutes past this point to ensure that stability can be maintained. The radiometric stability of the SQM immediately after powering on the lamps (*i.e.*, within 1 minute) is usually less than 0.2 % with preheating, and as much as 2 % without preheating depending on the environmental conditions. If a radiometer is subjected to some kind of trauma and needs to be checked as quickly as possible for an impending deployment, it is usually possible to check it to within reasonable limits using a rapid start of the SQM, particularly if the SQM is kept in the preheated mode.

If CERT sessions are conducted outside, the SQM should be shaded from direct sunlight and ambient wind conditions to prevent rapid changes in heating and cooling. A major source of noise in the stability of the lamps is vibration, particularly if the SQM is used at sea. Vibration damping is recommended under such conditions and 0.5 in. high density felt has been demonstrated to be a good damping material.

5.6 DATA ANALYSIS

The approach for presenting the data analysis procedures is assumed to involve more than one radiometer, since most deployment systems involve a solar reference and one or more above- or in-water instruments. In the most general terms, the quantity of interest is a voltage or digital count level associated with a radiometer (or DUT), $V^C(\lambda_i, t_j)$, where V is the voltage of the radiometer under illumination at the time of the measurement, C is the instrument code of the DUT, λ_i is an individual wavelength or channel of the instrument, and t_j is a particular time for the data record. The instrument code is just a simple mnemonic for keeping track of which DUT was measured when. A suitable coding scheme is to assign a letter for a particular type of radiometer (e.g., R for radiance, I for irradiance, etc.) and then to add on the serial number).

An SQM has two lamp sets, so multiple flux levels are possible. Under most circumstances the lamp sets are different, so three basic voltage levels for the SQM monitors and for the radiometers while they are mounted to the SQM are possible: L, M, and H, which correspond to low, medium, and high lamp levels, respectively. (In situations where the two lamp sets are identical, it is customary to denote the two levels as L and M.) In addition, dark voltages are measured for the radiometers (D^C) and the SQM internal monitors (D_S). For the latter, the S code denotes the internal monitor channel (B for blue, R for red, and W for white or broadband.) Note the SQM-II has a single internal monitor in the blue part of the spectrum. All of the data for a particular CERT session are acquired at a single lamp level.

The process of determining a parameter for monitoring the radiometric stability of a radiometer during a field deployment begins by first defining the average signal level acquired with the radiometer during a DAS:

$$\bar{V}^C(\lambda_i, \bar{t}_k) = \frac{1}{n} \sum_{j=1}^n V^C(\lambda_i, t_j), \quad (5.1)$$

where $\bar{V}^C(\lambda_i, \bar{t}_k)$ denotes a time average of the total number of samples, n , collected during a DAS, and \bar{t}_k is the average time over DAS time period k . Following (5.1), the average dark voltage for a DAS is defined as

$$\bar{D}^C(\lambda_i, \bar{t}_k) = \frac{1}{n} \sum_{j=1}^n D^C(\lambda_i, t_j). \quad (5.2)$$

In (5.2), the temporal assignment for the average dark voltage is associated with the average signal level even though the dark values are taken a few minutes before the signal data (this is a simplification in the process that is purely cosmetic).

The average internal monitor signal level acquired during a DAS while the DUT was mounted to the SQM is

$$\bar{V}_S(\bar{t}_k) = \frac{1}{n} \sum_{j=1}^n V_S(t_j), \quad (5.3)$$

where, again, S is used to denote the internal SQM monitor used for normalization: B, R, or W. The average dark voltage for an internal monitor is defined as

$$\bar{D}_S(\bar{t}_k) = \frac{1}{n} \sum_{j=1}^n D_S(t_j), \quad (5.4)$$

The internal monitor dark data is collected before the lamps are warmed up, so the temporal information is not important and has been omitted.

While the dark readings for a radiometer were being collected, a fiducial was placed inside the SQM and the signals from the internal SQM monitors were recorded. The voltages from the monitors are denoted by X_S^C where X can be either L, M, or H depending on the selected SQM lamp level, C is the instrument code for the DUT in the SQM, and S indicates the internal monitor under consideration: B for the blue monitor, R for the red monitor, and W for the broad-band or white monitor.

Changes in a radiometric signal can arise from changes in the light source, the digitization electronics, or the detector electronics. Tracking the performance of a radiometer over extended time periods must take into account these three influences on the signal. The basic parameter for tracking the radiometers is constructed by taking the average voltage from the radiometer when it was mounted to the SQM, subtracting the average dark voltage, and then normalizing the difference by one of the average internal SQM monitor voltages yields

$$\tilde{V}_S^C(\lambda_i, \bar{t}_k) = \frac{\bar{V}^C(\lambda_i, \bar{t}_k) - \bar{D}^C(\lambda_i, \bar{t}_k)}{\bar{V}_S^C(\bar{t}_k) - \bar{D}_S}, \quad (5.5)$$

where \tilde{V}_S^C denotes a normalized result for a DAS. Within the uncertainties of the measurements, $\tilde{V}_S^C(\lambda_i)$ should be a constant from one CERT session to the next, since an increase (decrease) in SQM intensity should coincide with an increase (decrease) in the radiometer signal.

If N is the total number of CERT sessions at a particular lamp level, the average normalized signal for a particular radiometer at that lamp level is given by

$$\hat{V}_S^C(\bar{t}_k) = \frac{1}{N} \sum_{j=1}^N \tilde{V}_S^C(\lambda_i, t_j), \quad (5.6)$$

where $\hat{V}_S^C(\bar{t}_k)$ denotes the average of the normalized signals.

The temporal performance of a radiometer is determined by calculating the percent deviation of the radiometer (during a particular DAS time, t_k) from the average of all of the normalized signals (5.4) as

$$\tilde{V}_S^C(\lambda_i, \bar{t}_k) = 100 \left[\frac{\tilde{V}_S^C(\lambda_i, \bar{t}_k)}{\tilde{V}_S^C(\lambda_k)} - 1 \right], \quad (5.7)$$

where \tilde{V}_S^C denotes the percent deviation of the normalized signals with respect to the average for a particular lamp level, the average being determined from the time series of data collected during a field deployment. Thus, $\tilde{M}_W^{R21}(421)$ is the percent deviation of the radiances for the 412 nm channel of radiometer OCR-200 serial number 21 (instrument code R21) at the medium lamp level normalized with the white SQM internal monitor.

The time series of corresponding fiducial measurements are formed in a similar fashion. The only data available for a fiducial is the internal SQM monitor data, so the equivalent of (5.5) for a fiducial is simply the average signal level for the monitor minus the average dark level, *i.e.*

$$\tilde{V}_S^C(\lambda_i) = \bar{V}_S^C(\bar{t}_k) - \bar{D}_S, \quad (5.8)$$

where C is the DUT code for a glass, black, or white fiducial (usually G, B, and W, respectively, although when many fiducials are available, the serial numbers of the fiducials are included in the coding scheme). The average signal over all CERT sessions is calculated using (5.6) and the individual percent deviations using (5.7).

The time series of fiducial measurements within a CERT gives the performance of the SQM during the CERT, and the time series of all fiducial measurements across the CERT sessions gives the long-term performance of the SQM. Because one fiducial is being used repeatedly, and two others are being used only once per CERT session, the ability to discern short- and long-term changes in the SQM is available, with the longer-term changes being measured by more than one fiducial.

5.7 FUTURE APPLICATIONS

Figure 5.4 presents a summary of SQM performance during three at-sea deployments. The data is from Atlantic Meridional Transect (AMT) cruises (Aiken et al. 2000) AMT-5 through AMT-7 plus laboratory experiments, and covers a time period of approximately 460 days. It shows the internal blue monitor signal as measured with the glass fiducial as a function of time, but presented as the percent difference with respect to the mean value for the entire time period (*i.e.*, across all CERT sessions). A confirmation of the signal is given by the R035 radiometer for the 443 nm channel (which is very similar to the blue internal monitor for the SQM), and it very nearly mirrors the internal monitor signal. The two detectors yield similar decay rates of approximately 0.007 % per day, or approximately 0.25 % for a 35 day cruise. This is an underestimate, however, because the degradation is due mostly to lamp usage, and this is obviously most significant during use, and not during shipping and storage. This is best seen by perusing the data from individual cruises, and comparing them to results of laboratory work done following AMT-7.

The stability and behavior of the SQM during AMT-5 was very similar to its performance on AMT-3 when it was first commissioned for field use (Hooker and Aiken 1998): the data indicate a stepwise change in the SQM flux level halfway through the cruise.

All three detectors show the change, and if the three detector signals are averaged together, the emitted flux of the SQM decreased by approximately 0.87 %. The change in flux was due to a partial short in one of the bulbs, which resulted in a 1.2 % decrease in the operating voltage of the lamp. The stability of the SQM during the periods before and after the change in light output, as estimated by one standard deviation (1σ) in the average of the three internal monitor signals, was to within 0.60 % and 0.53 %, respectively.

During AMT-6, the 1σ values of the red, blue, and white detectors while measuring the glass fiducial were 0.36 %, 0.46 %, and 0.39 %, respectively. The performance of the SQM during AMT-6 was the best out of all the cruises; no lamp anomalies were experienced and the standard deviation in the emitted flux was the lowest ever recorded in the field. The AMT-7 data show a stepwise change halfway through the cruise, as was seen during AMT-3 and AMT-5. Although the stability for the entire cruise was very good, to within ± 0.43 % as measured by the blue detector, the stability improves to ± 0.38 % and ± 0.28 % if the cruise is split into a first and second half, respectively.

Lamp performance after AMT-7 in the laboratory was very similar to that seen during AMT-6: the changes are all within 1 %. The long- and short-term stability of the SQM raises the possibility that this device can be used for absolute calibrations in the laboratory and in the field. Although a definitive analysis of using the SQM in this fashion has not been completed, one of the objectives of SIRREX-7 was to evaluate several SQMs for this purpose

(Hooker *et al.* 2000). The preliminary results indicate this may be possible, but a well-prescribed protocol is contingent upon completion of the SIRREX-7 data analysis and on acceptance through a rigorous independent review.

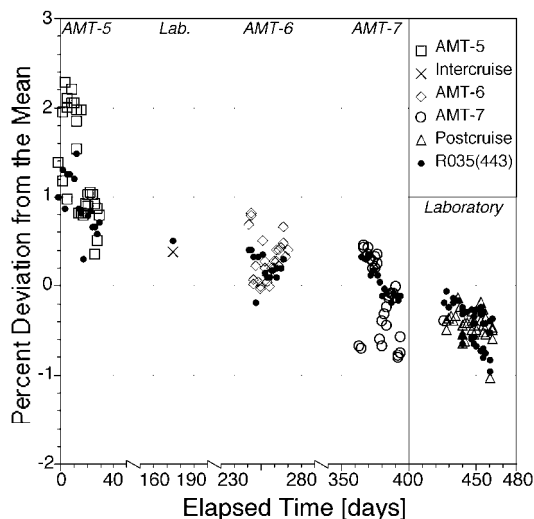


Figure 5.4: The long-term stability of the original SQM as measured, using its internal blue monitor and one radiometer (R035) at 433 nm, on a series of AMT cruises and laboratory exercises.

REFERENCES

- Aiken, J., D.G. Cummings, S.W. Gibb, N.W. Rees, R. Woodd-Walker, E.M.S. Woodward, J. Woolfenden, S.B. Hooker, J-F. Berthon, C.D. Dempsey, D.J. Suggett, P. Wood, C. Donlon, N. González-Benítez, I. Huskin, M. Quevedo, R. Barciela-Fernandez, C.de Vargas, and C. McKee, 1999: AMT-5 Cruise Report. *NASA Tech. Memo. 1998--206892, Vol. 2*, S.B. Hooker and E.R. Firestone, Eds., NASA Goddard Space Flight Center, Greenbelt, Maryland, 113 pp.
- Aiken, J., N. Rees, S. Hooker, P. Holligan, A. Bale, D. Robins, G. Moore, R. Harris, and D. Pilgrim, 2000: The Atlantic Meridional Transect; overview and synthesis of data. *Prog. Oceanogr.*, (in press).
- Hooker, S.B., and J. Aiken, 1998: Calibration evaluation and radiometric Testing of field radiometers with the SeaWiFS Quality Monitor (SQM). *J. Atmos. Oceanic Tech.*, **15**, 995-1,007.
- Hooker, S.B. and S. Maritorea, 2000: An evaluation of oceanographic radiometers and deployment methodologies. *J Atmos. Oceanic Technol.*, 17,811-830.
- Hooker, S.B., S. McLean, J. Sherman, M. Small, G. Zibordi, and J. Brown, 2000: The seventh SeaWiFS Intercalibration Round-Robin Experiment (SIRREX-7), March 1999. *NASA Tech. Memo. 2000--206892, Vol. 13*, S.B. Hooker and E.R. Firestone, Eds., NASA Goddard Space Flight Center, (in prep.)
- Johnson, B.C., P-S. Shaw, S.B. Hooker, and D. Lynch, 1998: Radiometric and engineering performance of the SeaWiFS Quality Monitor (SQM): A portable light source for field radiometers. *J. Atmos. Oceanic Tech.*, **15**, 1,008-1,022.
- McLean, S., S. Feener, J. Scrutton, M. Small, S. Hooker, and M. Lewis, 1998: SQM-II: A commercial portable light source for field radiometer quality assurance. *Proc. SPIE Ocean Optics XIV*, (in press).
- Mueller, J.L. and R. W. Austin, 1995: Ocean Optics Protocols for SeaWiFS Validation, Rev 1. *NASA Tech. Memo. 1995--104566, Vol. 25*, S.B. Hooker, E.R. Firestone and J.G. Aker, Eds., NASA Goddard Space Flight Center, Greenbelt, Maryland, 67 pp.